Please find the published version at Precambrian Research 167 (2008) 213-236

Provenance and tectonic setting of the Neoproterozoic Yanbian Group, western Yangtze Block (SW China)

Wei-Hua Sun [a,*], Mei-Fu Zhou [a], Dan-Ping Yan [b], Jian-Wei Li [c] and Yuxiao Ma [d]

[a] Department of Earth Sciences, University of Hong Kong, Hong Kong, China

[b] School of Earth Sciences and Resources, China University of Geosciences, Beijing 100083, China

[c] State Key Laboratory of Geological Processes and Mineral Resources, and Faculty of Earth Resources, China University of Geosciences, Wuhan 430074, China

[d] Department of Geochemistry, Chengdu University of Science and Technology, Chengdu, China

* Corresponding author. Tel.: +852 2859 8913; Fax: +852 2517 6912.

E-mail: weihua@hkusua.hku.hk Current email: weihuasun@yahoo.com

Abstract

Tectonic evolution of the Yangtze Block of South China during Neoproterozoic time has been a major focus of debate and is important in the reconstruction of the Rodinian supercontinent. The Yanbian Group in the western margin of the Yangtze Block is a well-preserved Neoproterozoic volcanic-sedimentary sequence and provides a rare opportunity to examine the provenance and tectonic setting. It consists of a lower part composed of ~1500 m thick basaltic lavas and an upper part with ~3500 m thick flysch deposits. The flysch sequence contains typical deep marine turbidites consisting mainly of fine-grained volcaniclastic sandstones and mudstones, indicating a submarine fan depositional system. Detrital zircon dating yields ages ranging from ca. 865 Ma to

1000 Ma with two peaks at ca. 900 Ma and 920 Ma, respectively. The Yanbian Group is intruded by the ~860- Ma Guandaoshan dioritic pluton, constraining its depositional age at ca. 870 Ma. The sandstones contain abundant feldspar and lithic fragments with minor amounts of quartz and have an average composition of $Q_{16}F_{35}L_{49}$, suggesting a proximal source and an undissected to transitional arc setting. The lithic fragments in the sandstones point to andesitic and felsic volcanic rock sources. The sandstones and mudstones have intermediate SiO_2/Al_2O_3 (typically 3-6), high Fe_2O_3+MgO contents (5-12 wt%), and moderate to high K_2O/Na_2O ratios (generally 0.1-1 and 1-10 for sandstones and mudstones, respectively). In comparison with average upper continental crust, they show strong Nb-Ta anomalies, slight depletion of Zr-Hf, La and Th, but moderate enrichment of V, Cr, Ni, and Sc. These rocks show LREE enrichment (La/Yb_N=5.3-7.4) with flat HREE, and pronounced negative Eu anomalies (Eu/Eu*=0.6-0.74) in chondrite-normalized REE patterns, similar to post-Archean shales. Geochemical data for these rocks suggest an arc setting and intermediate-felsic volcanic source, consistent with a back-arc basin scenario for the basaltic lavas in the lower Yanbian Group. Together with regional geological evidence, the turbidites of the Yanbian Group strongly support a model in which the western margin of the Yangtze Block was a major magmatic arc, active probably from ~920 Ma to 740 Ma, a period of more than 180 million years.

Key words: turbidite, detrital zircon dating, geochemistry, provenance, Yanbian Group, Yangtze Block

1. Introduction

Siliciclastic rocks are useful for investigating provenance and tectonic setting of sedimentary basins (Dickinson, 1970, 1985; Bhatia, 1983, 1985; Roser and Korsch, 1986, 1988; Floyd and Leveridge, 1987). Provenance regions, especially those at destructive plate margins, are rarely well preserved because of subsequent erosion and destruction. In such circumstances, studies of related sedimentary rocks have considerable potential for determining the source rocks and the history of ancient continental margins. A combination of traditional mineralogical (especially for sandstones) and geochemical methods and detrital zircon U-Pb analysis has greatly contributed to our understanding of the provenance, tectonic setting and tectonomagmatic evolution of sedimentary basins and their siliciclastic deposits (McLennan et al., 1990, 1995; Maas and McCulloch, 1991; Taylor and McLennan, 1995; Dickinson and Gehrels, 2000; DeGraaff-Surpless et al, 2002; Cope et al., 2005; She et al., 2006).

The tectonic evolution of the Yangtze Block of South China is of importance for the reconstruction of the supercontinent Rodinia and has been a matter of hot debate (Li Z.X. et al., 1999, 2003; Li X.H. et al., 2003, 2006; Zhou et al., 2002a, b, 2006a, b). Previous work has focused mainly on the Neoproterozoic igneous rocks, and studies of the associated sedimentary sequences are sparse. The Neoproterozoic Yanbian Group in the western margin of the Yangtze Block has been a subject of several recent studies (Du et al., 2005; Zhou et al., 2006a; Li X.H. et al., 2006; Sun et al., 2007), because it is not only one of the best-preserved volcano-sedimentary sequences in South China, but is spatially

associated with several contemporaneous intermediate to mafic plutons, making it ideal for investigating the tectonic affinities of the Yangtze Block. Previous studies on the volcanic rocks in the lower part of the Yanbian Group and the related intrusive rocks have interpreted the Yanbian Group as a relict ophiolite (Sun and Vuagnat, 1992) or a back-arc basin sequence (Du et al., 2005; Zhou et al., 2006a; Li X.H. et al., 2006, Sun et al., 2007). So far, there is no agreement about the depositional age of the Yanbian Group (Du et al., 2005; Zhou et al., 2006a; Li X.H. et al., 2006), causing additional ambiguity in its tectonic interpretation. In particular, no studies are available regarding the chemical composition and petrology of the sedimentary rocks, which are crucial to better understanding the source rocks and tectonic setting.

In this paper, we present petrographic, detrital zircon U-Pb geochronological and geochemical data for the upper siliciclastic rocks of the Yanbian Group, in an attempt to constrain the age of the sediments and to infer their provenance and tectonic setting. The results also provide insights into the tectonic evolution of the Yangtze Block during Neoproterozoic time.

2. Geological background

South China consists of the Yangtze Block in the northwest and the Cathaysia Block in the southeast (Fig. 1). The Yangtze Block is separated from the North China Craton by the Qinling-Dabie orogenic belt and is bounded to the west by the Songpan-Ganze Terrane of the Tibetan Plateau. The Songpan-Ganze Terrane is a prominent triangular region filled with Triassic deep-marine

95 flysch deposits (Zhou and Graham, 1996). The Yangtze Block comprises
96 metamorphic basement complexes and Neoproterozoic to Cenozoic cover
97 sequences (Yan D.P. et al., 2003). The basement complexes contain gneiss,
98 mica schist, amphibolite, marble and quartzite, whereas the cover sequences are
99 mainly composed of carbonate, clastic and volcanic rocks (SBGMR, 1991).

100 Along the western margin of the Yangtze Block, a ~1000-km-long, NS-
101 trending, Neoproterozoic igneous and metamorphic belt crops out from Kangding
102 in Sichuan Province to Yuanjiang in Yunnan Province (Fig. 1). This belt has been
103 recently interpreted as a major Neoproterozoic continental arc, named the
104 Hannan-Panxi arc, in which the igneous rocks have ages mostly ranging from
105 860 to 740 Ma (Zhou et al., 2002a, b, 2006a, b; Zhao and Zhou, 2007; Sun and
106 Zhou, 2008). The occurrence of this huge continental arc indicates an Andean-
107 type continental margin with oceanic crust being subducted eastward beneath
108 the western margin of the Yangtze Block during that time (Zhou et al., 2002b;
109 Sun and Zhou, 2008).

110 In the belt, the igneous plutons intrude high-grade (granitic gneisses and
111 amphibolite) and low-grade metamorphic rocks (Pan et al., 1987; Li F.H. et al.,
112 1988). The high-grade metamorphic rocks, including the Kangding and
113 Dahongshan complexes, were traditionally considered to be late Archean to
114 Paleoproterozoic crystalline basement; the low-grade metamorphic rocks, such
115 as the Kunyang, Huili, Yanbian and Bikou Groups, were interpreted to be
116 Mesoproterozoic and to constitute the folded basement in this region (Chen and
117 Chen, 1987).

The Yanbian Group is unconformably overlain by Sinian (latest Neoproterozoic) strata known as the Lieguliu Formation (Sun et al., 2007), which is composed of glacial deposits, comparable to those of similar age on other continents (Elsbacher, 1985). The Yanbian Group is intruded by a magmatic association that consists of the ~860-Ma Guandaoshan dioritic pluton (Li X.H. et al., 2003; Sun and Zhou, 2008), 810-820-Ma Tongde dioritic-gabbroic pluton (Li Z.X. et al., 2003) and ~810-Ma Gaojiacun and Lengshuiqing mafic plutons (Zhou et al., 2006a) (Fig. 1). These, together with the ~740 Ma Dadukou gabbroic intrusion south of Tongde Town (Zhao and Zhou, 2007), have been interpreted as part of the Hannan-Panxi arc along the western margin of the Yangtze Block (Sun and Zhou, 2008).

3. Stratigraphy and depositional environment

Cropping out over an area of approximately 500 km^2, the Yanbian Group is composed of two principal units: a lower volcanic sequence ca. 1500 m thick, known as the Fangtian Formation, and an upper flysch more than 5000 m thick, comprising the Yumen, Xiaoping and Zagu Formations (Fig. 2)

The Fangtian Formation is composed of massive basalt, pillow basalt and volcanic breccias with subordinate interbeds of chert, and pelitic and siliceous slate. It is conformably overlain by the ca.1700-m-thick Yumen Formation, which consists primarily of thin- to medium-bedded, dark-gray, carbonaceous and siliceous slates with interbeds of fine- to coarse-grained sandstone (Fig. 3a). Lenses of limestone are locally present. An ~5-cm-thick layer of black chert

141 marks the base of the Yumen Formation where it overlies the basaltic breccias of
142 the Fangtian Formation (Fig. 3a). The slates and sandstones have regular
143 parallel bedding, typical of distal turbidites. In this formation, turbidites generally
144 display T_{bce} of the Bouma sequences.

145 The ~2200-m-thick Xiaoping Formation comprises dark gray slates,
146 carbonaceous slates, fine- to coarse-grained sandstones and siltstones,
147 representing turbidites and associated mudstones. The basal and top parts of the
148 succession are dominated by sandstones in beds up to 1.5 m thick, suggesting
149 small-scale channel-fill deposits. The sandstone channels usually display an
150 eroded base and a concave-upward morphology, with the grain size fining
151 upward. Conglomerates are locally present as thin, discontinuous lag beds at
152 the base of the coarse sandstone layers. The sandstones have lenticular or flat
153 beds with thicknesses of 10-20 cm, but ranging from 2 to 50 cm. Sedimentary
154 structure, such as scours, slumps, and load and flame structure, are locally well
155 developed (Figs. 3b, c). Most sandstone beds are normally graded and follow the
156 Bouma sequence. Partial Bouma sequences are more common than complete
157 ones, with the T_{abc} sequence being the most common, followed in abundance by
158 T_{ae} (Fig. 3d). Thin limestone lenses and stromatolithic limestones are also
159 observed locally. Pyrite is common in the slates and siltstones, especially along
160 some layer boundaries.

161 The ~1300-m-thick Zagu Formation is composed of dark gray slates, black
162 dolomitic slates and dolomitic limestones. There is a thin (10-15 m) layer of
163 conglomerate and pebbly sandstone at the base, representing a medium-scale

channel-fill deposit. The conglomerate clasts are typically subangular to subrounded, generally 2-4 cm in diameter, and consist mainly of intermediate-felsic volcanic rocks (50-60%), chert (20-25%), fragments of carbonaceous rock (10-15%) and siltstone (~10%). The conglomerates and sandstones are also well graded. The Zagu Formation is unconformably overlain by the Sinian Lieguliu Formation (Sun et al., 2007).

The Yanbian Group consists mainly of thin- to medium-bedded, fine-grained, turbiditic volcaniclastic sandstones and mudstones with little variation in sedimentary facies and minor input of coarse clastic material. These sedimentary rocks most likely represent submarine fan deposits, especially mid-fan deposits. This thick turbidite package lacking shallow-water deposits indicates a marine environment below wave base. The presence of limestones throughout the section indicates that the seafloor was above the carbonate compensation depth and suggests a low-latitude, warm-water environment.

4. Sandstone petrography

The sandstones are mostly fine- to medium-grained, poorly sorted and contain angular to subangular grains of low to moderate sphericity. They are mainly composed of quartz, feldspar and lithic fragments. Quartz is relatively minor in volume and is generally subangular to angular, mostly being monocrystalline and lacking inclusions and undulatory extinction (Fig. 4a). Subrounded feldspar is the dominant mineral and is partly altered to saussurite and sericite. Plagioclase is much more common than alkali feldspar (Fig. 4b).

Lithic fragments are dominantly rhyolite and andesite with felsitic and microlitic textures, although sedimentary and metamorphic varieties are also present (Figs. 4c,d,e).

Biotite and muscovite occur as elongate laths or short plates and are locally accompanied by chlorite and glauconite. Sparse heavy minerals include magnetite, zircon, apatite, titanite, pyrite, rutile and tourmaline. Most of these grains are angular to subangular, although some are well-rounded. Amphibole and pyroxene grains are locally present but extremely rare (Fig. 4f).

The matrix of the sandstones consists of clay minerals, comminuted and altered lithic and feldspathic fragments, fine-grained quartz, micas, opaque minerals, carbonate and some aphanitic material. Matrix is commonly between 10 to 15%, but may be overestimated due to the pseudomatrix problem (Dickinson, 1970). Silica is the dominant cement in these rocks but calcite is also common.

Thirty-one medium-grained sandstones were selected for petrographic study using the Gazzi-Dickinson method (Ingersoll et al., 1984). About five to six hundred framework grains were counted from each sample. Matrix (<~0.03 mm) and cement were not counted. The Gazzi-Dickinson method divides volcanic lithic clasts into various textural types (Dickinson, 1970), which is especially significant in magmatic-arc settings, where volcaniclastic components may constitute as much as 100% of the sand fraction (Marsaglia and Ingersoll, 1992). Point-count categories and recalculated parameters are defined in Table 1.

The modal point-count data are shown in Table 2 and Figure 5. In general, the sandstones are characterized by low quartz (Q), moderate feldspar (F) and high lithic (L) abundances, with L/F ratios of 1-3, indicating that the sandstones were derived almost exclusively from volcanic sources (Dickinson, 1970). The Yumen, Xiaoping and Zagu Formations have average compositions of $Q_{22}F_{30}L_{48}$, $Q_{15}F_{36}L_{49}$, and $Q_{14}F_{34}L_{52}$, respectively. In the discrimination diagrams (Fig. 5), they plot in the magmatic-arc field, indicating an undissected-transitional arc provenance.

5. Geochronology and geochemistry

5.1. Detrital zircon geochronology

Single-grain U-Pb dating were performed using the laser ablation ICP-MS technique at China University of Geosciences (Wuhan). The detailed analytical procedures follow Yuan et al. (2004). A GeoLas 2005M laser-ablation system equipped with a 193 nm ArF-excimer laser was used in connection with an Agilent 7500 ICP-MS. Helium was used as the carrier gas to enhance the transport efficiency of the ablated material. The spot diameter was 32 μm. Raw data were processed using the Glitter program (Jackson et al., 2004). All measurements were normalized relative to standard zircon 91500. Standard silicate glass NIST SRM610 was used to calculate U and Th concentrations. The data were processed using the ISOPLOT program (Ludwig, 1999).

Zircons from these rocks are commonly transparent to orange in color, 100-200 μm in size and subrounded to subangular. A total of two hundred and ninety-

232 eight analyses were performed on zircon grains from five samples (Table 3). Of
233 those, 40 analyses with a degree of discordance >3% were discarded. However,
234 only a very few of these discordant analyses yield ages outside the range defined
235 by the remaining relatively concordant analyses. $^{207}Pb/^{206}Pb$ and $^{206}Pb/^{238}U$ ages
236 were applied for zircons older and younger than 1000 Ma, respectively. The
237 dataset yields ages mainly of ~900-920 Ma with only a very minor, statistically
238 insignificant, component of older continental-derived zircons in the Yumen and
239 Xiaoping Formations. The Zagu Formation, on the other hand, has a relatively
240 high content of older continental material (Fig. 6).

241 **5.1.1. Yumen Formation**

242 Sample F38, a coarse-grained sandstone specimen, was collected near the
243 base of the Yumen Formation (N26.53.39, E101.30.80) for zircon dating. Of the
244 60 grains analyzed, 4 were highly discordant and thus were discarded. The
245 remaining forty-six grains yielded $^{206}Pb/^{238}U$ apparent ages ranging from 865 to
246 975 Ma, with a single peak at 917±6 Ma (Fig. 6).

247 Sample F3, consisting of coarse-grained, feldspar-lithic sandstone, was
248 collected from the upper part of the Yumen Formation (N26.54.47, E101.28.89).
249 Of 58 spot analyses, 41 have concordant ages ranging from 860 to 990 Ma with
250 a weighted mean of 918±8 Ma. Only one concordant grain has a significantly
251 older age of ~2000 Ma (Fig. 6). The remaining 16 analyses are highly discordant
252 but have ages within the younger age population. Thus, the age distribution of
253 zircons from the Yumen Formation suggests uniform source rocks.
254

255 **5.1.2. Xiaoping Formation**

256 A medium- to coarse-grained, feldspar-lithic sandstone, sample F4, was
257 collected from the middle part of the Xiaoping Formation (N26.55.96,
258 E101.27.45). Of the 60 grains analyzed, 45 concordant grains yielded apparent
259 $^{206}Pb/^{238}U$ ages between 850 and 960 Ma, with a prominent peak at ~920 Ma.
260 Three concordant grains gave much older ages from ~2200 to 2600 Ma (Fig. 6).
261 This age spectrum is very similar to that of samples F38 and F3 of the Yumen
262 Formation. However, half of the remaining 12 analyses with varying degrees of
263 discordance (>3%) yield older ages of around 2200-2600, suggesting a
264 somewhat greater input of older material input relative to the Yumen Formation.
265 Several concordant ages are as young as ~850 Ma (Fig. 6).

266 Sample F26 (N26.58.76, E101.32.17) was collected near the top of the
267 Xiaoping Formation. 42 of 60 spot analyses have concordant ages ranging from
268 860 to 970 Ma, with two peaks of 897±6 Ma and 934±5 Ma, respectively (Fig. 6).
269 The remaining 18 discordant analyses also show similar age ranges.

270 **5.1.3. Zagu Formation**

271 A pebbly sandstone, sample F23 (N26.58.96, E101.32.17), was collected
272 from the base of the Zagu Formation. Of 60 grains analyzed, 46 are concordant.
273 This sample yields an age distribution mainly between~ 870 Ma and 930 Ma, but
274 it is characterized by sharp increase of older zircons with several minor peaks at
275 1800, 2000, 2600 and 3000 Ma (Fig. 6). Coupled with a rapid coarsening in the
276 stratigraphic section, this suggests increased uplift and erosion in the source
277 terrane.

5.2. Whole rock geochemistry

Major oxides and selected trace elements of whole-rock samples were determined by X-ray fluorescence (XRF) on fused glass beads at the University of Hong Kong. Trace elements were analyzed with a VG PQ Excell ICP-MS, also at the University of Hong Kong. The samples for ICP-MS analysis were prepared in closed beakers in high-pressure bombs to ensure complete digestion (Qi et al., 2000). We used pure elemental standards for external calibration, and BHVO-1 (basalt) and SY-4 (syenite) as reference materials for all analyses. Accuracies of the XRF analyses are estimated to be better than 1% for SiO_2, better than 2% for major oxides present in concentrations greater than 0.5 wt% and 5% for trace elements. The ICP-MS analyses yielded accuracies better than 5%.

5.2.1. Major elements

The majority of the Yanbian Group sandstones and mudstones have intermediate SiO_2 (55-73 wt%), high Fe_2O_3+MgO (usually 5-12 wt%; total Fe as Fe_2O_3) and TiO_2 (0.6-1.2 wt%) and low CaO (mostly <1 wt%) (Table 4). In general, SiO_2 increases whereas TiO_2, Al_2O_3, Fe_2O_3, MnO, MgO, CaO, and Na_2O decrease with enhanced mineralogical maturity, indicating an increase in the quartz content and a decrease in chemically unstable detrital grains (e.g., feldspar and volcanic rock fragments) (Bhatia, 1983). There are no systematic stratigraphic variations from the Yumen through Xiaoping to Zagu Formations, possibly reflecting inadequate sampling from the Yumen and Zagu Formations.

Due to enrichment in clay minerals, the mudstones generally have higher K_2O and Al_2O_3 and lower Na_2O contents, resulting in much higher K_2O/Na_2O ratios (typically 1-10) than those of the corresponding sandstones (commonly 0.1-1). Most sandstone samples are immature, with SiO_2/Al_2O_3 ratios between 3 to 6 and Na_2O/K_2O ratios between 1 to 3.5, and plot within the graywacke field in the plot of Pettijohn (1987) (Fig. 7).

5.2.2. Trace elements

Rocks from the three Formations are virtually indistinguishable in their trace element contents, and are characterized by variable contents of Rb (7-140 ppm), Sr (10-377 ppm), Cs (0.4-8 ppm), Ba (80-1200 ppm), Th (2.6-12 ppm) and U (0.5-3.2 ppm) (Table 4). In comparison with average upper continental crust, they show strong Nb-Ta, anomalies, slight depletion of Zr-Hf, La and Th, but moderate enrichment of V (17-257 ppm), Cr (15-185 ppm), Ni (<80 ppm), and Sc (8-22 ppm) (Fig. 8a). In addition, the mudstones commonly have higher Rb, Ba, Th, U and Cs contents than the sandstones (Fig 8a), likely reflecting the abundance of clay minerals (e.g., illite and sericite) in these rocks (McLennan et al., 1983).

Both the sandstones and mudstones exhibit subparallel chondrite-normalized REE patterns, characterized by moderate fractionation between light REE and heavy REE (La/Yb_N=5.3-7.4), with obvious negative Eu anomalies (Eu/Eu*=0.6-0.74) (Fig. 8b), features typical of post-Archean sedimentary rocks (Taylor and McLennan, 1985). Moreover, the mudstones generally have slightly more fractionated REE patterns than the sandstones and ~20% higher total REE abundances.

6. Discussion

6.1. Age of the Yanbian Group

The depositional age of the unfossiliferous Yanbian Group has long been debated. It was traditionally thought to be Mesoproterozoic (Pan et al., 1987; SBGMR, 1991). However, newly obtained SHRIMP U-Pb zircon ages of 782±53 Ma (Du et al., 2005) for the basaltic lavas of the lower Yanbian Group strongly suggest a Neoproterozoic age. Similarly, Zhou et al. (2006a) reported a maximum depositional age of 837±6 Ma based on LA-ICP-MS detrital zircon dating. By contrast, Li X.H. et al. (2003, 2006) proposed a minimum age of 857±13 Ma, inferred from the emplacement age of the Guandaoshan pluton that intrudes the Yanbian Group. Thus the depositional age of the Yanbian Group should be no younger than 857 ± 13 Ma. The present geochronological results provide reliable and tight constraints on the maximum depositional age of the Yanbian Group. Although eight youngest zircons from the Yanbian Group give ages as young as 852±6 Ma (Fig. 6), we adopt here a somewhat older age of 868±6 Ma defined by another ten youngest zircon dates in the concordant dataset (Table 3). The ten zircons are from different samples but yield similar ages within quoted errors. We therefore suggest that the Yanbian Group was most likely not older than ~870 Ma. Furthermore, the Yanbian Group was probably deposited in a syn-magmatic basin, based on the short time delay between deposition of the sediments and emplacement of the 857±13 Ma Guandaoshan pluton.

6.2. Effect of chemical weathering

Chemical weathering strongly affects the mineralogy and major element geochemistry of siliciclastic sediments (Nesbitt and Young, 1982, 1996). The chemical index of alteration (CIA) is very useful in evaluating effects of weathering on sedimentary rock composition and is defined by Nesbitt and Young (1982) as:

$$CIA = [Al_2O_3/(Al_2O_3+CaO^*+Na_2O+K_2O)]\times 100$$

Where CaO* represents Ca in the silicate minerals only (i.e. excluding calcite, dolomite and apatite) (Fedo et al., 1995). High CIA values reflect the removal of labile cations (e.g., Na^+, K^+ and Ca^+) in preference to relatively stable residual constituents (e.g. Al^+), corresponding to high degrees of chemical weathering. The values vary from about 50 for the average upper continental crust to about 100 for residual clays. Shales typically have intermediate values of about 70-75, indicating that weathering did not proceed to the stage where alkali and alkaline earth elements were substantially removed from the clay minerals (Nesbitt and Young, 1982). The Yanbian sandstones have CIA values ranging broadly from 49 to 73 and the mudstones from 57 to 84 (Table 4 and Fig. 9). In turbidites, physical sorting during transport and deposition would yield mudstone with high concentration of fine-grained, aluminous clay minerals of high-CIA value (e.g., kaolinite, gibbsite) derived from the upper parts of weathering profiles, and sandstone relatively enriched in coarse-grained low-CIA residue (e.g., quartz, vestigial feldspars) derived from the lower parts of weathering profiles (Nesbitt et al., 1996). The CIA values of mudstones, therefore, will give a better

understanding of the intensity of weathering in the source. Most mudstones have CIA values ranging from 65 to 77, reflecting only moderate source weathering. However, 6 mudstone samples in the Xiaoping Formation and 1 sample from the Zagu Formation having much higher CIA values in the range of 79-84 than typical shales of 70-75. If these values were corrected for K metasomatism (Fedo et al., 1995), their CIA values would be even greater than 90 (Fig. 9), indicative of severe weathering in the source. One possible explanation for the higher CIA values in the few samples from the Xiaoping and Zagu Formations may indicate a contribution of a greater proportion of distal high-CIA detritus from older cratonic source, which is consistent with our detrital zircon data.

The A-CN-K (Al_2O_3-CaO*+Na_2O-K_2O) triangular plot can also be used to constrain the initial compositions of the source rocks (Fedo et al., 1995). The sandstones and mudstones from the Yanbian Group form a linear trend, which is generally subparallel to the A-CN join, but is slightly below the predicted weathering trend, especially for the fine-grained mudstones (Fig. 9). This probably indicates that the mudstones were more profoundly affected by illitization. Their weathering trends suggest a provenance of tonalitic or granodioritic rocks for the Yanbian sediments.

Differential weathering at the source and subsequent diagenesis/metamorphism tend to mobilize and change the relative abundance of large-ion lithophile elements (Nesbitt et al., 1980). However, the Yanbian sandstones and mudstones commonly show linear correlation in the elemental plots of K vs. Rb, K vs. Ba, Ce vs. Sm and U vs. Th (Fig. 10), indicating that

these elements were probably not changed significantly. Moreover, because the sandstones studied here are relatively uniform in grain size, we believe that the grain-size effect is not important.

6.3. Tectonic setting of the Yanbian Group

The pillow basalts and marine sedimentary rocks of the Yanbian Group, and the spatially associated Gaojiacun and Lengshuiqing mafic intrusions, were previously regarded as the Yanbian ophiolite (Sun and Vuagnat, 1992). However, recent studies suggest that the mafic plutons postdate the Yanbian volcano-sedimentary sequence, arguing against an ophiolite model (Zhou et al., 2006a). Based on the geochemistry of the basaltic lavas, the Yanbian Group has been reinterpreted as a back-arc basin sequence (Du et al., 2005; Li X.H. et al., 2006; Sun et al., 2007), but evidence from the sedimentary sequence was not available. Our new geochronological, petrographical and geochemical data thus provide new constraints on a back-arc basin scenario.

The Yanbian Group was deposited at ~870 Ma and derived from a proximal magmatic arc with ages generally between 900 and 920 Ma (Figs. 5 and 6). The presence of almost contemporaneous volcanic arc magmatism indicates an active continental margin setting (DeGraaf-Surpless et al., 2002), in contrast to a passive continental margin where sediments are commonly derived from weathering of older continental crust (Goodge et al., 2002). The immature volcaniclastic graywackes, turbidites of the Yanbian Group are also consistent with an active margin setting (Crook, 1974; Pettijohn et al., 1987), where such rocks are commonly associated with pillow lavas or ‘greenstones’ (Pettijohn et al.,

415 1987 and references therein) and are commonly observed in modern back-arc
416 basins.

417 The sandstones from the Yanbian Group have about 15% modal quartz with
418 mostly 60-73 wt% SiO_2 and K_2O/Na_2O ratios <1, and are quartz-intermediate,
419 indicating a mixed provenance and depositional setting typical of an active
420 continental margin (Crook, 1974). Roser and Korsch (1986) examined the
421 K_2O/Na_2O-SiO_2 systematics of sandstone-mudstone suites from passive
422 continental margins (PM), active continental margins (ACM) and oceanic island
423 arcs (ARC), and found that the chemistry of the fine-grained members, and the
424 coupled sand-mud trends, were more useful indicators of tectonic setting than
425 the sandstones alone. Sandstones from the Yanbian Group plot exclusively in
426 the ARC and ACM fields, whereas most mudstones plot in the ACM field (Fig.
427 11). The coupled sand-mud trends (chain-dashed tie lines in Fig. 11) show one
428 trend parallel to the field boundaries and the other perpendicular to the first,
429 indicating a back-arc basin setting (Roser and Korsch, 1986). Using Bhatia's
430 (1983) scheme, the majority of samples from the Yanbian Group plot in the
431 oceanic island arc (OIA) to continental island arc (CIA) fields (Fig. 12). The
432 observed scatter of some points is probably due to a combination of sandstone
433 maturity and interelement variation.

434 The trace-element geochemistry of fine-grained clastic sediments has also
435 been widely used to determine tectonic setting (Bhatia and Crook, 1986; Floyd et
436 al., 1991). On the La-Th-Sc and Th-Sc-Zr/10 ternary plots (Fig. 13), most of the
437 Yanbian Group sandstones also fall within the OIA and CIA fields. The elemental

compositions of different greywackes can be most easily compared by utilizing upper continental crust-normalized, multi-element patterns. As shown in Figure 8a, the Yanbian rocks have pronounced negative Nb-Ta anomalies, clearly indicative of subduction-related magmatic rock source (Floyd et al., 1991). For further comparison, the data were also normalized to the standard tectonic setting values and the results show that the Yanbian rocks are mostly affiliated with a continental arc+active margin (Fig. 14).

REE patterns of clastic rocks are mainly controlled by provenance (Taylor and McLennan, 1985; McLennan, 1989) and are believed to be faithfully preserved in flysch deposited by turbidity currents and mass-flow processes (Hiscott and Gill, 1992). The Yanbian rocks have REE elements and ratios similar to those of continental arc settings (Table 5), in good agreement with the proposed back-arc basin scenario.

6.4. Provenance of the Yanbian Group

Petrographic, geochronological and geochemical evidence not only indicates that rocks of the Yanbian Group rocks were mainly derived from a magmatic arc, but also provides important constraints for the nature of this arc, which was not preserved in the modern exposures.

High feldspar contents (generally >30%) of the Yanbian sandstones indicates derivation directly from crystalline rocks (Boggs, 2001), because feldspars are chemically and physically unstable and thus less likely to survive recycling than a mineral like quartz. Presence of other unstable minerals such as magnetite, pyroxene and amphibole also support this view. The poorly sorted and immature

461 nature of the Yanbian greywackes, and their deposition in a back-arc basin,
462 further points to a proximal arc source with short transport distance and little or
463 no reworking.

464 The source area for the Yanbian Group sediments was an undissected to
465 transitional volcanic arc, in which only minor plutonic rocks were exposed. This
466 interpretation is supported by the abundance of volcanic rock fragments in the
467 sediments, the dominance of plagioclase over K-feldspar and the presence of
468 only minor quartz (Fig. 5 a, b and c). It is also consistent with the negative Zr-Hf
469 anomalies of these rocks relative to the average continent upper crust, reflecting
470 a lack of zircon input from silicic plutonic rocks (Fig. 8a).

471 The abundant intermediate and felsic volcanic rock fragments and sparse
472 mafic rock clasts in the Yanbian sandstones provide the most direct evidence for
473 the composition of these volcanic rocks (Table 2). Moreover, the trace element
474 characteristics of the sediments provide additional constraints on the nature of
475 the provenance. Because silicic rocks are significantly richer in La and Th, and
476 poorer in Sc, Cr, and Co than mafic rocks (Cullers, 1994 and references therein),
477 La/Sc, Th/Sc, Th/Co, and Cr/Th ratios are good indicators of the source rocks.
478 The Yanbian rocks have relatively low and constant La/Th ratios with an average
479 of 1.5 but more variable Co/Th ratios (Fig. 15a), suggesting mixing of felsic and
480 intermediate components. Similarly, a plot of La/Th against Hf also points to
481 mixed sources (Fig. 15b). In addition, the Yanbian rocks mostly have Cr/Th ratios
482 of 5-25 (Table 4), clearly indicative of silicic-intermediate source rocks (Cullers,
483 1994). The low Cr (mostly<150 ppm) and Ni (<80 ppm) of the Yanbian rocks and

484 slight V-Cr-Ni anomalies (Fig. 8a) is also consistent with minor mafic-ultramafic
485 input from the source area (Floyd et al., 1991; Garver et al., 1996).

486 **6.5. An integrated tectonic model**

487 Although the tectonic affinity of the western margin of the Yangtze Block
488 during the Neoproterozoic has been a matter of debate, it has been confirmed
489 that a number of plutons in this region were subduction-related. In the Yanbian
490 area, these intrusions include the ~860-Ma Guandaoshan dioritic pluton (Sun and
491 Zhou, 2008), the ~810-Ma Gaojiacun and Lengshuiqing mafic intrusions (Zhou et
492 al., 2006a) and the ~740-Ma Dadukou gabbroic pluton (Zhao and Zhou, 2007).
493 Determination of the age and tectonic provenance of the Yanbian Group has
494 significant implications for the regional tectonic evolution during Neoproterozoic
495 time. This study provides a window into a Neoproterozoic magmatic arc on the
496 western margin of the Yangtze Block, and reveals the presence of a ~900-920
497 Ma felsic and intermediate volcanic arc in this region, although such a feature
498 has not yet been widely identified directly.

499 Available data allow us to propose a model involving the development of a
500 volcanic arc and formation of the Yanbian back-arc basin and the closely
501 associated subduction-related plutons in this region (Fig. 16). Subduction-related
502 volcanic rocks of mainly felsic and intermediate composition were produced at ca.
503 900-920 Ma owing to the eastward subduction of oceanic lithosphere along the
504 western margin of the Yangtze Block (Fig. 16a). Rifting occurred as a
505 consequence of diapiric upwelling of metasomatized mantle to create the
506 Yanbian back-arc basin and generate the basaltic lavas of the Fangtian

Formation (Fig. 16b). According to Crawford et al. (1981), arc volcanism appears to cease around the time that back-arc opening commences. This basin was built on the ~900-920 Ma volcanic arc sequence which provided materials to fill the adjacent Yanbian basin above the lavas, to form the Yumen, Xiaoping and Zagu Formations (Fig. 16b). With continued erosion, the relief of the source region decreased and hence slowed down the supply of materials for the basin, resulting in biochemical deposition of the carbonates in the Zagu Formation (Fig. 16b). Subduction-related magmatism was then re-activated to generate the subduction-related plutons (Fig. 16c). The oldest pluton is the ~860-Ma Guandaoshan dioritic pluton, followed by the ~810-Ma Gaojiacun and Lengshuiqing and the youngest ~740 Ma Dadukou gabbroic plutons (Fig. 16c). This period of igneous activity suggests continuous subduction along the western margin of the Yangtze Block between about 920 and 740 Ma. This arc was thus active for at least ~180 million years. Eventually, this region probably became a passive margin and the Sinian Lieguliu Formation was unconformably deposited over the Yanbian Group, marking the termination of the arc setting (Fig. 16d).

The subduction-related environment may extend along the entire western margin of the Yangtze Block. Similar sequences also occurred in the northwest margin including the Bikou Group (Fig. 1), which has detrital zircon ages ranging from 700 to 850 Ma and has been interpreted as fore-arc basin deposits (Yan Q.R. et al., 2004; Druschke et al., 2006). Thus our proposed model implies that the western margin of the Yangtze Block was a major continental arc during the Neoproterozoic, and thus probably flanked the Rodinia supercontinent.

7. Conclusions

The Yanbian Group is a typical deep marine, volcaniclastic succession deposited in a back-arc basin. Detrital zircon dating and geological constraints indicate that the Yanbian Group was formed at ~870 Ma. The immature nature of the Yanbian sandstones indicates a proximal arc source with ages of ~900-920 Ma. The Yanbian Group and spatially associated subduction-related plutons in the Yanbian region make up a typical arc assemblage, being part of a major continental arc along the western margin of the Yangtze Block for at least 180 m.y. (920-740 Ma). We infer that the Yangtze Block probably flanked the Rodinia supercontinent.

Acknowledgments

This work was financially supported by the National Science Foundation of China (NSFC grant 40672037/D0204), Chinese Education Ministry 111 project (No. B07011) and the International Innovation Partnership Program of CAS & SAFEA. We thank Xiao Fu, Jianfeng Gao, Shijian Bi and Jiangman Zhang for help with the analyses. Paul Robinson is thanked for reading this manuscript. We appreciate thorough reviews by Barry P. Roser, Keith A.W. Crook and Pater A. Cawood, whose insights led to substantial improvements in this paper.

References

Bhatia, M.R., 1983. Plate tectonics and geochemical composition of sandstones. J. Geol. 91, 611-627.

Bhatia, M.R., 1985. Rare earth element geochemistry of Australian Paleozoic graywackes and mudstones: Provenance and tectonic control. Sediment. Geol. 45, 97-113.

Bhatia, M.R., Crook, K.A.W., 1986. Trace element characteristics of graywackes and tectonic setting discrimination of sedimentary basins. Contrib. Mineral. Petrol. 92, 181-193.

BGMRSP (Bureau of Geology and Mineral Resources of the Sichuan Province), 1972. Regional Geological Survey of People's Republic of China, the Yanbian Sheet (G-47-XII; geological part), scale 1:200,000 (in Chinese).

Boggs, S., 2001. Principles of sedimentology and stratigraphy (Third editon). New Jersey, Prentice-Hall, 726p.

Chen, Z.L., Chen, S.Y., 1987. On the tectonic evolution of the west margin of the Yangzi block. Chongqing, China, Chongqing Publishing House, 172p. (in Chinese).

Cope, T., Ritts, B.D., Darby, B.J., Fildani, A., Graham, S.A., 2005. Late Paleozoic Sedimentation on the Northern Margin of the North China Block: Implications for Regional Tectonics and Climate Change. Int. Geol. Rev. 47, 270-296.

Crawford, A.J., Beccaluva, L., Serri, G., 1981. Tectono-magmatic evolution of the west Philippine-Mariana region and the origin of boninites. Earth Planet. Sci. Lett. 54, 346-356.

573 Crook, K.A.W., 1974. Lithogenesis and geotectonics: The significance of
574 compositional variations in flysch arenites (graywackes). In: Dott, R.H.,
575 Shaver, R.H. (Eds.), Modern and Ancient Geosynclinal Sedimentation. SEPM
576 Spec. Publ. 19, pp. 304-310.
577 Cullers, R.L., 1994. The controls on the major and trace element variation of
578 shales, siltstones, and sandstones of Pennsylvanian-Permian age from
579 uplifted continental blocks in Colorado to platform sediment in Kansas, USA.
580 Geochim. Cosmochim. Acta 58, 4955-4972.
581 DeGraaff-Surpless, K., Graham, S.A., Wooden, J.L., McWilliams, M.O., 2002.
582 Detrital zircon provenance analysis of the Great Valley Group, California:
583 Evolution of an arc-forearc system. Geol. Soc. Am. Bull. 114, 1564-1580.
584 Dickinson, W.R., 1970. Interpreting detrital modes of graywacke and arkose. J.
585 Sediment. Petrol. 40, 695-707.
586 Dickinson, W.R., 1985. Interpreting provenance relations from detrital modes of
587 sandstones. In: Zuffa, G.G. (Eds.), Provenance of arenites. NATO ASI Series
588 C: Mathematical and Physical Sciences 48, D. Reidel Publishing Company,
589 pp. 333-361.
590 Dickinson, W.R., Gehrels, G.E., 2000. Sandstone petrofacies of detrital zircon
591 samples from Paleozoic and Triassic strata in suspect terranes of northern
592 Nevada and California. In: Soreghan, M.J., Gehrels, G.E. (Eds.), Paleozoic
593 and Triassic paleogeography and tectonics of western Nevada and northern
594 California. Boulder, Colorado, Geol. Soc. Am. Special Paper 347, pp. 151-171.

595 Druschke, P., Hanson, A.D., Yan, Q., Wang, Z., Wang, T., 2006. Stratigraphic
596 and U-Pb SHRIMP detrital zircon evidence for a Neoproterozoic continental
597 arc, Central China: Rodinia implications. J. Geol. 114, 627-636.
598 Du, L.L., Geng, Y.S., Yang, C.H., Wang, X.S., Ren, L.D., Zhou, X.W., Shi, Y.Y.,
599 Yang, Z.S., 2005. Geochemistry and SHRIMP U-Pb zircon chronology of
600 basalts from the Yanbian group in the western Yangtze Block. Acta Geologica
601 Sinica 76, 805-813 (in Chinese with English abstract).
602 Eisbacher, G.H., 1985. Late Proterozoic rifting, glacial sedimentation, and
603 sedimentary cycles in the light of Windermere deposition, western Canada.
604 Palaeogeogr. Palaeoclimatol. Palaeoecol. 51, 231-254.
605 Fedo, C.M., Nesbitt, H.W., Young, G.M., 1995. Unraveling the effects of
606 potassium metasomatism in sedimentary rocks and paleosols, with
607 implications for weathering conditions and provenance. Geology 23, 921-924.
608 Floyd, P.A., Leveridge, B.E., 1987. Tectonic environment of the Devonian
609 Gramscatho Basin, South Cornwall: Framework mode and geochemical
610 evidence from turbiditic sandstones. J. Geol. Soc. London 144, 531-542.
611 Floyd, P.A., Shail, R., Leveridge. B.E., Franke, W., 1991. Geochemistry and
612 provenance of Rhenohercynian synorogenic sandstones: implications for
613 tectonic environment discrimination. In: Morton, A.C., Todd, S.P., Haughton,
614 P.D.W. (Eds.), Developments in sedimentary provenance studies. Geol. Soc.
615 London, Spec. Publ. 57, 173-188.
616 Garver, J.I., Royce, P.R., Smick, T.A., 1996. Chromium and nickel in shale of the
617 Taconic Foreland: A case study for the provenance of fine-grained sediments

618 with an ultramafic source. J. Sediment. Res. 66, 100-106.
619 Goodge, J.W., Myrow, P., Williams, I.S., Bowring, S.A., 2002. Age and
620 provenance of the Beardmore Group, Antarctica: constraints on Rodinia
621 supercontinent breakup. J. Geol. 110, 393-406.
622 Gu, X.X., Liu, J.M., Zheng, M.H., Tang, J.X., Qi, L., 2002. Provenance and
623 tectonic setting of the Proterozoic turbidites in Hunan, South China:
624 geochemical evidence. J. Sediment. Res. 72, 393-407.
625 Hiscott, R.N., Gill, J.B., 1992. Major and trace element geochemistry of
626 Oligocene to Quaternary volcaniclastic sands and sandstones from the Izu-
627 Bonin arc. In: Taylor, B., Fujioka, K., et al. (Eds.), Proceedings of the Ocean
628 Drilling Program, Scientific Results 126. College Station, TX: Ocean Drilling
629 Program, pp. 467-485.
630 Ingersoll, R.V., Fullard, T.F., Ford, R.L., Grimm, J.P., Pickle, J.D., Sares, S.W.,
631 1984. The effect of grain size on detrital modes; a test of the Gazzi-Dickinson
632 point-counting method: J. Sediment. Petrol. 54, 103-116.
633 Jackson, S.E., Pearson, N.J., Griffin, W.L., Belousova, E.A., 2004. The
634 application of laser ablation-inductively coupled plasma-mass spectrometry
635 (LA-ICP-MS) to in-situ U-Pb zircon geochronology. Chem. Geol. 211, 331-335.
636 Li, F.H., Tan, J.M., Shen, Y.L., Yu, F.X., Zhou, G.F., Pan, X.N., Li, X.Z., 1988.
637 The pre-Sinian in the Kangdian area: Chongqing, China, Chongqing
638 Publishing House, 396p. (in Chinese).
639 Li, X.H., Li, Z.X., Zhou, H.W., Liu, Y., Liang, X.R., Li, W.X., 2003. SHRIMP U-Pb
640 zircon age, geochemistry and Nd isotope of the Guandaoshan pluton in SW

641 Sichuan: Petrogenesis and tectonic significance. Sci. China Ser. D (Supp.)
642 46, 73-83.
643 Li X.H., Li, Z.X., Sinclair, J.A., Li, W.X., Carter, G., 2006. Revisiting the “Yanbian
644 Terrane”: implications for Neoproterozoic tectonic evolution of the western
645 Yangtze Block, South China. Precambrian Res. 151, 14-30.
646 Li, Z.X., Li, X.H., Kinny, P., Wang, J., 1999. The breakup of Rodinia: did it start
647 with a mantle plume beneath South China. Earth Planet. Sci. Lett. 173, 171-
648 181.
649 Li, Z.X., Li, X.H., Kinny, P.D., Wang, J., Zhang, S., Zhou, H., 2003.
650 Geochronology of Neoproterozoic syn-rift magmatism in the Yangtze Craton,
651 South China and correlations with other continents: evidence for a mantle
652 superplume that broke up Rodinia. Precambrian Res. 122, 85-109.
653 Ludwig, K. R., 1999. Isoplot/Ex version 2.06: A geochronological tool kit for
654 Microsoft Excel. Berkeley Geochronology Center, Spec. Publ. 1a.
655 Maas, R., McCulloch, M.T., 1991. The provenance of Archean clastic
656 metasediments in the Narryer Geniss Complex, Western Australia: trace
657 element geochemistry, Nd isotopes, and U-Pb ages for detrital zircons.
658 Geochim. Cosmochim. Acta 55, 1915-1932.
659 Marsaglia, K.M., Ingersoll, R.V., 1992. Compositional trends in arc-related, deep-
660 marine sand and sandstone: a reassessment of magmatic-arc provenance.
661 Geol. Soc. Am. Bull. 104, 1637-1649.
662 McLennan, S.M., 1989. Rare earth elements in sedimentary rocks: Influence of
663 provenance and sedimentary processes. Rev. Mineral. Geochem. 21, 169-200.

McLennan, S.M., 1993. Weathering and Global Denudation. J. Geol. 101, 295-303.

McLennan, S.M., Taylor, S.R., Eriksson, K.A., 1983. Geochemistry of Archean shales from the Pilbara Supergroup, Western Australia. Geochim. Cosmochim. Acta 47, 1211-1222.

McLennan, S.M., Taylor, S.R., McCulloch, M.T., Maynard, J.B., 1990. Geochemical and Nd-Sr isotopic composition of deep-sea turbidites: Crustal evolution and plate tectonic associations. Geochim. Cosmochim. Acta 54, 2015-2050.

McLennan, S.M., Hemming, S.R., Taylor, S.R., Eriksson, K.A., 1995. Early Proterozoic crustal evolution: Geochemical and Nd-Pb isotopic evidence from metasedimentary rocks, southwestern North America. Geochim. Cosmochim. Acta 59, 1153-1177.

Nesbitt, H.W., Markovics, G., Price, R.C., 1980. Chemical processes affecting alkalies and alkaline earths during continental weathering: Geochim. Cosmochim. Acta 44, 1659-1666.

Nesbitt, H.W., Young, G.M., 1982. Early Proterozoic climates and plate motions inferred from major element chemistry of lutites. Nature 299, 715-717.

Nesbitt, H.W., Young, G.M., 1996. Petrogenesis of sediments in the absence of chemical weathering: effects of abrasion and sorting on bulk composition and mineralogy. Sedimentology 43, 341-358.

685 Nesbitt, H.W., Young, G.M., McLennan, S.M., and Keays, R.R., 1996. Effects of
686 chemical weathering and sorting on the petrogenesis of siliciclastic sediments,
687 with implications for provenance studies. J. Geol. 104, 525-542.
688 Pettijohn, F.J., Potter, P.E., Siever, R., 1987. Sand and sandstone (Second
689 editon), Springer-Verkag, 553p.
690 Pan, X.N., Zhao, J.X., Zhan, X.Y., Zhen, H.X., Yan, Z.H., Zhou, G.F., Tao, D.L.,
691 1987. Tectonics and rifting in the Kangdian area: Chongqing, China,
692 Chongqing Publishing House, 295p. (in Chinese).
693 Qi, L., Hu, J., Gregoire, D.C., 2000. Determination of trace elements in granites
694 by inductively coupled plasma-mass spectrometry. Talanta 51, 507-513.
695 Roser, B.P., Korsch, R.J., 1986. Determination of tectonic setting of sandstone-
696 mudstone suites using SiO_2 content and K_2O/Na_2O ratio. J. Geol. 94, 635-650.
697 Roser, B.P., Korsch, R.J., 1988. Provenance signatures of sandstone-mudstone
698 suites determined using discriminant function analysis of major-element data.
699 Chem. Geol. 67, 119-139.
700 SBGMR (Sichuan Bureau of Geology and Mineral Resources). 1991. Regional
701 Geology of Sichuan Province. Beijing, China, Geological Memoirs 23.
702 Geological Publishing House (in Chinese with English summary).
703 She, Z.B., Ma, C.Q., Mason, R., Li, J.W., Wang, G.C., Lei, Y.H., 2006.
704 Provenance of the Triassic Songpan-Ganzi flysch, west China. Chem. Geol.
705 231, 159-175.
706 Sun, C.M., Vuagnat, M., 1992. Proterozoic ophiolites from Yanbian and Shimian
707 (Sichuan Province, China): Petrography, geochemistry, petrogenesis, and

geotectonic environment. Schweiz. Mineral. Petrograph. Mitt. 72, 389-413.

Sun, W.H., Zhou, M.-F., Zhao J.H., 2007. Geochemistry and tectionic significance of basaltic lavas in the Neoproterozoic Yanbian Group (Southern Sichuan Province, SW China). Int. Geol. Rev. 49, 554-571.

Sun, W.H., Zhou, M.-F., 2008. The ~860-Ma, Cordilleran-type Guandaoshan dioritic pluton in the Yangtze Block, SW China: Implications for the origin of Neoproterozoic magmatism. J. Geol. 116, 238-253.

Taylor, S.R., McLennan, S.M., 1985. The Continental Crust; Its Composition and Evolution. London, Blackwell, 312 p.

Taylor, S.R., McLennan, S.M., 1995. The Geochemical Evolution of the Continental Crust. Rev. Geophys. 33, 241-265.

Yan, D.P., Zhou, M.-F., Song, H. L., Wang, X.W., Malpas, J., 2003. Origin and tectonic significance of a Mesozoic multi-layer over-thrust within the Yangtze block (South China). Tectonophysics 361, 239-254.

Yan, Q.R., Hanson, A.D., Wang, Z.Q., Druschke, P.A., Yan, Z., Wang, T., Liu, D.Y., Song, B., Pan, P., Zhou, H., Jiang, C.F., 2004. Late Proterozoic subduction and rifting on the northern margin of the Yangtze Plate, China: implications for Rodinia reconstruction. Int. Geol. Rev. 46, 817-832.

Yuan, H.L., Gao, S., Liu, X.M., Li, H.M., Gunther, D.,Wu, F.Y., 2004. Accurate U-Pb age and trace element determinations of zircon by laser ablation-inductively coupled plasma-mass spectrometry. Geostandard. Geoanal. Res. 28, 353-370.

730 Zhao, J.H., Zhou, M.-F., 2007. Geochemistry of Neoproterozoic mafic intrusions
731 in the Panzhihua district (Sichuan Province, SW China): implications for
732 subduction-related metasomatism in the upper mantle. Precambrian Res. 152,
733 27-47.
734 Zhou, M.-F., Kennedy, A.K., Sun, M., Malpas, J., Lesher, C.M., 2002a. Late
735 Proterozoic arc-related mafic intrusions along the northern margin of South
736 China: implications for the accretion of Rodinia. J. Geol. 110, 611-618.
737 Zhou, M.-F., Yan, D.P., Kennedy, A.K., Li, Y.Q., Ding, J., 2002b. SHRIMP U-Pb
738 zircon geochronological and geochemical evidence for Late Proterozoic arc-
739 magmatism along the western margin of the Yangtze Block, South China.
740 Earth Planet. Sci. Lett. 196, 51-67.
741 Zhou, M.-F., Ma, Y.X., Yan, D.P., Xia, X.P., Zhao, J.H., Sun, M., 2006a. The
742 Yanbian Terrane (Southern Sichuan Province, SW China): A Late Proterozoic
743 arc assemblage in the western margin of the Yangtze Block. Precambrian
744 Res. 144, 19-38.
745 Zhou, M.-F., Yan, D.P., Wang, C.L., Qi, L., Kennedy, A., 2006b. Subduction-
746 related origin of the 750 Ma Xuelongbao adakitic complex (Sichuan Province,
747 China): Implications for the tectonic setting of the giant Neoproterozoic
748 magmatic event in South China. Earth Planet. Sci. Lett. 248, 286-300.
749 Zhou, D., Graham, S.A., 1996. The Songpan-Ganzi complex of the West Qinling
750 Shan as a Triassic remnant ocean basin. In: Yin, A., Harrison, T.M. (Eds.),
751 The Tectonic Evolution of Asia. New York, Cambridge University Press, pp.
752 281-299.

753 **Figure captions**

754 Fig. 1. Simplified geological map of the Yanbian region, Sichuan Province, SW
755 China (after BGMRSP, 1972). The insert map showing the tectonic units of South
756 China and general distribution of Neoproterozoic rocks in the margins of the
757 Yangtze Block.

758 Fig. 2. Stratigraphy of the Yanbian Group based on a measured cross section
759 (BGMRSP, 1972) and our field mapping. Stars indicate samples for detrital zircon
760 analysis. The sandstone beds shown in the column are not strictly to scale
761 because they are typically thin layers interbedded with slate.

762 Fig. 3. (a) Contact between the clastic Yumen Formation and the volcanic
763 Fangtian Formation. (b) A scour structure in the Xiaoping Formation. (c) Slumped
764 siltstone in the Xiaoping Formation. (d) Well-exposed Bouma sequences in the
765 Xiaoping Formation.

766 Fig. 4. (a) Photomicrographs of grain types and features in the Yanbian
767 sandstones. (a) General view showing sub-angular monocrystalline quartz (Q)
768 (T3-3). (b) Sub-rounded plagioclase feldspar (Pl) and K-feldspar (Kf) grains (T3-
769 1-2). (c) A metamorphic grain (Lm) and volcanic grains (Lv) with felsitic and
770 microlitic texture (B11). (d) Siltstone fragments (Ls) (B11). (e) A typical volcanic
771 rock fragment with microlitic texture that we interpret to be derived from
772 intermediate composition (B9). (f) A clinopyroxene grain (Cpx) (F6). All samples
773 are in cross-polarized light. Scale bar in each photograph is 0.3 mm.

774 Fig. 5. Ternary plots of sandstone point count data for the Yanbian Group. (a)
775 QFL plot. (b) QmFLt plot. (c) QLvmLsm plot. (d) QmPK plot. Provenance fields

776 are from Dickinson (1985). The large open triangles represent arithmetic means
777 of data and polygonal box represents one standard deviation.
778 Fig. 6. Detrital zircon data for the sandstone samples of the Yanbian Group. (a)
779 Neoproterozoic (860-1000 Ma) detrital zircon age histogram and cumulative
780 probability plot, showing number of grains analyzed and percentage of
781 Neoproterozoic ages as a fraction of total discordant and concordant ages. (b)
782 Histogram and cumulative probability plot of total concordant detrital zircon ages.
783 Total number of concordant ages for each sample is shown, with number of
784 analyses (concordant plus discordant ages) shown in parenthesis.
785 Fig. 7. (a) Geochemical classification of sandstones from the Yanbian Group
786 (Pettijohn et al., 1987).
787 Fig. 8. (a) Upper crust-normalized, multi-element diagrams for the Yanbian
788 samples; (b) Chondrite-normalized REE patterns of the Yanbian sandstones and
789 mudstones. Post-Archean average Australian shale (PAAS) is also plotted as a
790 heavy dashed line "+" for comparison. Values are from Taylor and McLennan
791 (1985).
792 Fig. 9. CIA ternary diagram, A-CN-K=Al_2O_3 -CaO*+Na_2O-K_2O, after Nesbitt and
793 Young (1982) showing Yanbian sandstones and mudstones as well as average
794 compositions of tonalite and granodiorite (from Fedo et al., 1995). Approximate
795 correction for carbonate content was made by assuming reasonable Ca/Na ratios
796 in silicate material (McLennan, 1993). After correcting phosphate using P_2O_5, if
797 the remaining mole fraction of CaO ≤Na_2O, then this value of CaO is adopted; if
798 CaO >Na_2O, CaO* is assumed to be equivalent to Na_2O. Due to relatively low

carbonate contents in most samples, however, the calculated proportions are thus very close to actual values.

Fig. 10. Plots of K vs. Rb, K vs. Ba, Ce vs. Sm, and U vs. Th, showing linear correlations.

Fig 11. K_2O/Na_2O-SiO_2 plot for the Yanbian rocks. PM = passive margin; ACM = active continental margin; ARC = oceanic island arc. (after Roser and Korsch, 1986).

Fig.12. Tectonic discrimination diagrams for the Yanbian Group sandstones: PM = passive margin; ACM = active continental margin; CIA = continental island arc; OIA =oceanic island arc (after Bhatia, 1983).

Fig. 13. Triangular trace element plots for Yanbian sandstones (after Bhatia and Crook, 1986). Abbreviations as in Fig. 11.

Fig. 14. Normalized multi-element diagrams for the Yanbian sandstones. CAAM = continental arc+active margin; OIA = oceanic island arc; PM = passive margin; OWP = oceanic within-plate. Normalizing values are from Floyd et al. (1991).

Fig. 15. Source rock discrimination diagrams for the Yanbian rocks; (a) Co/Th vs. La/Sc diagram (after Gu et al., 2002), showing derivation from mixed felsic-basic volcanic source, (b) La/Th vs. Hf diagram (after Floyd and Leveridge, 1987), indicating mixed of felsic/basic source rocks.

Fig. 16. Model for the development of the Yanbian Group and the spatially associated subduction-related intrusions in the Yanbian region, SW China.

Provenance and tectonic setting of the Neoproterozoic Yanbian Group, western Yangtze Block (SW China)

Wei-Hua Sun [a, *], Mei-Fu Zhou [a], Dan-Ping Yan [b], Jian-Wei Li [c] and Yuxiao Ma [d]

[a] Department of Earth Sciences, University of Hong Kong, Hong Kong, China

[b] School of Earth Sciences and Resources, China University of Geosciences, Beijing 100083, China

[c] State Key Laboratory of Geological Processes and Mineral Resources, and Faculty of Earth Resources, China University of Geosciences, Wuhan 430074, China

[d] Department of Geochemistry, Chengdu University of Science and Technology, Chengdu, China

* Corresponding author. Tel.: +852 2859 8913; Fax: +852 2517 6912.

E-mail: weihua@hkusua.hku.hk

Abstract

Tectonic evolution of the Yangtze Block of South China during Neoproterozoic time has been a major focus of debate and is important in the reconstruction of the Rodinian supercontinent. The Yanbian Group in the western margin of the Yangtze Block is a well-preserved Neoproterozoic volcanic-sedimentary sequence and provides a rare opportunity to examine the provenance and tectonic setting. It consists of a lower part composed of ~1500 m thick basaltic lavas and an upper part with ~3500 m thick flysch deposits. The flysch sequence contains typical deep marine turbidites consisting mainly of fine-grained volcaniclastic sandstones and mudstones, indicating a submarine fan depositional system. Detrital zircon dating yields ages ranging from ca. 865 Ma to

1000 Ma with two peaks at ca. 900 Ma and 920 Ma, respectively. The Yanbian Group is intruded by the ~860- Ma Guandaoshan dioritic pluton, constraining its depositional age at ca. 870 Ma. The sandstones contain abundant feldspar and lithic fragments with minor amounts of quartz and have an average composition of $Q_{16}F_{35}L_{49}$, suggesting a proximal source and an undissected to transitional arc setting. The lithic fragments in the sandstones point to andesitic and felsic volcanic rock sources. The sandstones and mudstones have intermediate SiO_2/Al_2O_3 (typically 3-6), high Fe_2O_3+MgO contents (5-12 wt%), and moderate to high K_2O/Na_2O ratios (generally 0.1-1 and 1-10 for sandstones and mudstones, respectively). In comparison with average upper continental crust, they show strong Nb-Ta anomalies, slight depletion of Zr-Hf, La and Th, but moderate enrichment of V, Cr, Ni, and Sc. These rocks show LREE enrichment (La/Yb_N=5.3-7.4) with flat HREE, and pronounced negative Eu anomalies (Eu/Eu*=0.6-0.74) in chondrite-normalized REE patterns, similar to post-Archean shales. Geochemical data for these rocks suggest an arc setting and intermediate-felsic volcanic source, consistent with a back-arc basin scenario for the basaltic lavas in the lower Yanbian Group. Together with regional geological evidence, the turbidites of the Yanbian Group strongly support a model in which the western margin of the Yangtze Block was a major magmatic arc, active probably from ~920 Ma to 740 Ma, a period of more than 180 million years.

Key words: turbidite, detrital zircon dating, geochemistry, provenance, Yanbian Group, Yangtze Block

1. Introduction

Siliciclastic rocks are useful for investigating provenance and tectonic setting of sedimentary basins (Dickinson, 1970, 1985; Bhatia, 1983, 1985; Roser and Korsch, 1986, 1988; Floyd and Leveridge, 1987). Provenance regions, especially those at destructive plate margins, are rarely well preserved because of subsequent erosion and destruction. In such circumstances, studies of related sedimentary rocks have considerable potential for determining the source rocks and the history of ancient continental margins. A combination of traditional mineralogical (especially for sandstones) and geochemical methods and detrital zircon U-Pb analysis has greatly contributed to our understanding of the provenance, tectonic setting and tectonomagmatic evolution of sedimentary basins and their siliciclastic deposits (McLennan et al., 1990, 1995; Maas and McCulloch, 1991; Taylor and McLennan, 1995; Dickinson and Gehrels, 2000; DeGraaff-Surpless et al, 2002; Cope et al., 2005; She et al., 2006).

The tectonic evolution of the Yangtze Block of South China is of importance for the reconstruction of the supercontinent Rodinia and has been a matter of hot debate (Li Z.X. et al., 1999, 2003; Li X.H. et al., 2003, 2006; Zhou et al., 2002a, b, 2006a, b). Previous work has focused mainly on the Neoproterozoic igneous rocks, and studies of the associated sedimentary sequences are sparse. The Neoproterozoic Yanbian Group in the western margin of the Yangtze Block has been a subject of several recent studies (Du et al., 2005; Zhou et al., 2006a; Li X.H. et al., 2006; Sun et al., 2007), because it is not only one of the best-preserved volcano-sedimentary sequences in South China, but is spatially

associated with several contemporaneous intermediate to mafic plutons, making it ideal for investigating the tectonic affinities of the Yangtze Block. Previous studies on the volcanic rocks in the lower part of the Yanbian Group and the related intrusive rocks have interpreted the Yanbian Group as a relict ophiolite (Sun and Vuagnat, 1992) or a back-arc basin sequence (Du et al., 2005; Zhou et al., 2006a; Li X.H. et al., 2006, Sun et al., 2007). So far, there is no agreement about the depositional age of the Yanbian Group (Du et al., 2005; Zhou et al., 2006a; Li X.H. et al., 2006), causing additional ambiguity in its tectonic interpretation. In particular, no studies are available regarding the chemical composition and petrology of the sedimentary rocks, which are crucial to better understanding the source rocks and tectonic setting.

In this paper, we present petrographic, detrital zircon U-Pb geochronological and geochemical data for the upper siliciclastic rocks of the Yanbian Group, in an attempt to constrain the age of the sediments and to infer their provenance and tectonic setting. The results also provide insights into the tectonic evolution of the Yangtze Block during Neoproterozoic time.

2. Geological background

South China consists of the Yangtze Block in the northwest and the Cathaysia Block in the southeast (Fig. 1). The Yangtze Block is separated from the North China Craton by the Qinling-Dabie orogenic belt and is bounded to the west by the Songpan-Ganze Terrane of the Tibetan Plateau. The Songpan-Ganze Terrane is a prominent triangular region filled with Triassic deep-marine

95 flysch deposits (Zhou and Graham, 1996). The Yangtze Block comprises
96 metamorphic basement complexes and Neoproterozoic to Cenozoic cover
97 sequences (Yan D.P. et al., 2003). The basement complexes contain gneiss,
98 mica schist, amphibolite, marble and quartzite, whereas the cover sequences are
99 mainly composed of carbonate, clastic and volcanic rocks (SBGMR, 1991).

100 Along the western margin of the Yangtze Block, a ~1000-km-long, NS-
101 trending, Neoproterozoic igneous and metamorphic belt crops out from Kangding
102 in Sichuan Province to Yuanjiang in Yunnan Province (Fig. 1). This belt has been
103 recently interpreted as a major Neoproterozoic continental arc, named the
104 Hannan-Panxi arc, in which the igneous rocks have ages mostly ranging from
105 860 to 740 Ma (Zhou et al., 2002a, b, 2006a, b; Zhao and Zhou, 2007; Sun and
106 Zhou, 2008). The occurrence of this huge continental arc indicates an Andean-
107 type continental margin with oceanic crust being subducted eastward beneath
108 the western margin of the Yangtze Block during that time (Zhou et al., 2002b;
109 Sun and Zhou, 2008).

110 In the belt, the igneous plutons intrude high-grade (granitic gneisses and
111 amphibolite) and low-grade metamorphic rocks (Pan et al., 1987; Li F.H. et al.,
112 1988). The high-grade metamorphic rocks, including the Kangding and
113 Dahongshan complexes, were traditionally considered to be late Archean to
114 Paleoproterozoic crystalline basement; the low-grade metamorphic rocks, such
115 as the Kunyang, Huili, Yanbian and Bikou Groups, were interpreted to be
116 Mesoproterozoic and to constitute the folded basement in this region (Chen and
117 Chen, 1987).

The Yanbian Group is unconformably overlain by Sinian (latest Neoproterozoic) strata known as the Lieguliu Formation (Sun et al., 2007), which is composed of glacial deposits, comparable to those of similar age on other continents (Elsbacher, 1985). The Yanbian Group is intruded by a magmatic association that consists of the ~860-Ma Guandaoshan dioritic pluton (Li X.H. et al., 2003; Sun and Zhou, 2008), 810-820-Ma Tongde dioritic-gabbroic pluton (Li Z.X. et al., 2003) and ~810-Ma Gaojiacun and Lengshuiqing mafic plutons (Zhou et al., 2006a) (Fig. 1). These, together with the ~740 Ma Dadukou gabbroic intrusion south of Tongde Town (Zhao and Zhou, 2007), have been interpreted as part of the Hannan-Panxi arc along the western margin of the Yangtze Block (Sun and Zhou, 2008).

3. Stratigraphy and depositional environment

Cropping out over an area of approximately 500 km^2, the Yanbian Group is composed of two principal units: a lower volcanic sequence ca. 1500 m thick, known as the Fangtian Formation, and an upper flysch more than 5000 m thick, comprising the Yumen, Xiaoping and Zagu Formations (Fig. 2)

The Fangtian Formation is composed of massive basalt, pillow basalt and volcanic breccias with subordinate interbeds of chert, and pelitic and siliceous slate. It is conformably overlain by the ca.1700-m-thick Yumen Formation, which consists primarily of thin- to medium-bedded, dark-gray, carbonaceous and siliceous slates with interbeds of fine- to coarse-grained sandstone (Fig. 3a). Lenses of limestone are locally present. An ~5-cm-thick layer of black chert

141 marks the base of the Yumen Formation where it overlies the basaltic breccias of
142 the Fangtian Formation (Fig. 3a). The slates and sandstones have regular
143 parallel bedding, typical of distal turbidites. In this formation, turbidites generally
144 display T_{bce} of the Bouma sequences.

145 The ~2200-m-thick Xiaoping Formation comprises dark gray slates,
146 carbonaceous slates, fine- to coarse-grained sandstones and siltstones,
147 representing turbidites and associated mudstones. The basal and top parts of the
148 succession are dominated by sandstones in beds up to 1.5 m thick, suggesting
149 small-scale channel-fill deposits. The sandstone channels usually display an
150 eroded base and a concave-upward morphology, with the grain size fining
151 upward. Conglomerates are locally present as thin, discontinuous lag beds at
152 the base of the coarse sandstone layers. The sandstones have lenticular or flat
153 beds with thicknesses of 10-20 cm, but ranging from 2 to 50 cm. Sedimentary
154 structure, such as scours, slumps, and load and flame structure, are locally well
155 developed (Figs. 3b, c). Most sandstone beds are normally graded and follow the
156 Bouma sequence. Partial Bouma sequences are more common than complete
157 ones, with the T_{abc} sequence being the most common, followed in abundance by
158 T_{ae} (Fig. 3d). Thin limestone lenses and stromatolithic limestones are also
159 observed locally. Pyrite is common in the slates and siltstones, especially along
160 some layer boundaries.

161 The ~1300-m-thick Zagu Formation is composed of dark gray slates, black
162 dolomitic slates and dolomitic limestones. There is a thin (10-15 m) layer of
163 conglomerate and pebbly sandstone at the base, representing a medium-scale

channel-fill deposit. The conglomerate clasts are typically subangular to subrounded, generally 2-4 cm in diameter, and consist mainly of intermediate-felsic volcanic rocks (50-60%), chert (20-25%), fragments of carbonaceous rock (10-15%) and siltstone (~10%). The conglomerates and sandstones are also well graded. The Zagu Formation is unconformably overlain by the Sinian Lieguliu Formation (Sun et al., 2007).

The Yanbian Group consists mainly of thin- to medium-bedded, fine-grained, turbiditic volcaniclastic sandstones and mudstones with little variation in sedimentary facies and minor input of coarse clastic material. These sedimentary rocks most likely represent submarine fan deposits, especially mid-fan deposits. This thick turbidite package lacking shallow-water deposits indicates a marine environment below wave base. The presence of limestones throughout the section indicates that the seafloor was above the carbonate compensation depth and suggests a low-latitude, warm-water environment.

4. Sandstone petrography

The sandstones are mostly fine- to medium-grained, poorly sorted and contain angular to subangular grains of low to moderate sphericity. They are mainly composed of quartz, feldspar and lithic fragments. Quartz is relatively minor in volume and is generally subangular to angular, mostly being monocrystalline and lacking inclusions and undulatory extinction (Fig. 4a). Subrounded feldspar is the dominant mineral and is partly altered to saussurite and sericite. Plagioclase is much more common than alkali feldspar (Fig. 4b).

187 Lithic fragments are dominantly rhyolite and andesite with felsitic and microlitic
188 textures, although sedimentary and metamorphic varieties are also present (Figs.
189 4c,d,e).

190 Biotite and muscovite occur as elongate laths or short plates and are locally
191 accompanied by chlorite and glauconite. Sparse heavy minerals include
192 magnetite, zircon, apatite, titanite, pyrite, rutile and tourmaline. Most of these
193 grains are angular to subangular, although some are well-rounded. Amphibole
194 and pyroxene grains are locally present but extremely rare (Fig. 4f).

195 The matrix of the sandstones consists of clay minerals, comminuted and
196 altered lithic and feldspathic fragments, fine-grained quartz, micas, opaque
197 minerals, carbonate and some aphanitic material. Matrix is commonly between
198 10 to 15%, but may be overestimated due to the pseudomatrix problem
199 (Dickinson, 1970). Silica is the dominant cement in these rocks but calcite is also
200 common.

201 Thirty-one medium-grained sandstones were selected for petrographic study
202 using the Gazzi-Dickinson method (Ingersoll et al., 1984). About five to six
203 hundred framework grains were counted from each sample. Matrix (<~0.03 mm)
204 and cement were not counted. The Gazzi-Dickinson method divides volcanic
205 lithic clasts into various textural types (Dickinson, 1970), which is especially
206 significant in magmatic-arc settings, where volcaniclastic components may
207 constitute as much as 100% of the sand fraction (Marsaglia and Ingersoll, 1992).
208 Point-count categories and recalculated parameters are defined in Table 1.

The modal point-count data are shown in Table 2 and Figure 5. In general, the sandstones are characterized by low quartz (Q), moderate feldspar (F) and high lithic (L) abundances, with L/F ratios of 1-3, indicating that the sandstones were derived almost exclusively from volcanic sources (Dickinson, 1970). The Yumen, Xiaoping and Zagu Formations have average compositions of $Q_{22}F_{30}L_{48}$, $Q_{15}F_{36}L_{49}$, and $Q_{14}F_{34}L_{52}$, respectively. In the discrimination diagrams (Fig. 5), they plot in the magmatic-arc field, indicating an undissected-transitional arc provenance.

5. Geochronology and geochemistry

5.1. Detrital zircon geochronology

Single-grain U-Pb dating were performed using the laser ablation ICP-MS technique at China University of Geosciences (Wuhan). The detailed analytical procedures follow Yuan et al. (2004). A GeoLas 2005M laser-ablation system equipped with a 193 nm ArF-excimer laser was used in connection with an Agilent 7500 ICP-MS. Helium was used as the carrier gas to enhance the transport efficiency of the ablated material. The spot diameter was 32 μm. Raw data were processed using the Glitter program (Jackson et al., 2004). All measurements were normalized relative to standard zircon 91500. Standard silicate glass NIST SRM610 was used to calculate U and Th concentrations. The data were processed using the ISOPLOT program (Ludwig, 1999).

Zircons from these rocks are commonly transparent to orange in color, 100-200 μm in size and subrounded to subangular. A total of two hundred and ninety-

eight analyses were performed on zircon grains from five samples (Table 3). Of those, 40 analyses with a degree of discordance >3% were discarded. However, only a very few of these discordant analyses yield ages outside the range defined by the remaining relatively concordant analyses. $^{207}Pb/^{206}Pb$ and $^{206}Pb/^{238}U$ ages were applied for zircons older and younger than 1000 Ma, respectively. The dataset yields ages mainly of ~900-920 Ma with only a very minor, statistically insignificant, component of older continental-derived zircons in the Yumen and Xiaoping Formations. The Zagu Formation, on the other hand, has a relatively high content of older continental material (Fig. 6).

5.1.1. Yumen Formation

Sample F38, a coarse-grained sandstone specimen, was collected near the base of the Yumen Formation (N26.53.39, E101.30.80) for zircon dating. Of the 60 grains analyzed, 4 were highly discordant and thus were discarded. The remaining forty-six grains yielded $^{206}Pb/^{238}U$ apparent ages ranging from 865 to 975 Ma, with a single peak at 917±6 Ma (Fig. 6).

Sample F3, consisting of coarse-grained, feldspar-lithic sandstone, was collected from the upper part of the Yumen Formation (N26.54.47, E101.28.89). Of 58 spot analyses, 41 have concordant ages ranging from 860 to 990 Ma with a weighted mean of 918±8 Ma. Only one concordant grain has a significantly older age of ~2000 Ma (Fig. 6). The remaining 16 analyses are highly discordant but have ages within the younger age population. Thus, the age distribution of zircons from the Yumen Formation suggests uniform source rocks.

5.1.2. Xiaoping Formation

A medium- to coarse-grained, feldspar-lithic sandstone, sample F4, was collected from the middle part of the Xiaoping Formation (N26.55.96, E101.27.45). Of the 60 grains analyzed, 45 concordant grains yielded apparent $^{206}Pb/^{238}U$ ages between 850 and 960 Ma, with a prominent peak at ~920 Ma. Three concordant grains gave much older ages from ~2200 to 2600 Ma (Fig. 6). This age spectrum is very similar to that of samples F38 and F3 of the Yumen Formation. However, half of the remaining 12 analyses with varying degrees of discordance (>3%) yield older ages of around 2200-2600, suggesting a somewhat greater input of older material input relative to the Yumen Formation. Several concordant ages are as young as ~850 Ma (Fig. 6).

Sample F26 (N26.58.76, E101.32.17) was collected near the top of the Xiaoping Formation. 42 of 60 spot analyses have concordant ages ranging from 860 to 970 Ma, with two peaks of 897±6 Ma and 934±5 Ma, respectively (Fig. 6). The remaining 18 discordant analyses also show similar age ranges.

5.1.3. Zagu Formation

A pebbly sandstone, sample F23 (N26.58.96, E101.32.17), was collected from the base of the Zagu Formation. Of 60 grains analyzed, 46 are concordant. This sample yields an age distribution mainly between~ 870 Ma and 930 Ma, but it is characterized by sharp increase of older zircons with several minor peaks at 1800, 2000, 2600 and 3000 Ma (Fig. 6). Coupled with a rapid coarsening in the stratigraphic section, this suggests increased uplift and erosion in the source terrane.

5.2. Whole rock geochemistry

Major oxides and selected trace elements of whole-rock samples were determined by X-ray fluorescence (XRF) on fused glass beads at the University of Hong Kong. Trace elements were analyzed with a VG PQ Excell ICP-MS, also at the University of Hong Kong. The samples for ICP-MS analysis were prepared in closed beakers in high-pressure bombs to ensure complete digestion (Qi et al., 2000). We used pure elemental standards for external calibration, and BHVO-1 (basalt) and SY-4 (syenite) as reference materials for all analyses. Accuracies of the XRF analyses are estimated to be better than 1% for SiO_2, better than 2% for major oxides present in concentrations greater than 0.5 wt% and 5% for trace elements. The ICP-MS analyses yielded accuracies better than 5%.

5.2.1. Major elements

The majority of the Yanbian Group sandstones and mudstones have intermediate SiO_2 (55-73 wt%), high Fe_2O_3+MgO (usually 5-12 wt%; total Fe as Fe_2O_3) and TiO_2 (0.6-1.2 wt%) and low CaO (mostly <1 wt%) (Table 4). In general, SiO_2 increases whereas TiO_2, Al_2O_3, Fe_2O_3, MnO, MgO, CaO, and Na_2O decrease with enhanced mineralogical maturity, indicating an increase in the quartz content and a decrease in chemically unstable detrital grains (e.g., feldspar and volcanic rock fragments) (Bhatia, 1983). There are no systematic stratigraphic variations from the Yumen through Xiaoping to Zagu Formations, possibly reflecting inadequate sampling from the Yumen and Zagu Formations.

Due to enrichment in clay minerals, the mudstones generally have higher K_2O and Al_2O_3 and lower Na_2O contents, resulting in much higher K_2O/Na_2O ratios (typically 1-10) than those of the corresponding sandstones (commonly 0.1-1). Most sandstone samples are immature, with SiO_2/Al_2O_3 ratios between 3 to 6 and Na_2O/K_2O ratios between 1 to 3.5, and plot within the graywacke field in the plot of Pettijohn (1987) (Fig. 7).

5.2.2. Trace elements

Rocks from the three Formations are virtually indistinguishable in their trace element contents, and are characterized by variable contents of Rb (7-140 ppm), Sr (10-377 ppm), Cs (0.4-8 ppm), Ba (80-1200 ppm), Th (2.6-12 ppm) and U (0.5-3.2 ppm) (Table 4). In comparison with average upper continental crust, they show strong Nb-Ta, anomalies, slight depletion of Zr-Hf, La and Th, but moderate enrichment of V (17-257 ppm), Cr (15-185 ppm), Ni (<80 ppm), and Sc (8-22 ppm) (Fig. 8a). In addition, the mudstones commonly have higher Rb, Ba, Th, U and Cs contents than the sandstones (Fig 8a), likely reflecting the abundance of clay minerals (e.g., illite and sericite) in these rocks (McLennan et al., 1983).

Both the sandstones and mudstones exhibit subparallel chondrite-normalized REE patterns, characterized by moderate fractionation between light REE and heavy REE (La/Yb_N=5.3-7.4), with obvious negative Eu anomalies (Eu/Eu*=0.6-0.74) (Fig. 8b), features typical of post-Archean sedimentary rocks (Taylor and McLennan, 1985). Moreover, the mudstones generally have slightly more fractionated REE patterns than the sandstones and ~20% higher total REE abundances.

6. Discussion

6.1. Age of the Yanbian Group

The depositional age of the unfossiliferous Yanbian Group has long been debated. It was traditionally thought to be Mesoproterozoic (Pan et al., 1987; SBGMR, 1991). However, newly obtained SHRIMP U-Pb zircon ages of 782±53 Ma (Du et al., 2005) for the basaltic lavas of the lower Yanbian Group strongly suggest a Neoproterozoic age. Similarly, Zhou et al. (2006a) reported a maximum depositional age of 837±6 Ma based on LA-ICP-MS detrital zircon dating. By contrast, Li X.H. et al. (2003, 2006) proposed a minimum age of 857±13 Ma, inferred from the emplacement age of the Guandaoshan pluton that intrudes the Yanbian Group. Thus the depositional age of the Yanbian Group should be no younger than 857 ± 13 Ma. The present geochronological results provide reliable and tight constraints on the maximum depositional age of the Yanbian Group. Although eight youngest zircons from the Yanbian Group give ages as young as 852±6 Ma (Fig. 6), we adopt here a somewhat older age of 868±6 Ma defined by another ten youngest zircon dates in the concordant dataset (Table 3). The ten zircons are from different samples but yield similar ages within quoted errors. We therefore suggest that the Yanbian Group was most likely not older than ~870 Ma. Furthermore, the Yanbian Group was probably deposited in a syn-magmatic basin, based on the short time delay between deposition of the sediments and emplacement of the 857±13 Ma Guandaoshan pluton.

6.2. Effect of chemical weathering

Chemical weathering strongly affects the mineralogy and major element geochemistry of siliciclastic sediments (Nesbitt and Young, 1982, 1996). The chemical index of alteration (CIA) is very useful in evaluating effects of weathering on sedimentary rock composition and is defined by Nesbitt and Young (1982) as:

$$CIA = [Al_2O_3/(Al_2O_3+CaO^*+Na_2O+K_2O)]\times 100$$

Where CaO* represents Ca in the silicate minerals only (i.e. excluding calcite, dolomite and apatite) (Fedo et al., 1995). High CIA values reflect the removal of labile cations (e.g., Na^+, K^+ and Ca^+) in preference to relatively stable residual constituents (e.g. Al^+), corresponding to high degrees of chemical weathering. The values vary from about 50 for the average upper continental crust to about 100 for residual clays. Shales typically have intermediate values of about 70-75, indicating that weathering did not proceed to the stage where alkali and alkaline earth elements were substantially removed from the clay minerals (Nesbitt and Young, 1982). The Yanbian sandstones have CIA values ranging broadly from 49 to 73 and the mudstones from 57 to 84 (Table 4 and Fig. 9). In turbidites, physical sorting during transport and deposition would yield mudstone with high concentration of fine-grained, aluminous clay minerals of high-CIA value (e.g., kaolinite, gibbsite) derived from the upper parts of weathering profiles, and sandstone relatively enriched in coarse-grained low-CIA residue (e.g., quartz, vestigial feldspars) derived from the lower parts of weathering profiles (Nesbitt et al., 1996). The CIA values of mudstones, therefore, will give a better

understanding of the intensity of weathering in the source. Most mudstones have CIA values ranging from 65 to 77, reflecting only moderate source weathering. However, 6 mudstone samples in the Xiaoping Formation and 1 sample from the Zagu Formation having much higher CIA values in the range of 79-84 than typical shales of 70-75. If these values were corrected for K metasomatism (Fedo et al., 1995), their CIA values would be even greater than 90 (Fig. 9), indicative of severe weathering in the source. One possible explanation for the higher CIA values in the few samples from the Xiaoping and Zagu Formations may indicate a contribution of a greater proportion of distal high-CIA detritus from older cratonic source, which is consistent with our detrital zircon data.

The A-CN-K (Al_2O_3-CaO*+Na_2O-K_2O) triangular plot can also be used to constrain the initial compositions of the source rocks (Fedo et al., 1995). The sandstones and mudstones from the Yanbian Group form a linear trend, which is generally subparallel to the A-CN join, but is slightly below the predicted weathering trend, especially for the fine-grained mudstones (Fig. 9). This probably indicates that the mudstones were more profoundly affected by illitization. Their weathering trends suggest a provenance of tonalitic or granodioritic rocks for the Yanbian sediments.

Differential weathering at the source and subsequent diagenesis/metamorphism tend to mobilize and change the relative abundance of large-ion lithophile elements (Nesbitt et al., 1980). However, the Yanbian sandstones and mudstones commonly show linear correlation in the elemental plots of K vs. Rb, K vs. Ba, Ce vs. Sm and U vs. Th (Fig. 10), indicating that

these elements were probably not changed significantly. Moreover, because the sandstones studied here are relatively uniform in grain size, we believe that the grain-size effect is not important.

6.3. Tectonic setting of the Yanbian Group

The pillow basalts and marine sedimentary rocks of the Yanbian Group, and the spatially associated Gaojiacun and Lengshuiqing mafic intrusions, were previously regarded as the Yanbian ophiolite (Sun and Vuagnat, 1992). However, recent studies suggest that the mafic plutons postdate the Yanbian volcano-sedimentary sequence, arguing against an ophiolite model (Zhou et al., 2006a). Based on the geochemistry of the basaltic lavas, the Yanbian Group has been reinterpreted as a back-arc basin sequence (Du et al., 2005; Li X.H. et al., 2006; Sun et al., 2007), but evidence from the sedimentary sequence was not available. Our new geochronological, petrographical and geochemical data thus provide new constraints on a back-arc basin scenario.

The Yanbian Group was deposited at ~870 Ma and derived from a proximal magmatic arc with ages generally between 900 and 920 Ma (Figs. 5 and 6). The presence of almost contemporaneous volcanic arc magmatism indicates an active continental margin setting (DeGraaf-Surpless et al., 2002), in contrast to a passive continental margin where sediments are commonly derived from weathering of older continental crust (Goodge et al., 2002). The immature volcaniclastic graywackes, turbidites of the Yanbian Group are also consistent with an active margin setting (Crook, 1974; Pettijohn et al., 1987), where such rocks are commonly associated with pillow lavas or ‘greenstones’ (Pettijohn et al.,

415 1987 and references therein) and are commonly observed in modern back-arc
416 basins.

417 The sandstones from the Yanbian Group have about 15% modal quartz with
418 mostly 60-73 wt% SiO_2 and K_2O/Na_2O ratios <1, and are quartz-intermediate,
419 indicating a mixed provenance and depositional setting typical of an active
420 continental margin (Crook, 1974). Roser and Korsch (1986) examined the
421 K_2O/Na_2O-SiO_2 systematics of sandstone-mudstone suites from passive
422 continental margins (PM), active continental margins (ACM) and oceanic island
423 arcs (ARC), and found that the chemistry of the fine-grained members, and the
424 coupled sand-mud trends, were more useful indicators of tectonic setting than
425 the sandstones alone. Sandstones from the Yanbian Group plot exclusively in
426 the ARC and ACM fields, whereas most mudstones plot in the ACM field (Fig.
427 11). The coupled sand-mud trends (chain-dashed tie lines in Fig. 11) show one
428 trend parallel to the field boundaries and the other perpendicular to the first,
429 indicating a back-arc basin setting (Roser and Korsch, 1986). Using Bhatia's
430 (1983) scheme, the majority of samples from the Yanbian Group plot in the
431 oceanic island arc (OIA) to continental island arc (CIA) fields (Fig. 12). The
432 observed scatter of some points is probably due to a combination of sandstone
433 maturity and interelement variation.

434 The trace-element geochemistry of fine-grained clastic sediments has also
435 been widely used to determine tectonic setting (Bhatia and Crook, 1986; Floyd et
436 al., 1991). On the La-Th-Sc and Th-Sc-Zr/10 ternary plots (Fig. 13), most of the
437 Yanbian Group sandstones also fall within the OIA and CIA fields. The elemental

compositions of different greywackes can be most easily compared by utilizing upper continental crust-normalized, multi-element patterns. As shown in Figure 8a, the Yanbian rocks have pronounced negative Nb-Ta anomalies, clearly indicative of subduction-related magmatic rock source (Floyd et al., 1991). For further comparison, the data were also normalized to the standard tectonic setting values and the results show that the Yanbian rocks are mostly affiliated with a continental arc+active margin (Fig. 14).

REE patterns of clastic rocks are mainly controlled by provenance (Taylor and McLennan, 1985; McLennan, 1989) and are believed to be faithfully preserved in flysch deposited by turbidity currents and mass-flow processes (Hiscott and Gill, 1992). The Yanbian rocks have REE elements and ratios similar to those of continental arc settings (Table 5), in good agreement with the proposed back-arc basin scenario.

6.4. Provenance of the Yanbian Group

Petrographic, geochronological and geochemical evidence not only indicates that rocks of the Yanbian Group rocks were mainly derived from a magmatic arc, but also provides important constraints for the nature of this arc, which was not preserved in the modern exposures.

High feldspar contents (generally >30%) of the Yanbian sandstones indicates derivation directly from crystalline rocks (Boggs, 2001), because feldspars are chemically and physically unstable and thus less likely to survive recycling than a mineral like quartz. Presence of other unstable minerals such as magnetite, pyroxene and amphibole also support this view. The poorly sorted and immature

461 nature of the Yanbian greywackes, and their deposition in a back-arc basin,
462 further points to a proximal arc source with short transport distance and little or
463 no reworking.

464 The source area for the Yanbian Group sediments was an undissected to
465 transitional volcanic arc, in which only minor plutonic rocks were exposed. This
466 interpretation is supported by the abundance of volcanic rock fragments in the
467 sediments, the dominance of plagioclase over K-feldspar and the presence of
468 only minor quartz (Fig. 5 a, b and c). It is also consistent with the negative Zr-Hf
469 anomalies of these rocks relative to the average continent upper crust, reflecting
470 a lack of zircon input from silicic plutonic rocks (Fig. 8a).

471 The abundant intermediate and felsic volcanic rock fragments and sparse
472 mafic rock clasts in the Yanbian sandstones provide the most direct evidence for
473 the composition of these volcanic rocks (Table 2). Moreover, the trace element
474 characteristics of the sediments provide additional constraints on the nature of
475 the provenance. Because silicic rocks are significantly richer in La and Th, and
476 poorer in Sc, Cr, and Co than mafic rocks (Cullers, 1994 and references therein),
477 La/Sc, Th/Sc, Th/Co, and Cr/Th ratios are good indicators of the source rocks.
478 The Yanbian rocks have relatively low and constant La/Th ratios with an average
479 of 1.5 but more variable Co/Th ratios (Fig. 15a), suggesting mixing of felsic and
480 intermediate components. Similarly, a plot of La/Th against Hf also points to
481 mixed sources (Fig. 15b). In addition, the Yanbian rocks mostly have Cr/Th ratios
482 of 5-25 (Table 4), clearly indicative of silicic-intermediate source rocks (Cullers,
483 1994). The low Cr (mostly<150 ppm) and Ni (<80 ppm) of the Yanbian rocks and

484 slight V-Cr-Ni anomalies (Fig. 8a) is also consistent with minor mafic-ultramafic
485 input from the source area (Floyd et al., 1991; Garver et al., 1996).

486 **6.5. An integrated tectonic model**

487 Although the tectonic affinity of the western margin of the Yangtze Block
488 during the Neoproterozoic has been a matter of debate, it has been confirmed
489 that a number of plutons in this region were subduction-related. In the Yanbian
490 area, these intrusions include the ~860-Ma Guandaoshan dioritic pluton (Sun and
491 Zhou, 2008), the ~810-Ma Gaojiacun and Lengshuiqing mafic intrusions (Zhou et
492 al., 2006a) and the ~740-Ma Dadukou gabbroic pluton (Zhao and Zhou, 2007).
493 Determination of the age and tectonic provenance of the Yanbian Group has
494 significant implications for the regional tectonic evolution during Neoproterozoic
495 time. This study provides a window into a Neoproterozoic magmatic arc on the
496 western margin of the Yangtze Block, and reveals the presence of a ~900-920
497 Ma felsic and intermediate volcanic arc in this region, although such a feature
498 has not yet been widely identified directly.

499 Available data allow us to propose a model involving the development of a
500 volcanic arc and formation of the Yanbian back-arc basin and the closely
501 associated subduction-related plutons in this region (Fig. 16). Subduction-related
502 volcanic rocks of mainly felsic and intermediate composition were produced at ca.
503 900-920 Ma owing to the eastward subduction of oceanic lithosphere along the
504 western margin of the Yangtze Block (Fig. 16a). Rifting occurred as a
505 consequence of diapiric upwelling of metasomatized mantle to create the
506 Yanbian back-arc basin and generate the basaltic lavas of the Fangtian

Formation (Fig. 16b). According to Crawford et al. (1981), arc volcanism appears to cease around the time that back-arc opening commences. This basin was built on the ~900-920 Ma volcanic arc sequence which provided materials to fill the adjacent Yanbian basin above the lavas, to form the Yumen, Xiaoping and Zagu Formations (Fig. 16b). With continued erosion, the relief of the source region decreased and hence slowed down the supply of materials for the basin, resulting in biochemical deposition of the carbonates in the Zagu Formation (Fig. 16b). Subduction-related magmatism was then re-activated to generate the subduction-related plutons (Fig. 16c). The oldest pluton is the ~860-Ma Guandaoshan dioritic pluton, followed by the ~810-Ma Gaojiacun and Lengshuiqing and the youngest ~740 Ma Dadukou gabbroic plutons (Fig. 16c). This period of igneous activity suggests continuous subduction along the western margin of the Yangtze Block between about 920 and 740 Ma. This arc was thus active for at least ~180 million years. Eventually, this region probably became a passive margin and the Sinian Lieguliu Formation was unconformably deposited over the Yanbian Group, marking the termination of the arc setting (Fig. 16d).

The subduction-related environment may extend along the entire western margin of the Yangtze Block. Similar sequences also occurred in the northwest margin including the Bikou Group (Fig. 1), which has detrital zircon ages ranging from 700 to 850 Ma and has been interpreted as fore-arc basin deposits (Yan Q.R. et al., 2004; Druschke et al., 2006). Thus our proposed model implies that the western margin of the Yangtze Block was a major continental arc during the Neoproterozoic, and thus probably flanked the Rodinia supercontinent.

7. Conclusions

The Yanbian Group is a typical deep marine, volcaniclastic succession deposited in a back-arc basin. Detrital zircon dating and geological constraints indicate that the Yanbian Group was formed at ~870 Ma. The immature nature of the Yanbian sandstones indicates a proximal arc source with ages of ~900-920 Ma. The Yanbian Group and spatially associated subduction-related plutons in the Yanbian region make up a typical arc assemblage, being part of a major continental arc along the western margin of the Yangtze Block for at least 180 m.y. (920-740 Ma). We infer that the Yangtze Block probably flanked the Rodinia supercontinent.

Acknowledgments

This work was financially supported by the National Science Foundation of China (NSFC grant 40672037/D0204), Chinese Education Ministry 111 project (No. B07011) and the International Innovation Partnership Program of CAS & SAFEA. We thank Xiao Fu, Jianfeng Gao, Shijian Bi and Jiangman Zhang for help with the analyses. Paul Robinson is thanked for reading this manuscript. We appreciate thorough reviews by Barry P. Roser, Keith A.W. Crook and Pater A. Cawood, whose insights led to substantial improvements in this paper.

References

Bhatia, M.R., 1983. Plate tectonics and geochemical composition of sandstones. J. Geol. 91, 611-627.

Bhatia, M.R., 1985. Rare earth element geochemistry of Australian Paleozoic graywackes and mudstones: Provenance and tectonic control. Sediment. Geol. 45, 97-113.

Bhatia, M.R., Crook, K.A.W., 1986. Trace element characteristics of graywackes and tectonic setting discrimination of sedimentary basins. Contrib. Mineral. Petrol. 92, 181-193.

BGMRSP (Bureau of Geology and Mineral Resources of the Sichuan Province), 1972. Regional Geological Survey of People's Republic of China, the Yanbian Sheet (G-47-XII; geological part), scale 1:200,000 (in Chinese).

Boggs, S., 2001. Principles of sedimentology and stratigraphy (Third editon). New Jersey, Prentice-Hall, 726p.

Chen, Z.L., Chen, S.Y., 1987. On the tectonic evolution of the west margin of the Yangzi block. Chongqing, China, Chongqing Publishing House, 172p. (in Chinese).

Cope, T., Ritts, B.D., Darby, B.J., Fildani, A., Graham, S.A., 2005. Late Paleozoic Sedimentation on the Northern Margin of the North China Block: Implications for Regional Tectonics and Climate Change. Int. Geol. Rev. 47, 270-296.

Crawford, A.J., Beccaluva, L., Serri, G., 1981. Tectono-magmatic evolution of the west Philippine-Mariana region and the origin of boninites. Earth Planet. Sci. Lett. 54, 346-356.

573 Crook, K.A.W., 1974. Lithogenesis and geotectonics: The significance of
574 compositional variations in flysch arenites (graywackes). In: Dott, R.H.,
575 Shaver, R.H. (Eds.), Modern and Ancient Geosynclinal Sedimentation. SEPM
576 Spec. Publ. 19, pp. 304-310.
577 Cullers, R.L., 1994. The controls on the major and trace element variation of
578 shales, siltstones, and sandstones of Pennsylvanian-Permian age from
579 uplifted continental blocks in Colorado to platform sediment in Kansas, USA.
580 Geochim. Cosmochim. Acta 58, 4955-4972.
581 DeGraaff-Surpless, K., Graham, S.A., Wooden, J.L., McWilliams, M.O., 2002.
582 Detrital zircon provenance analysis of the Great Valley Group, California:
583 Evolution of an arc-forearc system. Geol. Soc. Am. Bull. 114, 1564-1580.
584 Dickinson, W.R., 1970. Interpreting detrital modes of graywacke and arkose. J.
585 Sediment. Petrol. 40, 695-707.
586 Dickinson, W.R., 1985. Interpreting provenance relations from detrital modes of
587 sandstones. In: Zuffa, G.G. (Eds.), Provenance of arenites. NATO ASI Series
588 C: Mathematical and Physical Sciences 48, D. Reidel Publishing Company,
589 pp. 333-361.
590 Dickinson, W.R., Gehrels, G.E., 2000. Sandstone petrofacies of detrital zircon
591 samples from Paleozoic and Triassic strata in suspect terranes of northern
592 Nevada and California. In: Soreghan, M.J., Gehrels, G.E. (Eds.), Paleozoic
593 and Triassic paleogeography and tectonics of western Nevada and northern
594 California. Boulder, Colorado, Geol. Soc. Am. Special Paper 347, pp. 151-171.

595 Druschke, P., Hanson, A.D., Yan, Q., Wang, Z., Wang, T., 2006. Stratigraphic
596 and U-Pb SHRIMP detrital zircon evidence for a Neoproterozoic continental
597 arc, Central China: Rodinia implications. J. Geol. 114, 627-636.
598 Du, L.L., Geng, Y.S., Yang, C.H., Wang, X.S., Ren, L.D., Zhou, X.W., Shi, Y.Y.,
599 Yang, Z.S., 2005. Geochemistry and SHRIMP U-Pb zircon chronology of
600 basalts from the Yanbian group in the western Yangtze Block. Acta Geologica
601 Sinica 76, 805-813 (in Chinese with English abstract).
602 Eisbacher, G.H., 1985. Late Proterozoic rifting, glacial sedimentation, and
603 sedimentary cycles in the light of Windermere deposition, western Canada.
604 Palaeogeogr. Palaeoclimatol. Palaeoecol. 51, 231-254.
605 Fedo, C.M., Nesbitt, H.W., Young, G.M., 1995. Unraveling the effects of
606 potassium metasomatism in sedimentary rocks and paleosols, with
607 implications for weathering conditions and provenance. Geology 23, 921-924.
608 Floyd, P.A., Leveridge, B.E., 1987. Tectonic environment of the Devonian
609 Gramscatho Basin, South Cornwall: Framework mode and geochemical
610 evidence from turbiditic sandstones. J. Geol. Soc. London 144, 531-542.
611 Floyd, P.A., Shail, R., Leveridge. B.E., Franke, W., 1991. Geochemistry and
612 provenance of Rhenohercynian synorogenic sandstones: implications for
613 tectonic environment discrimination. In: Morton, A.C., Todd, S.P., Haughton,
614 P.D.W. (Eds.), Developments in sedimentary provenance studies. Geol. Soc.
615 London, Spec. Publ. 57, 173-188.
616 Garver, J.I., Royce, P.R., Smick, T.A., 1996. Chromium and nickel in shale of the
617 Taconic Foreland: A case study for the provenance of fine-grained sediments

618 with an ultramafic source. J. Sediment. Res. 66, 100-106.
619 Goodge, J.W., Myrow, P., Williams, I.S., Bowring, S.A., 2002. Age and
620 provenance of the Beardmore Group, Antarctica: constraints on Rodinia
621 supercontinent breakup. J. Geol. 110, 393-406.
622 Gu, X.X., Liu, J.M., Zheng, M.H., Tang, J.X., Qi, L., 2002. Provenance and
623 tectonic setting of the Proterozoic turbidites in Hunan, South China:
624 geochemical evidence. J. Sediment. Res. 72, 393-407.
625 Hiscott, R.N., Gill, J.B., 1992. Major and trace element geochemistry of
626 Oligocene to Quaternary volcaniclastic sands and sandstones from the Izu-
627 Bonin arc. In: Taylor, B., Fujioka, K., et al. (Eds.), Proceedings of the Ocean
628 Drilling Program, Scientific Results 126. College Station, TX: Ocean Drilling
629 Program, pp. 467-485.
630 Ingersoll, R.V., Fullard, T.F., Ford, R.L., Grimm, J.P., Pickle, J.D., Sares, S.W.,
631 1984. The effect of grain size on detrital modes; a test of the Gazzi-Dickinson
632 point-counting method: J. Sediment. Petrol. 54, 103-116.
633 Jackson, S.E., Pearson, N.J., Griffin, W.L., Belousova, E.A., 2004. The
634 application of laser ablation-inductively coupled plasma-mass spectrometry
635 (LA-ICP-MS) to in-situ U-Pb zircon geochronology. Chem. Geol. 211, 331-335.
636 Li, F.H., Tan, J.M., Shen, Y.L., Yu, F.X., Zhou, G.F., Pan, X.N., Li, X.Z., 1988.
637 The pre-Sinian in the Kangdian area: Chongqing, China, Chongqing
638 Publishing House, 396p. (in Chinese).
639 Li, X.H., Li, Z.X., Zhou, H.W., Liu, Y., Liang, X.R., Li, W.X., 2003. SHRIMP U-Pb
640 zircon age, geochemistry and Nd isotope of the Guandaoshan pluton in SW

641 Sichuan: Petrogenesis and tectonic significance. Sci. China Ser. D (Supp.)
642 46, 73-83.
643 Li X.H., Li, Z.X., Sinclair, J.A., Li, W.X., Carter, G., 2006. Revisiting the “Yanbian
644 Terrane”: implications for Neoproterozoic tectonic evolution of the western
645 Yangtze Block, South China. Precambrian Res. 151, 14-30.
646 Li, Z.X., Li, X.H., Kinny, P., Wang, J., 1999. The breakup of Rodinia: did it start
647 with a mantle plume beneath South China. Earth Planet. Sci. Lett. 173, 171-
648 181.
649 Li, Z.X., Li, X.H., Kinny, P.D., Wang, J., Zhang, S., Zhou, H., 2003.
650 Geochronology of Neoproterozoic syn-rift magmatism in the Yangtze Craton,
651 South China and correlations with other continents: evidence for a mantle
652 superplume that broke up Rodinia. Precambrian Res. 122, 85-109.
653 Ludwig, K. R., 1999. Isoplot/Ex version 2.06: A geochronological tool kit for
654 Microsoft Excel. Berkeley Geochronology Center, Spec. Publ. 1a.
655 Maas, R., McCulloch, M.T., 1991. The provenance of Archean clastic
656 metasediments in the Narryer Geniss Complex, Western Australia: trace
657 element geochemistry, Nd isotopes, and U-Pb ages for detrital zircons.
658 Geochim. Cosmochim. Acta 55, 1915-1932.
659 Marsaglia, K.M., Ingersoll, R.V., 1992. Compositional trends in arc-related, deep-
660 marine sand and sandstone: a reassessment of magmatic-arc provenance.
661 Geol. Soc. Am. Bull. 104, 1637-1649.
662 McLennan, S.M., 1989. Rare earth elements in sedimentary rocks: Influence of
663 provenance and sedimentary processes. Rev. Mineral. Geochem. 21, 169-200.

McLennan, S.M., 1993. Weathering and Global Denudation. J. Geol. 101, 295-303.

McLennan, S.M., Taylor, S.R., Eriksson, K.A., 1983. Geochemistry of Archean shales from the Pilbara Supergroup, Western Australia. Geochim. Cosmochim. Acta 47, 1211-1222.

McLennan, S.M., Taylor, S.R., McCulloch, M.T., Maynard, J.B., 1990. Geochemical and Nd-Sr isotopic composition of deep-sea turbidites: Crustal evolution and plate tectonic associations. Geochim. Cosmochim. Acta 54, 2015-2050.

McLennan, S.M., Hemming, S.R., Taylor, S.R., Eriksson, K.A., 1995. Early Proterozoic crustal evolution: Geochemical and Nd-Pb isotopic evidence from metasedimentary rocks, southwestern North America. Geochim. Cosmochim. Acta 59, 1153-1177.

Nesbitt, H.W., Markovics, G., Price, R.C., 1980. Chemical processes affecting alkalies and alkaline earths during continental weathering: Geochim. Cosmochim. Acta 44, 1659-1666.

Nesbitt, H.W., Young, G.M., 1982. Early Proterozoic climates and plate motions inferred from major element chemistry of lutites. Nature 299, 715-717.

Nesbitt, H.W., Young, G.M., 1996. Petrogenesis of sediments in the absence of chemical weathering: effects of abrasion and sorting on bulk composition and mineralogy. Sedimentology 43, 341-358.

685 Nesbitt, H.W., Young, G.M., McLennan, S.M., and Keays, R.R., 1996. Effects of
686 chemical weathering and sorting on the petrogenesis of siliciclastic sediments,
687 with implications for provenance studies. J. Geol. 104, 525-542.
688 Pettijohn, F.J., Potter, P.E., Siever, R., 1987. Sand and sandstone (Second
689 editon), Springer-Verkag, 553p.
690 Pan, X.N., Zhao, J.X., Zhan, X.Y., Zhen, H.X., Yan, Z.H., Zhou, G.F., Tao, D.L.,
691 1987. Tectonics and rifting in the Kangdian area: Chongqing, China,
692 Chongqing Publishing House, 295p. (in Chinese).
693 Qi, L., Hu, J., Gregoire, D.C., 2000. Determination of trace elements in granites
694 by inductively coupled plasma-mass spectrometry. Talanta 51, 507-513.
695 Roser, B.P., Korsch, R.J., 1986. Determination of tectonic setting of sandstone-
696 mudstone suites using SiO_2 content and K_2O/Na_2O ratio. J. Geol. 94, 635-650.
697 Roser, B.P., Korsch, R.J., 1988. Provenance signatures of sandstone-mudstone
698 suites determined using discriminant function analysis of major-element data.
699 Chem. Geol. 67, 119-139.
700 SBGMR (Sichuan Bureau of Geology and Mineral Resources). 1991. Regional
701 Geology of Sichuan Province. Beijing, China, Geological Memoirs 23.
702 Geological Publishing House (in Chinese with English summary).
703 She, Z.B., Ma, C.Q., Mason, R., Li, J.W., Wang, G.C., Lei, Y.H., 2006.
704 Provenance of the Triassic Songpan-Ganzi flysch, west China. Chem. Geol.
705 231, 159-175.
706 Sun, C.M., Vuagnat, M., 1992. Proterozoic ophiolites from Yanbian and Shimian
707 (Sichuan Province, China): Petrography, geochemistry, petrogenesis, and

708 geotectonic environment. Schweiz. Mineral. Petrograph. Mitt. 72, 389-413.
709 Sun, W.H., Zhou, M.-F., Zhao J.H., 2007. Geochemistry and tectionic
710 significance of basaltic lavas in the Neoproterozoic Yanbian Group (Southern
711 Sichuan Province, SW China). Int. Geol. Rev. 49, 554-571.
712 Sun, W.H., Zhou, M.-F., 2008. The ~860-Ma, Cordilleran-type Guandaoshan
713 dioritic pluton in the Yangtze Block, SW China: Implications for the origin of
714 Neoproterozoic magmatism. J. Geol. 116, 238-253.
715 Taylor, S.R., McLennan, S.M., 1985. The Continental Crust; Its Composition and
716 Evolution. London, Blackwell, 312 p.
717 Taylor, S.R., McLennan, S.M., 1995. The Geochemical Evolution of the
718 Continental Crust. Rev. Geophys. 33, 241-265.
719 Yan, D.P., Zhou, M.-F., Song, H. L., Wang, X.W., Malpas, J., 2003. Origin and
720 tectonic significance of a Mesozoic multi-layer over-thrust within the Yangtze
721 block (South China). Tectonophysics 361, 239-254.
722 Yan, Q.R., Hanson, A.D., Wang, Z.Q., Druschke, P.A., Yan, Z., Wang, T., Liu,
723 D.Y., Song, B., Pan, P., Zhou, H., Jiang, C.F., 2004. Late Proterozoic
724 subduction and rifting on the northern margin of the Yangtze Plate, China:
725 implications for Rodinia reconstruction. Int. Geol. Rev. 46, 817-832.
726 Yuan, H.L., Gao, S., Liu, X.M., Li, H.M., Gunther, D.,Wu, F.Y., 2004. Accurate U-
727 Pb age and trace element determinations of zircon by laser ablation-
728 inductively coupled plasma-mass spectrometry. Geostandard. Geoanal. Res.
729 28, 353-370.

730 Zhao, J.H., Zhou, M.-F., 2007. Geochemistry of Neoproterozoic mafic intrusions
731 in the Panzhihua district (Sichuan Province, SW China): implications for
732 subduction-related metasomatism in the upper mantle. Precambrian Res. 152,
733 27-47.
734 Zhou, M.-F., Kennedy, A.K., Sun, M., Malpas, J., Lesher, C.M., 2002a. Late
735 Proterozoic arc-related mafic intrusions along the northern margin of South
736 China: implications for the accretion of Rodinia. J. Geol. 110, 611-618.
737 Zhou, M.-F., Yan, D.P., Kennedy, A.K., Li, Y.Q., Ding, J., 2002b. SHRIMP U-Pb
738 zircon geochronological and geochemical evidence for Late Proterozoic arc-
739 magmatism along the western margin of the Yangtze Block, South China.
740 Earth Planet. Sci. Lett. 196, 51-67.
741 Zhou, M.-F., Ma, Y.X., Yan, D.P., Xia, X.P., Zhao, J.H., Sun, M., 2006a. The
742 Yanbian Terrane (Southern Sichuan Province, SW China): A Late Proterozoic
743 arc assemblage in the western margin of the Yangtze Block. Precambrian
744 Res. 144, 19-38.
745 Zhou, M.-F., Yan, D.P., Wang, C.L., Qi, L., Kennedy, A., 2006b. Subduction-
746 related origin of the 750 Ma Xuelongbao adakitic complex (Sichuan Province,
747 China): Implications for the tectonic setting of the giant Neoproterozoic
748 magmatic event in South China. Earth Planet. Sci. Lett. 248, 286-300.
749 Zhou, D., Graham, S.A., 1996. The Songpan-Ganzi complex of the West Qinling
750 Shan as a Triassic remnant ocean basin. In: Yin, A., Harrison, T.M. (Eds.),
751 The Tectonic Evolution of Asia. New York, Cambridge University Press, pp.
752 281-299.

753 **Figure captions**

754 Fig. 1. Simplified geological map of the Yanbian region, Sichuan Province, SW
755 China (after BGMRSP, 1972). The insert map showing the tectonic units of South
756 China and general distribution of Neoproterozoic rocks in the margins of the
757 Yangtze Block.

758 Fig. 2. Stratigraphy of the Yanbian Group based on a measured cross section
759 (BGMRSP, 1972) and our field mapping. Stars indicate samples for detrital zircon
760 analysis. The sandstone beds shown in the column are not strictly to scale
761 because they are typically thin layers interbedded with slate.

762 Fig. 3. (a) Contact between the clastic Yumen Formation and the volcanic
763 Fangtian Formation. (b) A scour structure in the Xiaoping Formation. (c) Slumped
764 siltstone in the Xiaoping Formation. (d) Well-exposed Bouma sequences in the
765 Xiaoping Formation.

766 Fig. 4. (a) Photomicrographs of grain types and features in the Yanbian
767 sandstones. (a) General view showing sub-angular monocrystalline quartz (Q)
768 (T3-3). (b) Sub-rounded plagioclase feldspar (Pl) and K-feldspar (Kf) grains (T3-
769 1-2). (c) A metamorphic grain (Lm) and volcanic grains (Lv) with felsitic and
770 microlitic texture (B11). (d) Siltstone fragments (Ls) (B11). (e) A typical volcanic
771 rock fragment with microlitic texture that we interpret to be derived from
772 intermediate composition (B9). (f) A clinopyroxene grain (Cpx) (F6). All samples
773 are in cross-polarized light. Scale bar in each photograph is 0.3 mm.

774 Fig. 5. Ternary plots of sandstone point count data for the Yanbian Group. (a)
775 QFL plot. (b) QmFLt plot. (c) QLvmLsm plot. (d) QmPK plot. Provenance fields

776 are from Dickinson (1985). The large open triangles represent arithmetic means
777 of data and polygonal box represents one standard deviation.
778 Fig. 6. Detrital zircon data for the sandstone samples of the Yanbian Group. (a)
779 Neoproterozoic (860-1000 Ma) detrital zircon age histogram and cumulative
780 probability plot, showing number of grains analyzed and percentage of
781 Neoproterozoic ages as a fraction of total discordant and concordant ages. (b)
782 Histogram and cumulative probability plot of total concordant detrital zircon ages.
783 Total number of concordant ages for each sample is shown, with number of
784 analyses (concordant plus discordant ages) shown in parenthesis.
785 Fig. 7. (a) Geochemical classification of sandstones from the Yanbian Group
786 (Pettijohn et al., 1987).
787 Fig. 8. (a) Upper crust-normalized, multi-element diagrams for the Yanbian
788 samples; (b) Chondrite-normalized REE patterns of the Yanbian sandstones and
789 mudstones. Post-Archean average Australian shale (PAAS) is also plotted as a
790 heavy dashed line "+" for comparison. Values are from Taylor and McLennan
791 (1985).
792 Fig. 9. CIA ternary diagram, A-CN-K=Al_2O_3 -CaO*+Na_2O-K_2O, after Nesbitt and
793 Young (1982) showing Yanbian sandstones and mudstones as well as average
794 compositions of tonalite and granodiorite (from Fedo et al., 1995). Approximate
795 correction for carbonate content was made by assuming reasonable Ca/Na ratios
796 in silicate material (McLennan, 1993). After correcting phosphate using P_2O_5, if
797 the remaining mole fraction of CaO ≤Na_2O, then this value of CaO is adopted; if
798 CaO >Na_2O, CaO* is assumed to be equivalent to Na_2O. Due to relatively low

carbonate contents in most samples, however, the calculated proportions are thus very close to actual values.

Fig. 10. Plots of K vs. Rb, K vs. Ba, Ce vs. Sm, and U vs. Th, showing linear correlations.

Fig 11. K_2O/Na_2O-SiO_2 plot for the Yanbian rocks. PM = passive margin; ACM = active continental margin; ARC = oceanic island arc. (after Roser and Korsch, 1986).

Fig.12. Tectonic discrimination diagrams for the Yanbian Group sandstones: PM = passive margin; ACM = active continental margin; CIA = continental island arc; OIA =oceanic island arc (after Bhatia, 1983).

Fig. 13. Triangular trace element plots for Yanbian sandstones (after Bhatia and Crook, 1986). Abbreviations as in Fig. 11.

Fig. 14. Normalized multi-element diagrams for the Yanbian sandstones. CAAM = continental arc+active margin; OIA = oceanic island arc; PM = passive margin; OWP = oceanic within-plate. Normalizing values are from Floyd et al. (1991).

Fig. 15. Source rock discrimination diagrams for the Yanbian rocks; (a) Co/Th vs. La/Sc diagram (after Gu et al., 2002), showing derivation from mixed felsic-basic volcanic source, (b) La/Th vs. Hf diagram (after Floyd and Leveridge, 1987), indicating mixed of felsic/basic source rocks.

Fig. 16. Model for the development of the Yanbian Group and the spatially associated subduction-related intrusions in the Yanbian region, SW China.

Table 1. Definition of point-count and recalculated mode parameters (after Dickinson, 1970; Ingersoll et al., 1984)

Symbol	Definition
Point-counting Categories	
Qm	Monocrystalline quartz
Qpq	Polycrystalline quartz (not including chert)
Cht	Chert
P	Plagioclase feldspar
K	K-feldspar
Lvf	Volcanic-lithic with felsitic texture (mainly silicic volcanic rocks)
Lvm	Volcanic-lithic with microlitic texture (mainly intermediate lava)
Lvl	Volcanic-lithic with lathwork texture (mainly basaltic lava)
Lvv	Vitric volcanic-lithic grain
Lmv	Metavolcanic-lithic grain
Lms	Metamorphic-lithic grains except Lmv
Lss	Siltstone/shale sedimentary-lithic grain
Lsc	Carbonate grain
M	Phyllosilicates
Hv	Heavy minerals
FW	Total framework grains counted
Recalculated Parameters	
Qp	Polycrystalline quartz including chert (Qpq+Cht)
Q	Total quartzose grains (Qm+Qp)
F	Total feldspar grains (P+K)
Lvm	Total volcanic-lithic grains (Lvf+Lvm+Lvl+Lvv+Lmv)
Lsm	Total ~~volcanic~~ lithic grins (Lss+Lms)
L	Total unstable lithic grains (Lvm+Lsm)
Lt	Total lithics (L+Qp)

Table2

Table 2 Modal Point-count Data for the Yanbian Group, SW China

																(Q-F-L)			(Qm-F-Lt)			(Qm-P-K)			(Qp-Lv-Ls)				
Fm.	Sample	Qm	Qpq	Cht	P	K	Lvf	Lvm	Lvl	Lvv	Lmv	Lms	Lss	Lsc	M	Hv	FW	%Q	%F	%L	%Qm	%F	%Lt	%Qm	%P	%K	%Qp	%Lv	%Ls	Lv/L	P/F
ZG	F22	48	1	1	126	67	127	67			1	3	120	5	6	561	9	34	57	9	34	57	20	52	28	1	61	38	0.61	0.65
ZG	F23	50	2	1	119	96	122	39			1	2	157	3	4	589	9	37	54	8	37	55	19	45	36	1	50	49	0.50	0.55
ZG	B15	50	1	6	172	51	156	110					14	4	6	560	10	40	50	9	40	51	18	63	19	2	93	5	0.95	0.77
ZG	L18	59	6	32	122	41	155	56					61	4	5	532	18	31	51	11	31	58	27	55	18	12	68	20	0.78	0.75
ZG	YM6	75	5	46	136	25	134	48					77	4	9	546	23	29	47	14	29	57	32	58	11	16	59	25	0.70	0.84
XP	F20	27	1	5	148	19	126	207					9	2	7	542	6	31	63	5	31	64	14	76	10	2	96	3	0.97	0.89
XP	B9	28	1	4	103	18	204	117	2			2	86	3	9	563	6	21	73	5	21	74	19	69	12	1	78	21	0.79	0.85
XP	B10	27	1	5	128	21	176	195				3	20	4	7	576	6	26	68	5	26	69	15	73	12	2	93	6	0.94	0.86
XP	B11	13	1	4	94	5	125	185				9	120	3	6	556	3	18	79	2	18	80	12	84	4	1	70	29	0.71	0.95
XP	F4	73	2	69	215	3	138	8				1	31	1	3	4	540	27	40	33	14	40	46	25	74	1	29	59	13	0.82	0.99
XP	F5	69	7	74	209	8	129	7				2	53	1	3	7	558	27	39	34	12	39	49	24	73	3	30	50	20	0.71	0.96
XP	F6	19	1	19	222	5	18	228	1				7	1	2	6	519	8	44	49	4	44	53	8	90	2	7	90	3	0.97	0.98
XP	F7	17	1	13	218	4	17	243				1	3	3	4	517	6	43	51	3	43	54	7	91	2	5	94	1	0.98	0.98
XP	F8	18	1	12	216	5	16	265				3		1	7	536	6	41	53	3	41	55	8	90	2	4	95	1	0.99	0.98
XP	F9	61	2	82	193	8	83	34			1	1	123	3	3	588	25	34	41	10	34	55	23	74	3	26	36	38	0.49	0.96
XP	F10	72	3	53	89	28	181	110				3		1	5	539	24	22	55	13	22	65	38	47	15	16	83	1	0.99	0.76
XP	F11	79	4	21	215	12	102	124						1	4	557	19	41	41	14	41	45	26	70	4	10	90	0	1.00	0.95
XP	F14	11	1	1	125	4	3	373				3	6	1	2	5	527	2	24	73	2	24	73	8	89	3	1	97	2	0.98	0.97
XP	F33	93	4	38	331	24	62	43					43	3	3	638	21	56	23	15	56	30	21	74	5	22	55	23	0.71	0.93
XP	F34	89	3	39	218	21	168	47					56	3	4	641	20	37	42	14	37	49	27	66	6	13	69	18	0.79	0.91
XP	S6	65	4	26	85	28	267	4		15			2	3	6	496	19	23	58	13	23	64	37	48	16	9	90	1	0.99	0.75
XP	S8	66	1	12	174	49	96	52		1		4	93	4	4	548	14	41	45	12	41	47	23	60	17	5	58	37	0.61	0.78
XP	S3-1	87	4	19	203	18	164	31		3		1	2	3	5	532	21	42	38	16	42	42	28	66	6	10	88	1	0.99	0.92
XP	S5	99	4	21	236	27	106	71		1			12	1	5	577	21	46	33	17	46	37	27	65	7	12	83	6	0.94	0.90
XP	S4	86	3	27	326	53	38	21						3	4	554	21	68	11	16	68	16	18	70	11	34	66	0	1.00	0.86
XP	B4	77	3	26	131	19	204	69					6	3	4	535	20	28	52	14	28	58	34	58	8	9	89	2	0.98	0.87
XP	L6	43	3	38	84	26	225	44	1				80	3	6	543	15	20	64	8	20	72	28	55	17	10	69	20	0.77	0.76
YM	F3	41	2	58	196	1	93	5			1		136	2	7	533	19	37	44	8	37	55	17	82	0	20	34	46	0.42	0.99
YM	F38	74	5	27	96	19	113	73			1		112	2	5	520	20	22	58	14	22	64	39	51	10	10	56	34	0.63	0.83
YM	T3	128	1	18	131	16	212	8					26	2	4	540	27	27	46	24	27	49	47	48	6	7	83	10	0.89	0.89
YM	T3-1-2	108	2	16	171	22	208	23				1	12	2	5	563	22	34	43	19	34	47	36	57	7	7	88	5	0.95	0.89

Table3

Table 3. Zircon U-Pb LA-ICPMS data*

	Pb^{207}/Pb^{206}		Pb^{207}/U^{235}		Pb^{206}/U^{238}		Pb^{207}/Pb^{206}		Pb^{207}/U^{235}		Pb^{206}/U^{238}		Disc.	Best age estimate	
	Ratio	1σ	Ratio	1σ	Ratio	1σ	Age	1σ	Age	1σ	Age	1σ	%	Age(Ma)	1σ
Sample F23															
1	0.1747	0.0021	11.9588	0.1430	0.4964	0.0052	2603	20	2601	11	2599	22	0.2	2603	20
2	0.0676	0.0010	1.3793	0.0200	0.1479	0.0016	858	30	880	9	889	9	3.6		
3	0.0680	0.0010	1.3289	0.0197	0.1418	0.0015	868	31	858	9	855	9	1.5	**855**	**9**
4	0.0697	0.0016	1.4184	0.0322	0.1477	0.0017	918	47	897	14	888	10	3.4		
5	0.1110	0.0014	5.1468	0.0633	0.3362	0.0035	1816	22	1844	10	1868	17	2.8	1816	22
6	0.0687	0.0011	1.3693	0.0212	0.1446	0.0016	889	32	876	9	871	9	2.1	**871**	**9**
7	0.1225	0.0017	6.1327	0.0837	0.3631	0.0039	1993	24	1995	12	1997	19	0.2	1993	24
8	0.0694	0.0010	1.4550	0.0214	0.1520	0.0016	911	30	912	9	912	9	0.1	912	9
9	0.0674	0.0010	1.3556	0.0208	0.1458	0.0016	851	32	870	9	877	9	3.0	877	9
10	0.0697	0.0015	1.4726	0.0321	0.1533	0.0018	918	45	919	13	920	10	0.2	920	10
11	0.0691	0.0016	1.3990	0.0327	0.1468	0.0017	903	48	889	14	883	10	2.2	883	10
12	0.0680	0.0009	1.3527	0.0180	0.1443	0.0015	869	27	869	8	869	9	0	**869**	**9**
13	0.0717	0.0010	1.5399	0.0205	0.1557	0.0016	978	27	947	8	933	9	4.7		
14	0.0683	0.0012	1.3789	0.0232	0.1464	0.0016	879	35	880	10	881	9	0.2	881	9
15	0.1270	0.0017	6.9029	0.0925	0.3943	0.0042	2057	23	2099	12	2143	20	4.1		
16	0.1796	0.0024	12.7856	0.1673	0.5163	0.0056	2649	22	2664	12	2684	24	1.3	2649	22
17	0.0683	0.0013	1.3726	0.0251	0.1458	0.0016	877	38	877	11	877	9	0	877	9
18	0.0690	0.0009	1.3639	0.0172	0.1434	0.0015	898	26	874	7	864	8	3.9		
19	0.0688	0.0014	1.3452	0.0272	0.1419	0.0016	892	42	866	12	855	9	4.2		
20	0.0701	0.0010	1.4866	0.0201	0.1538	0.0016	931	27	925	8	922	9	0.9	922	9
21	0.0676	0.0011	1.3185	0.0214	0.1416	0.0015	855	34	854	9	854	9	0.2	**854**	**9**
22	0.0723	0.0018	1.6481	0.0412	0.1653	0.0020	995	51	989	16	986	11	0.9	986	11
23	0.1219	0.0015	6.1732	0.0778	0.3672	0.0039	1984	22	2001	11	2016	18	1.6	1984	22
24	0.0690	0.0009	1.4192	0.0192	0.1492	0.0016	898	28	897	8	897	9	0.1	897	9
25	0.0676	0.0011	1.3131	0.0220	0.1408	0.0015	857	35	852	10	849	9	0.9	**849**	**9**
26	0.0696	0.0014	1.4648	0.0284	0.1526	0.0017	917	40	916	12	915	10	0.2	915	10
27	0.0686	0.0011	1.3947	0.0215	0.1475	0.0016	887	32	887	9	887	9	0	887	9
28	0.1265	0.0016	6.5102	0.0847	0.3734	0.0040	2049	23	2047	11	2045	19	0.2	2049	23
29	0.1239	0.0016	5.9332	0.0756	0.3474	0.0037	2013	22	1966	11	1922	18	4.6		
30	0.1248	0.0016	6.2883	0.0815	0.3655	0.0039	2026	23	2017	11	2008	18	0.9	2026	23
31	0.0691	0.0012	1.4347	0.0254	0.1505	0.0017	903	36	904	11	904	9	0.1	904	9
32	0.1274	0.0016	6.6361	0.0858	0.3779	0.0040	2062	23	2064	11	2066	19	0.2	2062	23
33	0.0705	0.0011	1.5078	0.0223	0.1550	0.0017	944	30	934	9	929	9	1.6	929	9
34	0.0706	0.0015	1.4459	0.0307	0.1485	0.0017	947	44	908	13	892	10	5.9		
35	0.0687	0.0016	1.3731	0.0305	0.1450	0.0017	890	46	878	13	873	9	1.9	873	9
36	0.1097	0.0015	4.8656	0.0656	0.3218	0.0034	1794	24	1796	11	1799	17	0.3	1794	24
37	0.0692	0.0010	1.4371	0.0202	0.1506	0.0016	905	29	905	8	904	9	0.1	904	9
38	0.1288	0.0019	6.7728	0.0988	0.3814	0.0042	2082	26	2082	13	2083	19	0.1	2082	26
39	0.0733	0.0028	1.7131	0.0631	0.1695	0.0025	1022	75	1013	24	1009	13	1.2	1022	75
40	0.0677	0.0011	1.3448	0.0219	0.1440	0.0016	860	34	865	9	868	9	0.9	**868**	**9**
41	0.1247	0.0018	6.3380	0.0890	0.3685	0.0040	2025	25	2024	12	2023	19	0.1	2025	25
42	0.1256	0.0018	6.4518	0.0920	0.3726	0.0040	2037	25	2039	13	2042	19	0.2	2037	25
43	0.0692	0.0013	1.3666	0.0253	0.1433	0.0016	903	38	875	11	864	9	4.5		
44	0.0721	0.0012	1.5596	0.0252	0.1568	0.0017	990	33	954	10	939	10	5.2		
45	0.1230	0.0017	6.1609	0.0840	0.3632	0.0039	2000	24	1999	12	1997	18	0.2	2000	24
46	0.0689	0.0011	1.4897	0.0240	0.1567	0.0017	897	33	926	10	939	10	4.6		
47	0.0678	0.0011	1.3443	0.0222	0.1437	0.0016	863	34	865	10	866	9	0.3	**866**	**9**
48	0.0700	0.0013	1.4916	0.0282	0.1545	0.0017	929	39	927	11	926	10	0.3	926	10
49	0.0683	0.0017	1.3697	0.0326	0.1455	0.0017	877	49	876	14	876	10	0.2	876	10

*A total of 19 youngest concordant zircions used to define the maximum depostion age are shown in bold.

Table 3. Zircon U-Pb LA-ICPMS data (continued)

	Pb^{207}/Pb^{206}		Pb^{207}/U^{235}		Pb^{206}/U^{238}		Pb^{207}/Pb^{206}		Pb^{207}/U^{235}		Pb^{206}/U^{238}		Disc.	Best age estimate	
	Ratio	1σ	Ratio	1σ	Ratio	1σ	Age	1σ	Age	1σ	Age	1σ	%	Age(Ma)	1σ
50	0.0687	0.0010	1.4077	0.0209	0.1485	0.0016	891	30	892	9	893	9	0.2	893	9
51	0.0712	0.0019	1.4592	0.0380	0.1487	0.0018	963	53	914	16	894	10	7.4		
52	0.0685	0.0012	1.3267	0.0227	0.1405	0.0016	883	35	857	10	848	9	4.1		
53	0.0697	0.0030	1.4771	0.0630	0.1537	0.0023	919	87	921	26	922	13	0.3	922	13
54	0.1659	0.0024	10.8526	0.1550	0.4743	0.0051	2517	24	2511	13	2503	22	0.6	2517	24
55	0.0687	0.0013	1.4217	0.0261	0.1500	0.0017	890	38	898	11	901	9	1.2	901	9
56	0.1237	0.0018	6.2384	0.0916	0.3657	0.0040	2010	26	2010	13	2009	19	0	2010	26
57	0.2149	0.0031	17.1552	0.2512	0.5791	0.0063	2943	23	2944	14	2945	26	0.1	2943	23
58	0.0703	0.0012	1.4722	0.0241	0.1518	0.0017	938	33	919	10	911	9	2.9	911	9
59	0.0699	0.0012	1.4070	0.0233	0.1459	0.0016	926	34	892	10	878	9	5.3		
60	0.0697	0.0014	1.4298	0.0276	0.1487	0.0017	920	40	902	12	894	9	2.9	894	9
Sample F26															
1	0.0713	0.0010	1.4611	0.0203	0.1486	0.0016	966	28	915	8	893	9	7.8		
2	0.0700	0.0010	1.3875	0.0191	0.1439	0.0015	927	28	884	8	867	9	6.7		
3	0.0724	0.0010	1.5491	0.0211	0.1553	0.0016	996	28	950	8	930	9	6.8		
4	0.0708	0.0010	1.5402	0.0218	0.1578	0.0017	951	29	947	9	945	9	0.6	945	9
5	0.0704	0.0011	1.5070	0.0231	0.1553	0.0017	939	31	933	9	931	9	0.9	931	9
6	0.0688	0.0010	1.4104	0.0206	0.1486	0.0016	894	30	893	9	893	9	0	893	9
7	0.0720	0.0011	1.6095	0.0250	0.1622	0.0017	985	32	974	10	969	10	1.6	**969**	**10**
8	0.0712	0.0020	1.5768	0.0428	0.1607	0.0020	963	56	961	17	960	11	0.2	960	11
9	0.0689	0.0018	1.4175	0.0371	0.1492	0.0018	896	54	896	16	896	10	0	896	10
10	0.0681	0.0012	1.3846	0.0244	0.1476	0.0016	870	37	882	10	887	9	1.9	887	9
11	0.0716	0.0010	1.4686	0.0210	0.1488	0.0016	975	29	918	9	894	9	8.6		
12	0.1492	0.0031	3.4552	0.0696	0.1680	0.0021	2337	35	1517	16	1001	11	80		
13	0.0689	0.0014	1.4114	0.0288	0.1486	0.0017	895	42	894	12	893	9	0.2	893	9
14	0.0695	0.0010	1.3420	0.0196	0.1401	0.0015	913	30	864	9	845	8	7.8		
15	0.0664	0.0023	1.1731	0.0389	0.1282	0.0017	818	69	788	18	778	10	5.0		
16	0.0693	0.0010	1.3423	0.0189	0.1404	0.0015	908	29	864	8	847	8	6.9		
17	0.0781	0.0020	1.6387	0.0407	0.1521	0.0019	1151	50	985	16	913	10	23		
18	0.0691	0.0018	1.4277	0.0354	0.1500	0.0018	900	51	901	15	901	10	0	901	10
19	0.0696	0.0010	1.4677	0.0216	0.1529	0.0016	917	30	917	9	917	9	0	917	9
20	0.0712	0.0011	1.4712	0.0229	0.1498	0.0016	964	32	919	9	900	9	6.9		
21	0.0703	0.0011	1.5170	0.0233	0.1566	0.0017	936	31	937	9	938	9	0.2	938	9
22	0.0686	0.0009	1.3949	0.0189	0.1475	0.0016	886	28	887	8	887	9	0.1	887	9
23	0.0689	0.0016	1.4034	0.0322	0.1478	0.0017	895	47	890	14	889	10	0.7	889	10
24	0.0693	0.0013	1.4428	0.0260	0.1510	0.0017	907	37	907	11	907	9	0	907	9
25	0.0712	0.0011	1.5062	0.0237	0.1535	0.0017	962	32	933	10	921	9	4		
26	0.0730	0.0016	1.5189	0.0325	0.1509	0.0017	1015	43	938	13	906	10	11		
27	0.0696	0.0012	1.4573	0.0254	0.1518	0.0017	917	36	913	11	911	9	0.6	911	9
28	0.0718	0.0013	1.5011	0.0262	0.1517	0.0017	980	36	931	11	910	9	7.3		
29	0.0702	0.0011	1.5093	0.0237	0.1559	0.0017	935	32	934	10	934	9	0.1	934	9
30	0.0733	0.0033	1.7038	0.0739	0.1687	0.0027	1021	88	1010	28	1005	15	1.6	1005	15
31	0.0687	0.0011	1.4049	0.0223	0.1482	0.0016	891	33	891	9	891	9	0	891	9
32	0.0697	0.0011	1.4450	0.0231	0.1503	0.0016	920	33	908	10	903	9	1.9	903	9
33	0.0702	0.0011	1.5067	0.0239	0.1558	0.0017	933	33	933	10	933	9	0.1	933	9
34	0.0683	0.0010	1.3717	0.0197	0.1456	0.0016	878	30	877	8	877	9	0.2	877	9
35	0.0703	0.0011	1.4870	0.0235	0.1535	0.0017	937	32	925	10	920	9	1.8	920	9
36	0.0727	0.0012	1.5204	0.0242	0.1516	0.0016	1006	32	939	10	910	9	10		
37	0.0712	0.0014	1.4255	0.0273	0.1452	0.0016	964	39	900	11	874	9	9.8		
38	0.0725	0.0013	1.3722	0.0234	0.1373	0.0015	999	35	877	10	830	9	19		

Table 3. Zircon U-Pb LA-ICPMS data (continued)

	Pb^{207}/Pb^{206}		Pb^{207}/U^{235}		Pb^{206}/U^{238}		Pb^{207}/Pb^{206}		Pb^{207}/U^{235}		Pb^{206}/U^{238}		Disc.	Best age estimate	
	Ratio	1σ	Ratio	1σ	Ratio	1σ	Age	1σ	Age	1σ	Age	1σ	%	Age(Ma)	1σ
39	0.0716	0.0025	1.5722	0.0543	0.1592	0.0022	976	71	959	21	952	12	2.4	952	12
40	0.0706	0.0011	1.5263	0.0241	0.1567	0.0017	947	32	941	10	939	9	0.8	939	9
41	0.0705	0.0017	1.5075	0.0348	0.1551	0.0018	943	47	933	14	929	10	1.5	929	10
42	0.0702	0.0012	1.4962	0.0255	0.1547	0.0017	933	35	929	10	927	9	0.6	927	9
43	0.0699	0.0018	1.4769	0.0365	0.1534	0.0018	924	51	921	15	920	10	0.4	920	10
44	0.0699	0.0012	1.4815	0.0248	0.1538	0.0017	924	34	923	10	922	9	0.2	922	9
45	0.0698	0.0015	1.4757	0.0305	0.1533	0.0018	924	43	920	12	919	10	0.5	919	10
46	0.0700	0.0013	1.4972	0.0265	0.1550	0.0017	930	36	929	11	929	10	0.1	929	10
47	0.0683	0.0019	1.3724	0.0373	0.1457	0.0018	878	56	877	16	877	10	0.1	877	10
48	0.0683	0.0015	1.3725	0.0298	0.1457	0.0017	879	45	877	13	877	9	0.2	877	9
49	0.0709	0.0018	1.5599	0.0378	0.1596	0.0019	955	50	954	15	954	11	0.1	954	11
50	0.0693	0.0012	1.3932	0.0229	0.1459	0.0016	907	34	886	10	878	9	3.2		
51	0.0686	0.0014	1.3947	0.0284	0.1474	0.0017	887	42	887	12	886	9	0.1	886	9
52	0.0689	0.0012	1.4111	0.0246	0.1486	0.0016	895	36	894	10	893	9	0.2	893	9
53	0.0678	0.0015	1.3268	0.0295	0.1420	0.0017	861	46	858	13	856	9	0.6	856	9
54	0.0685	0.0013	1.3894	0.0255	0.1470	0.0016	885	38	884	11	884	9	0	884	9
55	0.0702	0.0013	1.4982	0.0264	0.1548	0.0017	934	36	930	11	928	10	0.6	928	10
56	0.0699	0.0012	1.5011	0.0244	0.1557	0.0017	926	33	931	10	933	9	0.8	933	9
57	0.0691	0.0023	1.4252	0.0454	0.1496	0.0020	902	66	900	19	899	11	0.3	899	11
58	0.0687	0.0012	1.3986	0.0244	0.1476	0.0016	890	36	888	10	888	9	0.3	888	9
59	0.0696	0.0012	1.4631	0.0247	0.1525	0.0017	916	35	915	10	915	9	0	915	9
60	0.0699	0.0012	1.4857	0.0253	0.1542	0.0017	925	35	925	10	925	9	0	925	9
Sample F4															
1	0.1817	0.0022	12.7955	0.1577	0.5107	0.0055	2669	20	2665	12	2660	23	0.3	2669	20
2	0.0682	0.0010	1.3674	0.0204	0.1454	0.0016	874	30	875	9	875	9	0.1	875	9
3	0.1707	0.0020	8.4354	0.1027	0.3584	0.0038	2565	20	2279	11	1975	18	26		
4	0.0690	0.0014	1.4184	0.0290	0.1490	0.0017	900	42	897	12	895	10	0.5	895	10
5	0.0703	0.0013	1.5193	0.0270	0.1568	0.0018	937	36	938	11	939	10	0.3	939	10
6	0.0696	0.0010	1.4647	0.0217	0.1526	0.0017	917	30	916	9	916	9	0.1	916	9
7	0.0690	0.0011	1.4226	0.0219	0.1496	0.0016	898	31	898	9	899	9	0.1	899	9
8	0.1196	0.0015	2.3069	0.0286	0.1400	0.0015	1949	22	1214	9	844	8	79		
9	0.1737	0.0021	10.7804	0.1330	0.4500	0.0048	2594	20	2504	11	2395	21	8.0		
10	0.0702	0.0019	1.5102	0.0391	0.1559	0.0019	935	53	935	16	934	11	0.1	934	11
11	0.0683	0.0009	1.3712	0.0185	0.1457	0.0016	877	27	877	8	877	9	0	877	9
12	0.0713	0.0012	1.5836	0.0272	0.1611	0.0018	965	35	964	11	963	10	0.2	963	10
13	0.0680	0.0009	1.3502	0.0186	0.1441	0.0016	867	28	868	8	868	9	0.1	868	9
14	0.0700	0.0010	1.4886	0.0219	0.1543	0.0017	927	30	926	9	925	9	0.2	925	9
15	0.0699	0.0010	1.4880	0.0217	0.1545	0.0017	924	29	926	9	926	9	0.2	926	9
16	0.0689	0.0009	1.4145	0.0194	0.1490	0.0016	894	28	895	8	895	9	0.1	895	9
17	0.0695	0.0011	1.4606	0.0231	0.1524	0.0017	913	32	914	10	915	9	0.1	915	9
18	0.0690	0.0011	1.4214	0.0219	0.1493	0.0016	900	31	898	9	897	9	0.3	897	9
19	0.0690	0.0011	1.4190	0.0222	0.1492	0.0017	898	32	897	9	897	9	0.2	897	9
20	0.0694	0.0008	1.2403	0.0139	0.1296	0.0014	911	22	819	6	785	8	15		
21	0.1626	0.0021	7.9200	0.1046	0.3533	0.0038	2483	22	2222	12	1950	18	24		
22	0.1580	0.0020	7.8123	0.1003	0.3586	0.0039	2434	21	2210	12	1976	18	21		
23	0.1380	0.0018	7.7464	0.1048	0.4070	0.0045	2203	23	2202	12	2201	20	0.1	2203	23
24	0.0695	0.0012	1.4544	0.0247	0.1517	0.0017	914	35	912	10	911	10	0.4	911	10
25	0.0700	0.0016	1.5050	0.0329	0.1558	0.0019	930	45	932	13	934	10	0.4	934	10
26	0.0674	0.0011	1.3110	0.0209	0.1410	0.0016	851	33	851	9	850	9	0.1	**850**	**9**
27	0.0689	0.0011	1.4126	0.0223	0.1487	0.0017	895	32	894	9	894	9	0.1	894	9

Table 3. Zircon U-Pb LA-ICPMS data (continued)

	Pb^{207}/Pb^{206}		Pb^{207}/U^{235}		Pb^{206}/U^{238}		Pb^{207}/Pb^{206}		Pb^{207}/U^{235}		Pb^{206}/U^{238}		Disc.	Best age estimate	
	Ratio	1σ	Ratio	1σ	Ratio	1σ	Age	1σ	Age	1σ	Age	1σ	%	Age(Ma)	1σ
28	0.0690	0.0010	1.4247	0.0204	0.1498	0.0016	898	29	899	9	900	9	0.2	900	9
29	0.0674	0.0009	1.3115	0.0178	0.1411	0.0015	850	27	851	8	851	9	0	**851**	**9**
30	0.0713	0.0013	1.5832	0.0295	0.1610	0.0019	966	38	964	12	963	10	0.3	963	10
31	0.0694	0.0020	1.4406	0.0410	0.1506	0.0019	909	59	906	17	905	11	0.5	905	11
32	0.0684	0.0009	1.3797	0.0194	0.1463	0.0016	880	28	880	8	880	9	0	880	9
33	0.0681	0.0009	1.3574	0.0191	0.1447	0.0016	870	28	871	8	871	9	0.1	**871**	**9**
34	0.0691	0.0010	1.4249	0.0202	0.1496	0.0016	900	29	899	8	899	9	0.2	899	9
35	0.1830	0.0025	13.0071	0.1780	0.5154	0.0056	2680	22	2680	13	2680	24	0	2680	24
36	0.0697	0.0010	1.4692	0.0219	0.1529	0.0017	919	30	918	9	917	9	0.1	917	9
37	0.0698	0.0014	1.4828	0.0300	0.1541	0.0018	923	41	923	12	924	10	0.1	924	10
38	0.0699	0.0011	1.4789	0.0242	0.1535	0.0017	925	33	922	10	921	10	0.4	921	10
39	0.0695	0.0016	1.4546	0.0331	0.1519	0.0018	912	47	912	14	911	10	0.1	911	10
40	0.0676	0.0011	1.3163	0.0223	0.1413	0.0016	855	35	853	10	852	9	0.3	852	9
41	0.0697	0.0011	1.4749	0.0236	0.1534	0.0017	921	32	920	10	920	10	0.1	920	10
42	0.0708	0.0011	1.5573	0.0242	0.1595	0.0018	952	31	953	10	954	10	0.2	954	10
43	0.0705	0.0015	1.5334	0.0315	0.1577	0.0019	944	42	944	13	944	10	0	944	10
44	0.0685	0.0016	1.3877	0.0327	0.1469	0.0018	883	48	884	14	884	10	0	884	10
45	0.0682	0.0010	1.5182	0.0222	0.1613	0.0018	876	29	938	9	964	10	9.6		
46	0.0850	0.0019	2.0445	0.0460	0.1744	0.0021	1316	44	1131	15	1036	12	24		
47	0.0699	0.0011	1.4864	0.0236	0.1542	0.0017	926	32	925	10	924	10	0.2	924	10
48	0.0667	0.0011	1.0473	0.0172	0.1139	0.0013	827	34	728	9	696	7	17		
49	0.0696	0.0011	1.4653	0.0236	0.1527	0.0017	916	32	916	10	916	10	0	916	10
50	0.0725	0.0012	1.6761	0.0284	0.1677	0.0019	999	34	1000	11	1000	11	0.1	1000	11
51	0.1884	0.0028	9.3023	0.1394	0.3581	0.0040	2728	24	2368	14	1973	19	32		
52	0.0689	0.0012	1.4161	0.0246	0.1490	0.0017	896	35	896	10	896	10	0	896	10
53	0.1401	0.0021	7.5719	0.1155	0.3918	0.0044	2229	26	2182	14	2131	20	4.5		
54	0.0696	0.0012	1.4702	0.0252	0.1531	0.0017	918	35	918	10	918	10	0.1	918	10
55	0.0675	0.0011	1.3140	0.0210	0.1413	0.0016	852	32	852	9	852	9	0	**852**	**9**
56	0.0698	0.0012	1.4766	0.0250	0.1535	0.0017	922	34	921	10	920	10	0.2	920	10
57	0.0687	0.0012	1.4093	0.0246	0.1487	0.0017	890	35	893	10	894	10	0.4	894	10
58	0.0672	0.0011	1.4552	0.0233	0.1571	0.0018	843	32	912	10	941	10	11		
59	0.0701	0.0013	1.4986	0.0283	0.1551	0.0018	931	38	930	11	929	10	0.2	929	10
60	0.0696	0.0013	1.4711	0.0268	0.1532	0.0018	918	37	919	11	919	10	0.1	919	10
Sample F3															
1	0.0695	0.0010	1.4595	0.0206	0.1524	0.0016	913	29	914	9	914	9	0.2	914	9
2	0.0707	0.0010	1.5490	0.0219	0.1588	0.0017	950	29	950	9	950	9	0	950	9
3	0.0692	0.0009	1.5022	0.0184	0.1574	0.0016	906	25	931	7	942	9	4.0	942	9
4	0.0680	0.0012	1.3491	0.0227	0.1439	0.0016	868	35	867	10	867	9	0.2	**867**	**9**
5	0.0696	0.0009	1.4639	0.0196	0.1526	0.0016	916	28	916	8	915	9	0.1	915	9
6	0.0711	0.0012	1.5710	0.0263	0.1602	0.0017	961	34	959	10	958	10	0.3	958	10
7	0.0686	0.0011	1.3903	0.0219	0.1471	0.0016	885	33	885	9	885	9	0	885	9
8	0.0691	0.0010	1.4291	0.0198	0.1499	0.0016	903	28	901	8	901	9	0.2	901	9
9	0.0724	0.0010	1.6640	0.0232	0.1668	0.0018	996	28	995	9	995	10	0.1	995	10
10	0.0685	0.0009	1.3850	0.0181	0.1467	0.0015	883	27	883	8	883	9	0	883	9
11	0.0682	0.0012	1.3712	0.0237	0.1457	0.0016	876	36	877	10	877	9	0.1	877	9
12	0.0697	0.0009	1.4707	0.0194	0.1531	0.0016	919	27	918	8	918	9	0.1	918	9
13	0.0692	0.0012	1.4355	0.0247	0.1505	0.0016	904	36	904	10	904	9	0	904	9
14	0.0688	0.0013	1.4070	0.0257	0.1482	0.0016	894	38	892	11	891	9	0.3	891	9
15	0.0806	0.0010	1.6356	0.0207	0.1472	0.0015	1211	25	984	8	885	9	31		
16	0.0691	0.0013	1.3720	0.0245	0.1441	0.0016	901	37	877	11	868	9	3.8	**868**	**9**
17	0.0918	0.0012	1.3533	0.0172	0.1069	0.0011	1464	24	869	7	655	6	76		

Table 3. Zircon U-Pb LA-ICPMS data (continued)

	Pb^{207}/Pb^{206}		Pb^{207}/U^{235}		Pb^{206}/U^{238}		Pb^{207}/Pb^{206}		Pb^{207}/U^{235}		Pb^{206}/U^{238}		Disc.	Best age estimate	
	Ratio	1σ	Ratio	1σ	Ratio	1σ	Age	1σ	Age	1σ	Age	1σ	%	Age(Ma)	1σ
18	0.0695	0.0009	1.4625	0.0191	0.1526	0.0016	913	27	915	8	916	9	0.3	916	9
19	0.0688	0.0011	1.4038	0.0214	0.1480	0.0016	892	31	891	9	890	9	0.3	890	9
20	0.0698	0.0009	1.4841	0.0188	0.1541	0.0016	924	26	924	8	924	9	0	924	9
21	0.0828	0.0014	1.6643	0.0273	0.1457	0.0016	1266	32	995	10	877	9	36		
22	0.0714	0.0011	1.5864	0.0243	0.1611	0.0017	969	31	965	10	963	10	0.6	963	10
23	0.0850	0.0015	1.8289	0.0322	0.1560	0.0017	1316	34	1056	12	934	10	34		
24	0.0685	0.0011	1.3891	0.0212	0.1470	0.0016	885	31	884	9	884	9	0.1	884	9
25	0.0688	0.0009	1.4106	0.0186	0.1488	0.0016	892	27	893	8	894	9	0.2	894	9
26	0.1196	0.0019	5.7505	0.0903	0.3486	0.0038	1951	28	1939	14	1928	18	1.2	1951	28
27	0.0690	0.0010	1.4279	0.0207	0.1500	0.0016	900	30	901	9	901	9	0.1	901	9
28	0.0694	0.0010	1.4474	0.0214	0.1514	0.0016	909	30	909	9	909	9	0.1	909	9
29	0.0733	0.0010	1.6188	0.0218	0.1602	0.0017	1022	27	978	8	958	9	6.5		
30	0.0702	0.0012	1.5064	0.0243	0.1556	0.0017	935	33	933	10	932	9	0.3	932	9
31	0.0699	0.0013	1.4860	0.0274	0.1542	0.0017	926	38	925	11	924	9	0.1	924	9
32	0.0698	0.0010	1.4762	0.0209	0.1535	0.0016	921	29	921	9	921	9	0.1	921	9
33	0.0760	0.0010	1.5237	0.0201	0.1454	0.0015	1096	26	940	8	875	9	22		
34	0.0706	0.0009	1.5371	0.0204	0.1579	0.0017	946	27	945	8	945	9	0.1	945	9
35	0.0722	0.0011	1.6521	0.0240	0.1660	0.0018	991	29	990	9	990	10	0	990	10
36	0.0706	0.0012	1.5393	0.0255	0.1581	0.0017	947	34	946	10	946	10	0.1	946	10
37	0.0699	0.0010	1.4841	0.0217	0.1540	0.0016	925	30	924	9	924	9	0.1	924	9
38	0.0775	0.0015	1.5968	0.0297	0.1495	0.0017	1133	37	969	12	898	9	23		
39	0.0695	0.0010	1.4613	0.0202	0.1525	0.0016	914	28	915	8	915	9	0.1	915	9
40	0.0724	0.0011	1.4769	0.0217	0.1480	0.0016	997	30	921	9	890	9	11.4		
41	0.0687	0.0010	1.3970	0.0204	0.1476	0.0016	889	30	888	9	887	9	0.1	887	9
42	0.0747	0.0012	1.5199	0.0250	0.1476	0.0016	1060	33	938	10	888	9	18		
43	0.0695	0.0011	1.4589	0.0226	0.1523	0.0016	914	32	914	9	914	9	0	914	9
44	0.0712	0.0013	1.5834	0.0277	0.1613	0.0018	964	36	964	11	964	10	0	**964**	**10**
45	0.0680	0.0012	1.3501	0.0239	0.1440	0.0016	868	37	868	10	868	9	0	**868**	**9**
46	0.0693	0.0011	1.4420	0.0222	0.1510	0.0016	907	32	907	9	906	9	0.1	906	9
47	0.0699	0.0011	1.4924	0.0229	0.1548	0.0017	926	31	927	9	928	9	0.2	928	9
48	0.0706	0.0010	1.4622	0.0212	0.1502	0.0016	946	30	915	9	902	9	4.8	902	9
49	0.0700	0.0012	1.4973	0.0243	0.1550	0.0017	930	33	929	10	929	9	0	929	9
50	0.0834	0.0013	1.3573	0.0209	0.1181	0.0013	1277	30	871	9	720	7	56		
51	0.0709	0.0017	1.5551	0.0359	0.1592	0.0019	953	47	953	14	952	10	0.1	952	10
52	0.0691	0.0012	1.4347	0.0251	0.1505	0.0016	903	36	904	10	904	9	0.1	904	9
53	0.0700	0.0012	1.4975	0.0262	0.1551	0.0017	928	36	929	11	930	9	0.1	930	9
54	0.0740	0.0011	1.5527	0.0232	0.1522	0.0016	1041	30	952	9	913	9	13		
55	0.0712	0.0013	1.4545	0.0253	0.1482	0.0016	963	35	912	10	891	9	7.8		
56	0.0701	0.0011	1.5066	0.0242	0.1558	0.0017	932	33	933	10	934	9	0.2	934	9
57	0.0786	0.0013	1.5576	0.0252	0.1437	0.0016	1162	32	954	10	866	9	29		
58	0.0710	0.0018	1.5655	0.0384	0.1600	0.0019	957	50	957	15	957	11	0	957	11
Sample F38															
1	0.0691	0.0008	1.4284	0.0169	0.1500	0.0015	901	24	901	7	901	9	0	901	9
2	0.0719	0.0026	1.4467	0.0503	0.1460	0.0020	983	71	909	21	878	11	12		
3	0.0689	0.0009	1.3850	0.0175	0.1459	0.0015	895	26	883	7	878	8	1.9	878	8
4	0.0692	0.0011	1.4367	0.0226	0.1506	0.0016	905	33	904	9	904	9	0.1	904	9
5	0.0688	0.0011	1.4100	0.0222	0.1487	0.0016	893	33	893	9	893	9	0.1	893	9
6	0.0688	0.0008	1.4194	0.0156	0.1497	0.0015	892	23	897	7	899	9	0.8	899	9
7	0.0688	0.0009	1.4073	0.0184	0.1484	0.0015	892	27	892	8	892	9	0.1	892	9
8	0.0697	0.0009	1.4699	0.0188	0.1531	0.0016	918	26	918	8	918	9	0	918	9
9	0.0685	0.0008	1.3890	0.0161	0.1471	0.0015	884	24	884	7	885	8	0.1	885	8

Table 3. Zircon U-Pb LA-ICPMS data (continued)

	Pb^{207}/Pb^{206}		Pb^{207}/U^{235}		Pb^{206}/U^{238}		Pb^{207}/Pb^{206}		Pb^{207}/U^{235}		Pb^{206}/U^{238}		Disc.	Best age estimate	
	Ratio	1σ	Ratio	1σ	Ratio	1σ	Age	1σ	Age	1σ	Age	1σ	%	Age(Ma)	1σ
10	0.0729	0.0035	1.6331	0.0753	0.1625	0.0027	1011	93	983	29	971	15	4.2		
11	0.0704	0.0014	1.5216	0.0301	0.1568	0.0017	939	41	939	12	939	10	0	939	10
12	0.0687	0.0014	1.4061	0.0276	0.1484	0.0016	891	41	892	12	892	9	0.1	892	9
13	0.0700	0.0013	1.4675	0.0261	0.1520	0.0017	929	37	917	11	912	9	1.9	912	9
14	0.0689	0.0012	1.4168	0.0247	0.1491	0.0016	896	36	896	10	896	9	0	896	9
15	0.0695	0.0008	1.4608	0.0157	0.1524	0.0015	914	22	914	6	914	9	0	914	9
16	0.0689	0.0011	1.4201	0.0228	0.1494	0.0016	897	33	897	10	898	9	0.1	898	9
17	0.0696	0.0008	1.4667	0.0164	0.1528	0.0016	917	23	917	7	917	9	0	917	9
18	0.0704	0.0013	1.5248	0.0278	0.1571	0.0017	940	38	940	11	941	10	0.1	941	10
19	0.0695	0.0008	1.4611	0.0160	0.1524	0.0015	915	22	915	7	915	9	0	915	9
20	0.0702	0.0009	1.5146	0.0198	0.1564	0.0016	935	27	936	8	937	9	0.2	937	9
21	0.0745	0.0013	1.5630	0.0265	0.1521	0.0017	1056	34.4	955.6	11	913	9	16		
22	0.0692	0.0011	1.4496	0.0236	0.1519	0.0016	905	34	910	10	912	9	0.7	912	9
23	0.0698	0.0010	1.4809	0.0199	0.1539	0.0016	923	28	923	8	923	9	0	923	9
24	0.0690	0.0010	1.4227	0.0200	0.1496	0.0016	898	29	899	8	899	9	0.1	899	9
25	0.0696	0.0008	1.4658	0.0173	0.1527	0.0016	917	24	916	7	916	9	0.1	916	9
26	0.0695	0.0010	1.4563	0.0200	0.1521	0.0016	913	28	913	8	912	9	0	912	9
27	0.0710	0.0013	1.5680	0.0290	0.1601	0.0018	958	38	958	11	957	10	0.1	957	10
28	0.0697	0.0012	1.4720	0.0247	0.1532	0.0016	920	35	919	10	919	9	0.1	919	9
29	0.0710	0.0012	1.5627	0.0268	0.1597	0.0017	957	35	956	11	955	10	0.1	955	10
30	0.0705	0.0008	1.5292	0.0175	0.1574	0.0016	941	23	942	7	943	9	0.1	943	9
31	0.0716	0.0018	1.6105	0.0385	0.1633	0.0019	973	49	974	15	975	11	0.2	975	11
32	0.0703	0.0013	1.5188	0.0277	0.1566	0.0017	938	38	938	11	938	10	0	938	10
33	0.0709	0.0012	1.5566	0.0269	0.1593	0.0017	953	35	953	11	953	10	0	953	10
34	0.0679	0.0041	1.3543	0.0792	0.1446	0.0027	867	120	869	34	871	15	0.4	**871**	**15**
35	0.0698	0.0012	1.4766	0.0242	0.1535	0.0016	921	34	921	10	921	9	0.1	921	9
36	0.0687	0.0018	1.3998	0.0353	0.1478	0.0018	890	52	889	15	889	10	0.1	889	10
37	0.0670	0.0015	1.2385	0.0267	0.1341	0.0015	837	45	818	12	811	9	3.2		
38	0.0685	0.0007	1.3834	0.0150	0.1466	0.0015	883	22	882	6	882	8	0.1	882	8
39	0.0700	0.0009	1.4932	0.0195	0.1547	0.0016	929	27	928	8	927	9	0.2	927	9
40	0.0694	0.0012	1.4509	0.0241	0.1517	0.0016	910	34	910	10	910	9	0	910	9
41	0.0696	0.0012	1.4661	0.0249	0.1528	0.0016	916	35	917	10	917	9	0.1	917	9
42	0.0702	0.0015	1.5076	0.0315	0.1557	0.0017	935	43	934	13	933	10	0.2	933	10
43	0.0700	0.0011	1.4933	0.0230	0.1548	0.0016	927	32	928	9	928	9	0.1	928	9
44	0.0693	0.0008	1.4454	0.0163	0.1512	0.0015	908	23	908	7	908	9	0	908	9
45	0.0707	0.0015	1.5425	0.0310	0.1583	0.0018	948	41	948	12	947	10	0.1	947	10
46	0.0685	0.0012	1.3849	0.0230	0.1467	0.0016	882	34	883	10	883	9	0.1	883	9
47	0.0709	0.0017	1.5593	0.0364	0.1595	0.0019	954	48	954	14	954	10	0	954	10
48	0.0678	0.0014	1.3427	0.0271	0.1436	0.0016	863	42	864	12	865	9	0.2	**865**	**9**
49	0.0699	0.0011	1.4892	0.0238	0.1545	0.0016	926	33	926	10	926	9	0	926	9
50	0.0691	0.0013	1.4266	0.0260	0.1498	0.0016	901	38	900	11	900	9	0.1	900	9
51	0.0703	0.0018	1.5147	0.0377	0.1564	0.0018	936	51	936	15	937	10	0.1	937	10
52	0.0699	0.0008	1.4896	0.0174	0.1545	0.0016	926	24	926	7	926	9	0	926	9
53	0.0703	0.0012	1.5111	0.0262	0.1559	0.0017	937	36	935	11	934	9	0.3	934	9
54	0.0705	0.0020	1.5338	0.0421	0.1577	0.0019	944	57	944	17	944	11	0	944	11
55	0.0701	0.0008	1.4976	0.0161	0.1551	0.0016	930	22	929	7	929	9	0.1	929	9
56	0.0701	0.0008	1.4999	0.0166	0.1552	0.0016	931	22	930	7	930	9	0.1	930	9
57	0.0696	0.0013	1.4614	0.0262	0.1524	0.0017	915	37	915	11	914	9	0.1	914	9
58	0.0700	0.0008	1.4927	0.0161	0.1547	0.0016	928	22	927	7	927	9	0.1	927	9
59	0.0690	0.0012	1.4206	0.0238	0.1493	0.0016	899	35	898	10	897	9	0.2	897	9
60	0.0700	0.0010	1.4989	0.0211	0.1553	0.0016	929	29	930	9	930	9	0.2	930	9

Table4

Table 4 Chemical compostion of the Yanbian rocks in the western margin of the Yangtze Block.

	Yumen Formation													
	Sandstone							Mudstone						
	F38	T3-1-2	T3-2	T-1	T-3	Z3	Average	st11	st12	st13	st14	st15	st16	Average
Major Oxides (wt%)														
SiO_2	69.7	79.8	65.2	64.1	80.1	67.7	71.1	65.7	62.1	64.1	65.7	65.3	73.4	66.0
TiO_2	0.99	0.48	0.81	1.02	0.30	0.79	0.73	0.89	0.85	0.76	0.93	0.98	0.84	0.88
Al_2O_3	12.7	10.4	15.5	15.7	10.9	13.9	13.2	14.0	16.3	14.7	13.3	17.8	14.3	15.1
Fe_2O_3	6.62	1.13	5.92	7.87	0.87	7.21	4.94	7.42	7.30	7.70	6.74	2.62	1.69	5.58
MnO	0.05	0.03	0.07	0.10	0.01	0.03	0.05	0.07	0.04	0.03	0.03	0.01	0.02	0.03
MgO	1.94	0.23	1.07	2.17	0.20	1.91	1.25	2.12	1.97	1.81	2.27	1.32	1.01	1.75
CaO	0.31	0.22	0.91	0.30	0.25	0.34	0.39	0.28	0.20	0.22	0.69	0.05	0.05	0.25
Na_2O	3.66	5.05	4.97	1.70	5.14	2.43	3.82	2.91	2.06	2.82	3.41	0.87	1.01	2.18
K_2O	1.11	0.50	2.23	2.45	0.43	1.50	1.37	1.71	2.57	1.95	1.34	3.55	3.76	2.48
P_2O_5	0.16	0.00	0.09	0.10	0.00	0.16	0.09	0.14	0.10	0.16	0.21	0.00	0.00	0.10
LOI	2.64	1.67	3.07	3.65	1.06	3.12	2.54	4.67	5.70	5.10	5.06	6.23	3.85	5.10
Total	99.9	99.6	99.8	99.2	99.3	99.1	99.5	99.9	99.2	99.3	99.7	98.7	100.0	99.5
CIA	63	53	56	73	54	70	61	67	72	68	63	77	71	70
Trace elements (ppm)														
Sc	11.8	7.85	12.8	17.5	6.29	17.1	12.2	16.0	19.3	15.9	17.2	19.1	19.7	17.8
V	89	17.7	46	127	20	115	69	108	137	114	134	257	206	159
Cr	260	14.9	37	74	19.0	152	93	186	182	170	261	148	81	171
Co	3.46	1.72	2.29	18.3	0.98	9.33	6.01	10.1	8.89	4.25	7.03	2.76	0.59	5.61
Ni	45.3	9.4	9.2	38.6	2.7	32.7	23.0	48.9	55.7	48.2	69.9	41.3	10.4	45.7
Rb	30.5	7.4	36.2	90.7	9.3	70.8	40.8	69.7	114	80.8	54.3	137	134	98
Sr	48	153	213	80	266	60	137	62	61	88	138	29	18	66
Y	19.7	6.0	28.0	21.6	10.1	21.7	17.8	18.7	24.6	35.6	20.1	26.1	25.9	25.1
Zr	125	89	214	193	119	162	150	122	135	119	129	153	170	138
Nb	5.14	5.23	9.59	11.40	6.21	6.18	7.29	6.41	10.04	7.94	6.20	10.52	13.24	9.06
Cs	1.98	0.38	2.52	3.85	0.43	3.47	2.10	3.39	5.71	5.07	2.82	8.03	7.62	5.44
Ba	170	125	352	324	132	255	226	271	419	296	295	417	618	386
La	22.2	8.5	15.0	22.3	17.4	21.9	17.89	20.6	29.5	32.0	13.1	41.5	29.9	27.8
Ce	45.8	15.5	28.8	44.3	28.9	51.7	35.83	46.0	61.9	81.8	26.8	83.6	57.0	59.5
Pr	6.00	1.94	3.91	4.95	3.82	6.14	4.46	5.19	6.75	9.12	3.49	9.45	6.37	6.73
Nd	27.4	8.15	17.3	19.4	14.1	26.6	18.82	21.9	26.1	38.1	15.7	40.5	26.2	28.1
Sm	6.43	1.68	4.14	4.07	2.62	6.20	4.19	4.61	5.21	8.48	3.62	8.16	4.73	5.80
Eu	0.94	0.28	1.01	0.96	0.56	1.48	0.87	1.16	1.32	2.33	0.89	1.72	0.90	1.39
Gd	5.29	1.69	3.94	3.60	2.01	5.20	3.62	4.66	5.05	9.21	3.71	6.75	4.55	5.66
Tb	0.94	0.28	0.70	0.62	0.34	0.89	0.63	0.58	0.76	1.29	0.55	0.96	0.67	0.80
Dy	5.71	1.70	4.79	3.63	1.82	4.44	3.68	3.54	4.24	6.91	3.43	5.30	4.50	4.65
Ho	1.12	0.32	1.14	0.78	0.40	0.87	0.77	0.71	1.02	1.35	0.78	1.08	0.99	0.99
Er	2.83	0.84	3.30	2.36	1.21	2.32	2.14	1.96	2.80	3.28	2.11	3.07	3.08	2.72
Tm	0.38	0.13	0.49	0.34	0.18	0.31	0.31	0.30	0.41	0.44	0.32	0.49	0.48	0.41
Yb	2.36	0.83	3.08	2.38	1.30	2.13	2.01	1.80	2.85	2.70	2.00	2.89	3.10	2.56
Lu	0.36	0.14	0.51	0.35	0.22	0.30	0.31	0.29	0.43	0.39	0.29	0.44	0.49	0.39
Hf	4.14	3.06	6.75	4.84	3.01	4.10	4.32	3.74	4.30	3.57	3.99	4.65	5.22	4.25
Ta	0.27	0.20	0.43	0.73	0.41	0.40	0.41	0.36	0.60	0.47	0.36	0.68	0.90	0.56
Pb	9.83	5.96	7.95	3.48	4.32	5.06	6.10	5.88	7.96	11.3	17.4	13.7	47.4	17.3
Th	4.57	2.99	6.03	7.68	3.64	5.45	5.06	5.19	8.66	6.58	4.72	8.94	14.50	8.10
U	1.31	0.93	1.72	1.50	0.69	1.16	1.22	1.53	2.12	1.65	1.42	3.26	3.95	2.32
Eu/Eu*	0.49	0.51	0.76	0.77	0.75	0.80	0.68	0.76	0.79	0.81	0.74	0.71	0.59	0.73
REE	128	42	88	110	75	130	96	113	148	197	77	206	143	147
La/Yb_N	6.33	6.92	3.28	6.31	9.01	6.92	6.46	7.69	6.95	7.98	4.41	9.65	6.49	7.20
La/Yb	9.40	10.29	4.87	9.37	13.38	10.28	9.60	11.43	10.33	11.86	6.56	14.34	9.65	10.7
Cr/Th	56.8	5.0	6.1	9.7	5.2	27.9	18.45	35.8	21.0	25.9	55.3	16.5	5.6	26.7

Table 4 (continued)

Xiaoping Formation																	
Sandstone																	
	F3	F4-1	F4-2	F5	F6	F7	F8	F9	F10	F11	F12	F13	F14	F15	F16	F17	F18
Major Oxides (wt%)																	
SiO_2	67.5	69.0	69.8	66.5	66.4	59.6	58.8	66.3	71.1	71.1	62.3	53.3	54.9	55.1	54.7	60.8	59.59
TiO_2	1.00	0.65	0.69	0.81	0.78	1.01	1.18	0.79	0.54	0.73	1.02	1.74	1.23	1.14	1.14	1.25	1.20
Al_2O_3	13.8	13.2	13.5	14.3	14.1	16.6	16.3	15.5	14.7	14.6	16.2	16.2	17.9	16.9	17.7	16.2	17.51
Fe_2O_3	5.97	4.86	5.09	5.97	5.86	8.11	8.43	6.52	2.12	1.91	6.17	10.71	9.50	6.94	8.84	6.49	7.17
MnO	0.08	0.09	0.06	0.07	0.08	0.11	0.13	0.05	0.02	0.03	0.11	0.26	0.23	0.18	0.22	0.14	0.14
MgO	1.63	1.22	1.15	1.51	1.84	2.85	3.12	1.60	0.75	0.47	1.82	3.24	2.63	1.97	2.62	1.86	1.72
CaO	0.29	1.64	0.35	0.98	0.35	0.82	1.07	0.16	0.31	0.32	2.26	4.67	3.52	5.33	3.39	2.88	1.22
Na_2O	2.80	4.05	4.31	3.02	5.07	6.21	6.04	2.73	3.76	5.82	4.58	3.63	3.65	4.78	3.45	5.54	4.09
K_2O	1.95	1.49	1.50	2.22	2.10	0.61	0.56	1.71	3.99	2.33	2.25	1.55	2.43	1.93	2.84	1.57	3.11
P_2O_5	0.13	0.08	0.07	0.07	0.10	0.15	0.17	0.08	0.06	0.02	0.16	0.27	0.25	0.28	0.24	0.18	0.18
LOI	3.51	3.22	2.97	3.01	2.71	3.05	3.17	3.78	2.18	1.90	2.55	4.21	3.50	5.22	3.60	2.83	3.39
Total	98.6	99.5	99.5	98.4	99.4	99.1	98.9	99.2	99.6	99.3	99.4	99.7	99.8	99.8	98.8	99.8	99.3
CIA	66	54	59	61	56	58	57	71	57	54	54	54	55	49	55	51	60
Trace elements (ppm)																	
Sc	12.5	11.6	10.4	10.2	12.6	13.5	14.5	11.5	13.4	14.4	14.6	18.4	14.5	15.9	14.0	10.8	14.9
V	93	64	60	70	94	130	158	102	36	33	93	228	147	105	125	38	117
Cr	72	56	53	72	74	51	60	78	28	33	47	147	77	47	70	30	62
Co	12.1	9.9	9.1	11.2	12.8	17.1	16.4	4.2	9.5	1.0	11.5	22.4	15.5	15.0	14.9	7.0	19.1
Ni	40.0	23.9	22.4	25.2	37.6	29.5	24.2	18.9	22.1	4.3	25.8	53.9	36.1	27.3	34.5	13.7	37.7
Rb	55.0	33.1	30.1	53.4	45.4	11.4	9.9	42.7	55.4	30.2	34.9	16.6	32.2	29.9	39.4	17.7	42.9
Sr	73	141	152	160	99	255	244	103	204	178	325	339	377	310	330	218	194
Y	17.8	16.0	18.2	17.0	16.0	18.1	15.8	66.7	49.7	15.8	25.4	24.7	21.6	24.9	22.1	21.7	29.0
Zr	202	119	99	140	117	101	104	123	146	164	171	158	154	147	160	47	174
Nb	12.0	6.21	5.64	7.99	5.59	4.91	5.12	5.99	8.12	8.38	9.89	9.31	8.94	8.27	8.95	2.93	10.14
Cs	2.97	1.32	1.44	2.93	2.29	0.76	1.23	1.46	2.43	1.32	1.46	1.24	2.32	1.84	2.63	0.88	1.65
Ba	308	278	284	355	303	195	179	316	943	424	480	407	650	589	568	341	1125
La	27.1	15.3	22.1	24.6	20.2	14.5	16.0	51.8	34.9	25.0	24.4	25.6	25.1	26.0	24.9	20.4	23.6
Ce	48.9	34.2	37.8	44.4	38.0	28.5	31.1	104	67.2	45.6	48.0	45.6	44.8	45.2	46.6	36.1	47.8
Pr	5.40	3.82	5.06	5.34	4.33	3.43	3.72	15	8.47	5.06	5.79	5.79	5.65	5.71	6.13	4.46	6.47
Nd	21.1	16.2	21.1	22.4	17.0	15.0	16.0	69.3	37.1	19.9	25.0	25.7	23.6	24.5	26.1	20.1	28.8
Sm	3.83	3.45	4.42	4.39	3.43	3.25	3.46	16	8.04	3.76	5.28	5.32	4.99	4.98	5.33	4.12	6.37
Eu	0.71	0.71	0.76	0.92	0.75	0.73	0.77	2.88	1.81	1.07	1.18	1.26	1.37	1.24	1.31	0.97	1.73
Gd	4.44	3.16	4.27	4.36	3.52	2.83	3.20	17	7.50	4.18	4.99	4.93	4.83	4.91	5.18	4.03	5.64
Tb	0.67	0.55	0.72	0.72	0.57	0.52	0.56	2.49	1.40	0.63	0.84	0.86	0.81	0.84	0.87	0.70	1.02
Dy	4.22	3.47	4.48	4.58	3.56	3.46	3.50	16	9.02	3.95	5.44	5.47	5.01	5.27	5.55	4.46	6.66
Ho	0.80	0.68	0.92	0.85	0.76	0.72	0.68	2.60	1.78	0.76	1.06	1.04	0.96	1.10	1.12	0.89	1.37
Er	2.27	1.84	2.57	2.36	2.09	2.05	2.01	6.05	4.62	2.14	2.87	2.82	2.43	3.02	3.09	2.51	3.61
Tm	0.34	0.29	0.36	0.32	0.30	0.30	0.28	0.85	0.60	0.30	0.42	0.40	0.36	0.45	0.44	0.36	0.51
Yb	2.19	1.80	2.22	2.10	1.92	1.88	1.77	5.04	3.53	1.91	2.72	2.54	2.32	2.72	2.70	2.32	3.25
Lu	0.36	0.27	0.34	0.32	0.30	0.29	0.28	0.74	0.55	0.32	0.41	0.40	0.37	0.43	0.42	0.38	0.5
Hf	5.90	3.61	3.44	4.43	3.76	3.15	3.25	4.26	4.78	4.89	5.10	4.80	4.74	4.58	5.03	1.72	5.45
Ta	0.38	0.23	0.22	0.29	0.24	0.20	0.22	0.27	0.30	0.32	0.33	0.31	0.31	0.30	0.32	0.11	0.4
Pb	17.2	15.6	15.0	15.6	18.6	5.78	8.56	22.7	10.1	8.46	9.90	5.44	4.74	8.99	6.77	4.68	10.2
Th	10.7	4.27	4.15	5.50	5.35	2.71	2.57	5.28	5.48	5.13	4.72	3.29	3.98	3.76	3.98	2.86	3.77
U	2.44	1.03	1.02	1.31	1.24	0.80	0.83	1.24	1.51	1.48	1.42	1.00	1.16	1.09	1.16	0.54	1.08
Eu/Eu*	0.53	0.66	0.53	0.64	0.66	0.74	0.71	0.54	0.71	0.82	0.70	0.75	0.85	0.77	0.76	0.73	0.88
REE	122	86	107	118	97	77	83	309	187	115	128	128	123	126	130	102	137
La/Yb_N	8.32	5.74	6.70	7.89	7.08	5.18	6.06	6.92	6.66	8.80	6.03	6.79	7.28	6.43	6.21	5.93	4.89
La/Yb	12.4	8.52	9.95	11.7	10.52	7.70	9.01	10	9.90	13.07	8.96	10.09	10.82	9.55	9.22	8.81	7.26
Cr/Th	6.7	13.1	12.8	13.1	13.9	19.0	23.5	14.7	5.1	6.4	9.9	44.6	19.4	12.6	17.5	10.4	16.3

Table 4 (continued)

	Xiaoping Formation																
	Sandstone																
	F19	F20	F21	F24	F25	F26	F27	F28	F29	F30	F31	F32	F33	F34	Z4	Z5	Average
Major Oxides (wt%)																	
SiO_2	64.2	62.7	62.7	61.9	60.3	62.1	60.9	62.3	68.6	72.1	66.9	62.0	68.9	72.5	66.2	63.4	63.8
TiO_2	1.09	1.14	1.04	1.21	1.21	1.14	1.20	1.25	1.06	0.83	0.87	0.92	0.75	0.66	0.72	0.92	1.00
Al_2O_3	15.8	15.0	15.0	15.3	15.5	15.3	16.1	15.1	13.8	12.2	14.6	15.0	14.1	12.5	13.8	14.4	15.11
Fe_2O_3	5.49	7.82	7.38	7.77	8.97	8.64	8.32	8.00	4.94	4.31	6.34	7.39	4.64	3.49	7.04	8.64	6.66
MnO	0.10	0.11	0.09	0.08	0.07	0.06	0.04	0.05	0.06	0.20	0.03	0.09	0.10	0.08	0.05	0.05	0.10
MgO	1.40	3.02	2.95	2.87	3.24	2.93	2.75	2.93	1.62	1.54	1.42	1.86	1.14	0.83	2.75	2.17	2.04
CaO	0.99	0.56	0.59	0.40	0.50	0.50	0.45	0.36	0.10	0.11	0.26	0.13	0.63	0.63	0.35	0.79	1.12
Na_2O	4.28	4.36	3.93	3.82	3.45	2.96	2.97	3.48	3.64	3.35	3.01	2.00	5.48	5.63	2.46	2.32	3.96
K_2O	3.03	1.87	2.09	2.08	1.95	2.18	2.24	1.92	1.64	1.19	1.93	2.01	1.44	1.08	2.24	1.85	1.97
P_2O_5	0.18	0.20	0.22	0.21	0.30	0.27	0.20	0.23	0.06	0.03	0.09	0.13	0.05	0.04	0.12	0.27	0.15
LOI	2.71	3.18	3.29	3.56	3.75	3.33	4.09	3.82	3.90	3.18	4.14	6.86	2.28	1.67	3.07	4.12	3.39
Total	99.2	100.0	99.3	99.2	99.2	99.4	99.2	99.5	99.4	99.0	99.6	98.4	99.6	99.1	98.8	98.9	99.3
CIA	57	61	62	64	66	67	68	66	64	64	67	73	55	52	67	68	59
Trace elements (ppm)																	
Sc	15.4	13.8	12.9	14.1	13.7	12.0	13.3	13.6	12.5	10.2	11.8	10.3	13.4	11.6	14.2	16.7	13.2
V	94	110	104	130	128	129	137	133	98	82	98	106	62	48	106	143	103
Cr	52	46	42	69	71	79	70	75	67	84	177	67	55	45	38	41	65
Co	15.3	12.1	12.4	11.5	13.4	11.6	10.4	10.1	6.8	2.6	7.8	4.5	7.0	8.4	11.3	22.1	11.4
Ni	24.1	28.2	31.0	30.0	34.0	37.1	30.6	28.5	22.2	16.5	37.9	21.3	16.9	18.3	16.8	22.2	27.0
Rb	39.7	42.3	47.6	52.2	49.6	53.8	51.7	41.8	41.8	31.7	53.4	42.8	27.8	16.3	59.4	63.7	39.3
Sr	189	60	54	57	56	48	49	51	63	80	75	51	107	112	75	83	149
Y	36.5	25.7	25.1	24.1	29.6	27.0	36.2	26.2	16.5	13.1	14.6	24.5	16.3	13.0	28.4	26.4	24.4
Zr	154	116	114	128	118	113	124	113	125	89	122	128	135	105	133	132	130
Nb	8.81	5.69	5.42	6.25	5.91	5.69	5.89	5.57	7.22	5.44	7.12	7.51	6.86	5.93	7.18	5.44	6.98
Cs	1.26	2.32	2.58	2.46	2.32	3.06	2.74	2.15	3.17	2.37	4.14	2.77	1.22	0.71	2.00	3.07	2.08
Ba	1215	336	349	337	320	349	427	351	283	223	235	275	317	259	523	408	423
La	26.6	15.2	15.1	16.6	18.1	16.1	24.1	15.9	15.8	18.9	24.1	20.3	15.4	11.0	22.8	14.1	21.6
Ce	51.6	34.2	34.7	34.7	40.9	34.9	43.8	35.4	32.0	32.7	48.1	37.7	32.6	20.2	45.0	33.4	42.0
Pr	6.72	4.01	4.41	4.19	5.19	4.49	6.59	4.62	3.74	4.17	5.46	4.77	3.86	2.38	5.30	4.10	5.26
Nd	29.3	18.8	20.3	18.9	24.1	20.2	30.7	21.5	15.0	15.9	22.9	20.2	16.2	9.7	21.7	18.3	22.8
Sm	6.22	4.37	4.79	4.22	5.59	5.04	7.23	5.27	3.16	3.15	4.63	4.21	3.50	2.04	4.87	4.27	4.93
Eu	1.69	0.91	0.93	0.81	0.93	1.04	1.49	1.05	0.64	0.55	0.78	0.83	0.73	0.59	1.23	1.21	1.08
Gd	5.97	4.23	4.59	3.49	4.44	4.09	5.71	4.17	3.14	3.42	4.56	4.06	3.22	2.03	4.76	4.31	4.70
Tb	1.06	0.74	0.76	0.67	0.89	0.80	1.10	0.83	0.54	0.50	0.73	0.73	0.57	0.34	0.85	0.76	0.81
Dy	6.94	4.74	5.10	4.61	5.96	5.37	7.32	5.60	3.56	3.14	4.45	4.80	3.77	2.34	5.00	4.70	5.18
Ho	1.44	1.05	1.07	1.05	1.28	1.16	1.51	1.19	0.75	0.59	0.90	1.05	0.78	0.54	1.03	1.03	1.05
Er	4.10	3.04	3.01	3.04	3.71	3.39	4.23	3.49	2.19	1.55	2.32	3.01	2.22	1.67	2.73	2.83	2.88
Tm	0.58	0.43	0.42	0.45	0.55	0.50	0.64	0.51	0.34	0.23	0.32	0.46	0.34	0.26	0.37	0.41	0.42
Yb	3.62	2.70	2.66	2.80	3.32	3.20	3.94	3.21	2.12	1.48	2.02	2.93	2.19	1.65	2.41	2.74	2.60
Lu	0.59	0.43	0.40	0.43	0.51	0.48	0.58	0.48	0.35	0.24	0.30	0.47	0.35	0.27	0.34	0.40	0.40
Hf	4.99	3.80	3.62	4.08	4.00	3.93	4.20	3.90	4.21	2.92	3.85	4.32	4.32	3.62	3.60	3.51	4.11
Ta	0.32	0.24	0.24	0.26	0.26	0.25	0.27	0.25	0.27	0.19	0.24	0.28	0.28	0.23	0.45	0.35	0.28
Pb	8.61	9.86	8.14	5.67	11.3	10.9	5.66	6.01	7.78	16.8	11.5	4.61	10.2	14.1	5.92	7.46	10.1
Th	3.34	3.04	3.12	3.66	3.30	3.27	3.48	3.06	5.40	4.01	5.30	6.03	4.83	4.31	5.49	2.93	4.31
U	1.08	0.78	0.81	0.95	0.90	0.87	0.92	0.80	1.34	1.07	1.39	1.45	1.26	1.10	0.88	0.42	1.10
Eu/Eu*	0.85	0.65	0.61	0.65	0.57	0.70	0.71	0.68	0.62	0.51	0.52	0.61	0.66	0.89	0.78	0.86	0.69
REE	146	95	98	96	115	101	139	103	83	87	121	105	86	55	118	93	116
La/Yb_N	4.95	3.78	3.83	3.99	3.66	3.39	4.12	3.33	5.01	8.59	8.02	4.65	4.72	4.47	6.37	3.46	5.7
La/Yb	7.35	5.61	5.69	5.93	5.44	5.04	6.13	4.94	7.45	12.8	11.9	6.91	7.02	6.64	9.46	5.15	8.5
Cr/Th	15.7	15.2	13.6	18.8	21.4	24.1	20.0	24.5	12.4	20.9	33.5	11.2	11.4	10.4	6.9	13.9	16.1

Table 4 (continued)

Xiaoping Formation																	
Mudstone																	
	st2	st4	st5	st6	st7	st8	st17	st18	st19	st20	st21	st22	St23	St24	St25	St26	Average
Major Oxides (wt%)																	
SiO_2	59.0	70.6	65.2	68.8	62.2	59.4	63.3	58.4	61.2	59.5	58.5	60.9	57.9	63.5	58.1	59.1	61.6
TiO_2	0.74	0.98	0.95	0.83	0.83	0.87	0.98	0.75	0.78	0.74	0.82	0.92	0.88	0.78	0.97	0.80	0.9
Al_2O_3	15.2	15.4	15.3	13.6	15.5	15.9	17.0	19.6	16.8	17.3	16.1	16.9	18.5	15.5	19.5	17.7	16.6
Fe_2O_3	6.55	2.70	5.42	5.22	7.67	8.68	3.94	8.11	7.30	8.59	9.51	6.99	7.45	5.68	5.15	7.59	6.7
MnO	0.13	0.04	0.04	0.02	0.15	0.07	0.04	0.04	0.15	0.05	0.10	0.06	0.03	0.12	0.04	0.03	0.1
MgO	3.21	1.37	1.92	1.31	2.50	2.16	1.77	1.26	2.20	1.99	2.90	2.39	1.99	1.77	1.72	1.89	2.0
CaO	2.54	0.06	0.09	0.31	0.37	0.40	0.09	0.06	0.24	0.08	0.57	0.99	0.26	0.88	1.29	0.13	0.5
Na_2O	2.34	0.14	2.97	2.90	1.70	1.66	0.35	0.17	0.93	0.54	2.16	2.51	0.57	2.76	1.41	0.69	1.5
K_2O	3.59	3.60	2.23	1.91	2.43	2.20	3.28	3.22	2.91	2.93	2.43	2.72	2.98	3.77	4.67	2.91	3.0
P_2O_5	0.13	0.02	0.06	0.09	0.13	0.18	0.01	0.11	0.06	0.10	0.32	0.18	0.10	0.06	0.21	0.12	0.1
LOI	5.82	4.77	5.02	4.14	5.96	7.52	8.06	7.84	6.37	7.34	5.44	4.45	7.99	4.50	5.62	7.91	6.2
Total	99.2	99.7	99.2	99.2	99.4	99.1	98.9	99.5	99.0	99.1	98.9	99.0	98.6	99.3	98.7	98.9	99.1
CIA	57	79	68	65	73	75	80	84	77	81	71	67	81	61	68	81	72
Trace elements (ppm)																	
Sc	19.5	22.3	19.8	15.4	19.2	18.8	20.9	19.5	20.5	17.4	19.2	22.2	9.3	14.6	13.9	9.6	17.6
V	133	241	145	110	143	140	238	141	133	125	132	142	136	80	106	124	142
Cr	57	119	61	157	111	78	102	96	112	100	91	89	99	57	38	83	91
Co	27.0	8.9	11.7	13.4	17.8	13.1	1.6	7.4	11.4	5.0	10.4	6.7	4.3	8.5	3.5	6.1	9.8
Ni	11.8	0	0	10.4	28.7	19.2	32.6	44.2	59.4	32.5	77.1	36.0	31.0	25.8	15.1	39.0	28.9
Rb	128	140	73.9	74.0	90.5	79.0	114	114	105	96.1	74.8	83.0	75.1	80.3	112	69.1	94.3
Sr	90	23	95	102	53	65	48	11	103	14	114	171	13	78	59	27	67
Y	25.6	22.0	20.4	17.8	23.2	27.6	33.9	28.3	28.8	28.0	23.8	31.1	24.6	20.4	42.1	43.5	27.6
Zr	158	178	150	147	158	164	176	166	158	161	135	147	147	166	206	125	159
Nb	10	13	8.55	8.13	9.96	9.16	12.0	12.1	10.9	10.6	8.87	9.11	9.61	10.01	12.6	7.97	10.15
Cs	7.08	8.42	4.63	4.61	4.97	3.24	5.39	6.33	4.65	3.70	3.12	4.16	4.06	6.83	6.16	2.79	5.01
Ba	519	554	472	283	413	340	602	576	652	530	393	579	491	725	966	531	539
La	27.9	36.3	22.4	25.1	31.8	24.3	38.8	39.9	38.9	16.4	13.3	24.8	27.4	26.4	14.9	43.5	28.3
Ce	53.9	72.4	46.7	53.8	60.7	43.6	72.7	78.7	75.0	19.1	29.2	55.2	50.9	47.2	35.6	51.7	52.9
Pr	5.79	7.44	5.18	6.06	6.86	5.60	9.58	9.19	8.19	4.07	4.34	6.77	7.28	5.72	5.68	11.0	6.80
Nd	21.9	27.2	19.8	24.2	26.7	23.4	37.9	37.8	31.8	18.5	19.7	28.4	31.7	22.9	27.3	47.6	27.9
Sm	4.67	4.81	4.23	5.37	5.42	5.73	7.29	7.26	5.50	3.99	4.66	6.12	7.10	4.53	7.51	10.5	5.92
Eu	1.03	1.04	0.98	1.21	1.20	1.30	1.76	1.69	1.36	1.12	1.11	1.90	1.32	1.03	1.43	1.86	1.33
Gd	4.54	4.28	3.76	4.79	5.02	5.78	7.12	5.80	5.22	4.64	4.70	6.06	6.31	4.76	6.63	9.06	5.53
Tb	0.79	0.66	0.61	0.69	0.75	0.87	0.93	0.83	0.74	0.67	0.67	0.91	1.08	0.74	1.15	1.67	0.86
Dy	4.61	3.91	3.63	3.71	4.31	4.82	5.92	4.97	5.12	4.47	4.07	5.78	6.72	4.85	7.94	10.6	5.34
Ho	0.95	0.82	0.82	0.73	0.90	1.01	1.29	1.10	1.11	1.01	0.94	1.23	1.32	0.95	1.71	2.10	1.12
Er	2.80	2.64	2.38	2.07	2.70	2.79	3.73	3.14	3.14	3.15	2.66	3.56	3.52	2.71	4.73	5.34	3.19
Tm	0.46	0.43	0.41	0.31	0.41	0.43	0.58	0.53	0.49	0.51	0.46	0.55	0.50	0.42	0.64	0.71	0.49
Yb	2.99	3.07	2.76	2.18	2.67	2.85	3.80	3.43	3.34	3.17	2.64	3.57	3.21	2.69	4.13	4.39	3.18
Lu	0.46	0.48	0.40	0.33	0.40	0.44	0.59	0.50	0.53	0.48	0.41	0.52	0.51	0.44	0.66	0.65	0.49
Hf	4.41	4.90	4.06	3.76	4.34	4.37	5.41	5.19	4.72	4.89	4.20	5.03	5.03	5.44	7.45	4.65	4.87
Ta	0.88	0.82	0.56	0.49	0.65	0.60	0.67	0.77	0.73	0.67	0.52	0.59	0.33	0.35	0.47	0.30	0.59
Pb	6.30	31.1	9.55	8.87	12.7	6.79	17.9	6.27	8.22	11.4	8.15	7.87	12.0	17.4	4.10	6.65	11.0
Th	11	10	5.79	5.34	8.52	6.21	10.41	10.40	12.2	8.27	7.59	7.75	7.14	7.06	7.76	6.92	8.27
U	1.63	2.30	1.52	1.47	1.64	1.38	4.74	2.30	2.31	1.73	1.72	1.75	1.89	2.31	1.81	1.53	2.00
Eu/Eu*	0.68	0.70	0.75	0.73	0.71	0.69	0.75	0.80	0.78	0.80	0.72	0.95	0.60	0.68	0.62	0.58	0.72
REE	133	166	114	131	150	123	192	195	180	81	89	145	149	125	120	201	143
La/Yb_N	6.28	7.95	5.45	7.75	8.04	5.74	6.88	7.83	7.84	3.48	3.38	4.67	5.75	6.61	2.42	6.66	6.0
La/Yb	9.33	11.8	8.10	11.51	11.95	8.53	10.22	11.63	11.6	5.17	5.02	6.94	8.54	9.83	3.60	9.90	9.0
Cr/Th	5.4	11.4	10.6	29.5	13.0	12.5	9.8	9.2	9.2	12.1	12.0	11.4	13.8	8.1	5.0	12.0	11.6

Table 4 (continued)

	Zagu							
	Sandstone				Mudstone			
	F22	F23	Z1	Average	st1	st9	st10	Average
Major Oxides (wt%)								
SiO_2	63.1	65.4	66.8	65.1	61.5	58.9	67.1	62.5
TiO_2	1.03	0.89	0.70	0.9	0.85	0.81	0.55	0.7
Al_2O_3	15.2	14.0	13.8	14.3	16.1	20.0	14.9	17.0
Fe_2O_3	7.44	6.63	6.32	6.8	8.04	7.26	5.84	7.0
MnO	0.05	0.05	0.05	0.0	0.14	0.02	0.05	0.1
MgO	3.15	2.80	2.50	2.8	3.28	2.02	1.91	2.4
CaO	0.37	0.31	0.49	0.4	0.27	0.08	0.30	0.2
Na_2O	3.45	3.34	2.40	3.1	2.52	0.26	1.73	1.5
K_2O	2.70	2.24	2.33	2.4	2.65	3.48	2.23	2.8
P_2O_5	0.15	0.13	0.19	0.2	0.14	0.11	0.05	0.1
LOI	2.98	3.39	3.13	3.2	4.27	6.21	4.69	5.1
Total	99.7	99.2	98.7	99.2	99.8	99.1	99.3	99.4
CIA	63	63	67	64	69	83	72	75
Trace elements (ppm)								
Sc	12.7	11.7	14.3	12.9	20.1	20.4	12.8	17.8
V	116	96	103	105	126	160	72	119
Cr	58	49	34	47	56	90	40	62
Co	11.8	6.7	10.5	9.7	18.5	10.2	10.1	12.9
Ni	26.0	21.1	16.7	21.3	5.96	25.9	0.00	10.6
Rb	52.3	44.8	63.6	53.6	85.9	122.9	78.3	95.7
Sr	70	68	85	74	51	16	75	47
Y	21.1	21.4	33.5	25.3	28.9	36.5	32.3	32.6
Zr	138	111	135	128	167	204	181	184
Nb	8.73	7.01	7.40	7.71	10.05	13.40	10.68	11.37
Cs	1.88	1.60	2.10	1.86	3.88	4.86	6.54	5.09
Ba	553	464	563	527	319	733	853	635
La	20.2	18.1	22.5	20.3	30.2	48.2	34.7	37.7
Ce	39.7	36.6	44.7	40.3	61.2	84.6	47.7	64.5
Pr	4.35	4.02	5.59	4.65	6.83	11.31	8.61	8.92
Nd	18.0	16.8	23.8	19.5	26.6	44.6	34.8	35.3
Sm	3.77	3.74	5.90	4.47	6.15	9.41	8.49	8.02
Eu	0.89	0.85	1.75	1.16	1.09	2.03	1.57	1.56
Gd	3.75	3.56	6.23	4.51	5.60	8.39	7.62	7.21
Tb	0.63	0.64	1.14	0.80	0.93	1.25	1.27	1.15
Dy	4.24	4.27	6.51	5.01	5.30	7.03	6.66	6.33
Ho	0.91	0.94	1.29	1.05	1.13	1.41	1.26	1.27
Er	2.58	2.74	3.23	2.85	3.31	3.98	3.59	3.63
Tm	0.41	0.39	0.43	0.41	0.53	0.60	0.56	0.56
Yb	2.57	2.44	2.69	2.57	3.75	3.95	3.67	3.79
Lu	0.43	0.39	0.37	0.40	0.53	0.58	0.54	0.55
Hf	4.64	3.70	3.68	4.01	4.61	5.74	5.08	5.14
Ta	0.30	0.24	0.46	0.33	0.65	0.95	0.80	0.80
Pb	10.2	6.68	6.27	7.72	1.58	15.8	3.88	7.09
Th	7.66	5.50	5.82	6.33	8.47	11.13	8.05	9.21
U	1.77	1.28	0.92	1.32	1.51	2.35	1.60	1.82
Eu/Eu*	0.72	0.71	0.88	0.77	0.57	0.70	0.60	0.62
REE	102	95	126	108	153	227	161	180
La/Yb_N	5.30	5.00	5.63	5.3	5.42	8.21	6.35	6.7
La/Yb	7.87	7.43	8.36	7.9	8.05	12.20	9.44	9.9
Cr/Th	7.6	9.0	5.8	7.5	6.6	8.1	4.9	6.5

Table 5

Table 5 Discriminating REE elements and ratios for the Yanbian sandstones (after Bhatia,1983)

Tectonic settings	La	Ce	∑REE	La/Yb	La/Yb_N	∑LREE/∑HREE	Eu/Eu*
Oceanic island arc	8±1.7	19±3.7	58±10	4.2±1.3	2.8±0.9	3.8±0.9	1.04±0.11
Andean-type continetnal margin	37	78	186	12.5	8.5	9.1	0.6
Passive margins	39	85	210	15.9	10.8	8.5	0.56
Continental island arc	27±4.5	59±8.2	146±20	11±3.6	7.5±2.5	7.7±1.7	0.79±0.13
Yanbian Group*	22	42	116	8.5	5.7	5.6	0.69

*Values are adopted from the mean values of the 33 sandstones in the Xiaoping Formation.

Figure1

Click here to download high resolution image

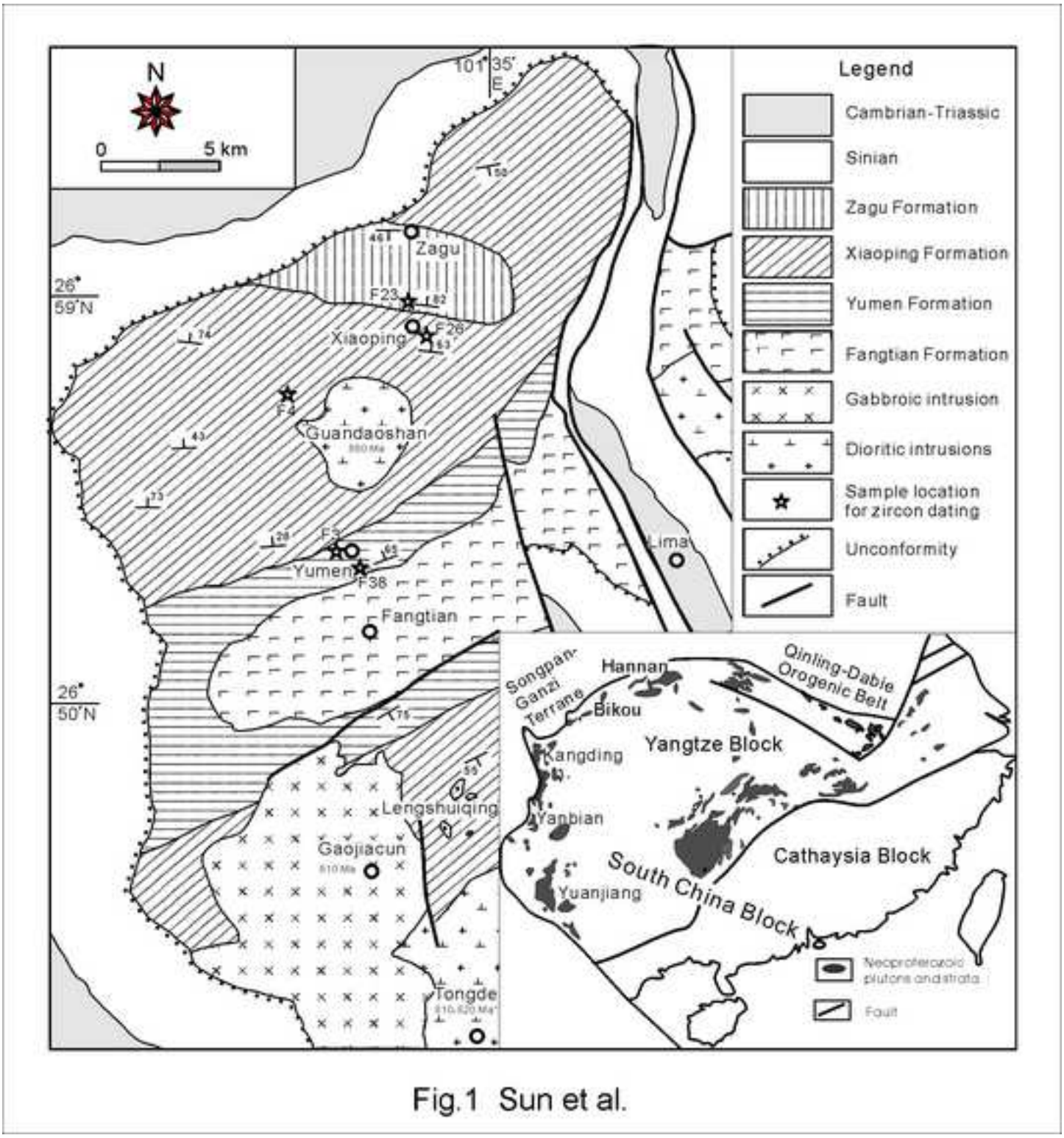

Fig.1 Sun et al.

2

Click here to download high resolution image

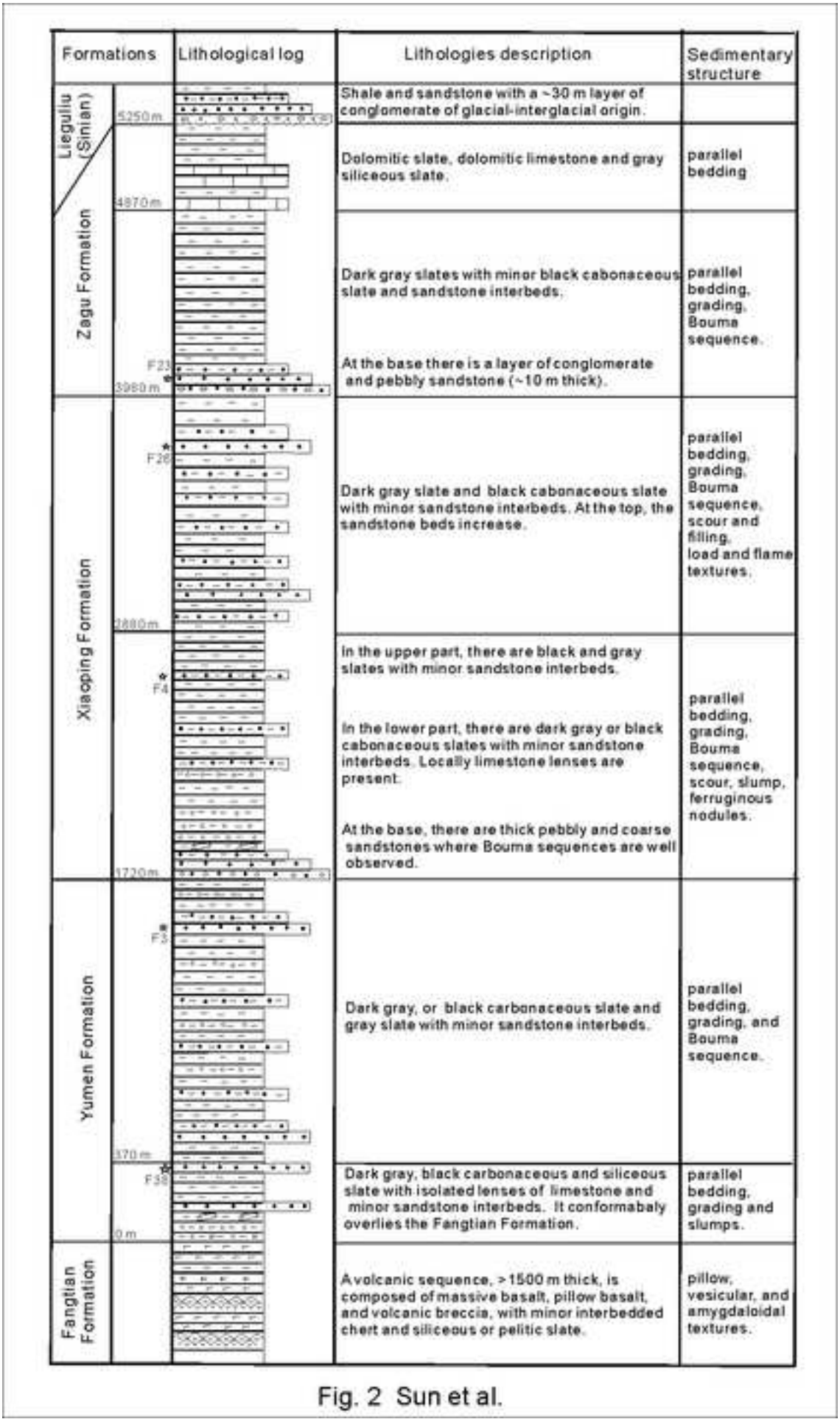

Fig. 2 Sun et al.

Click here to download high resolution image

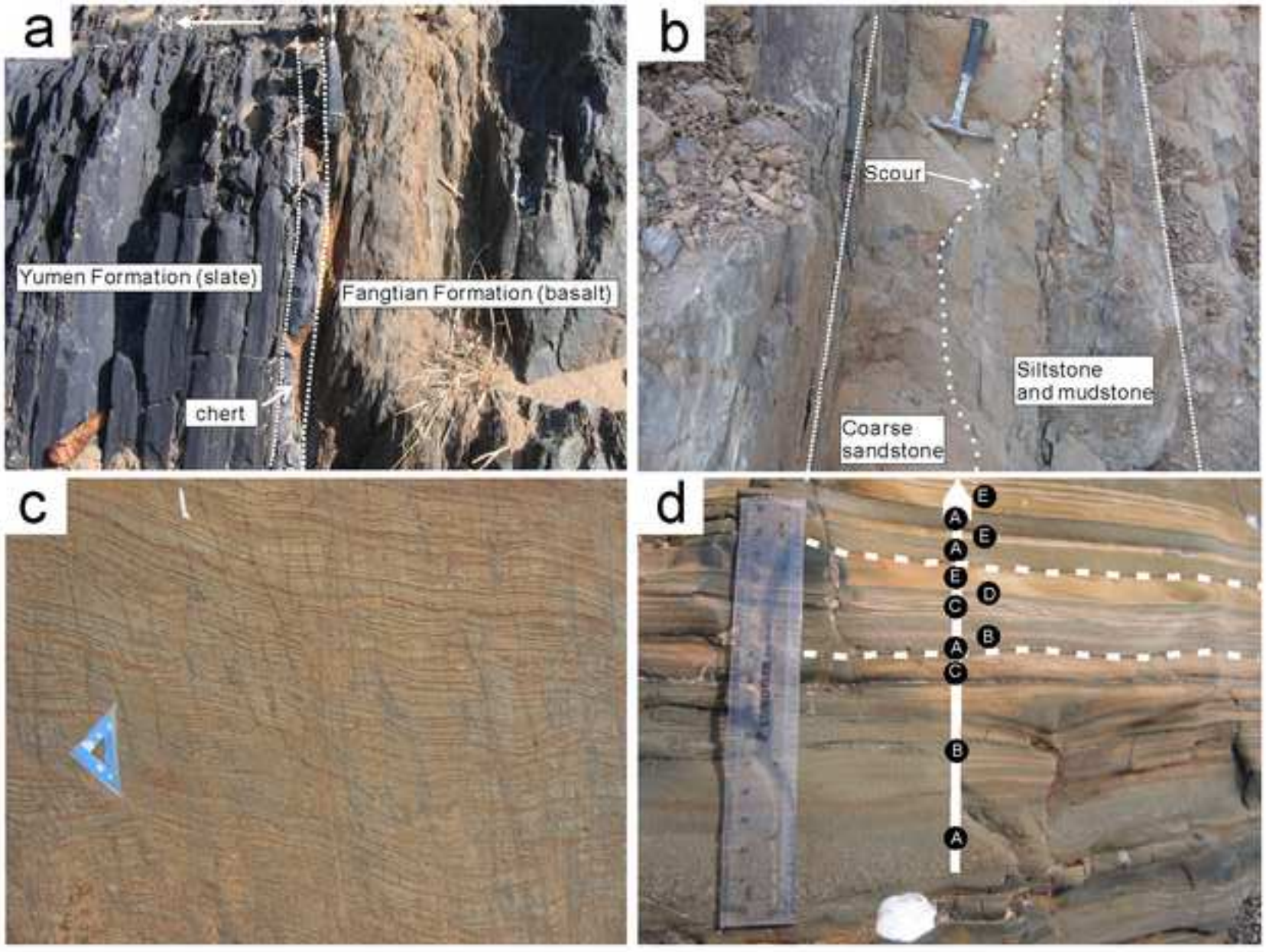

Fig. 3 Sun et al.

Click here to download high resolution image

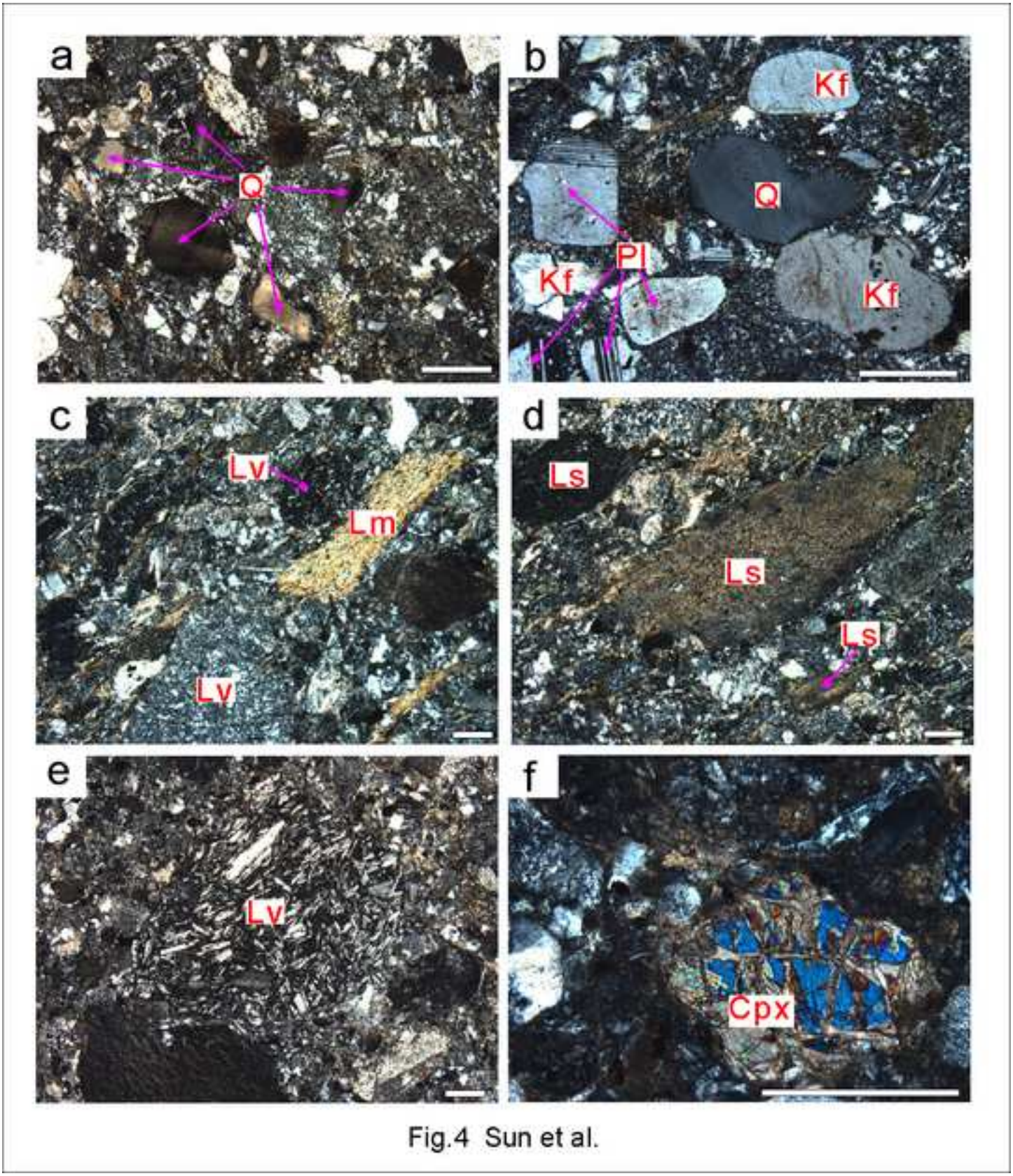

Fig.4 Sun et al.

5

Click here to download high resolution image

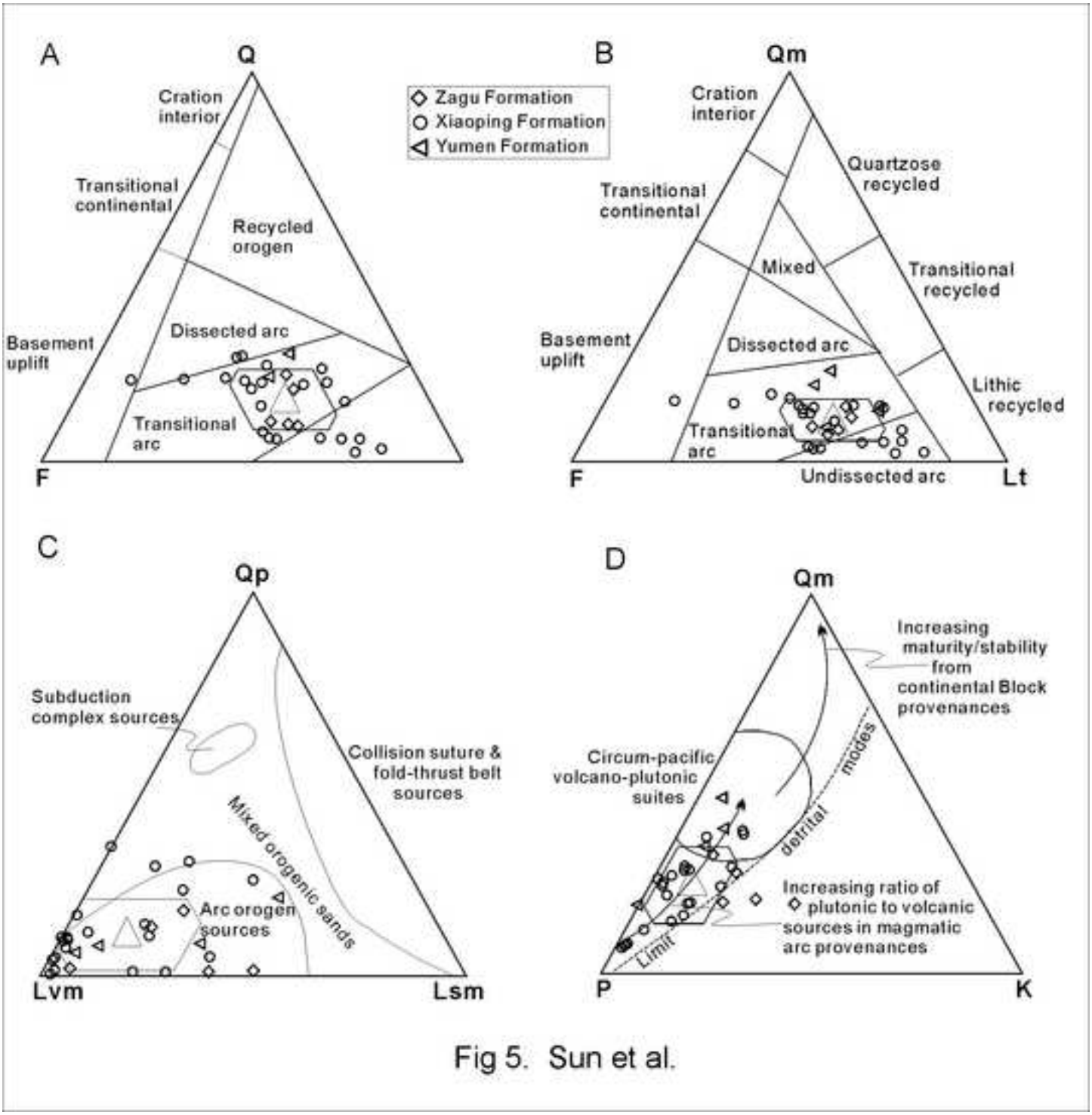

Fig 5. Sun et al.

Click here to download high resolution image

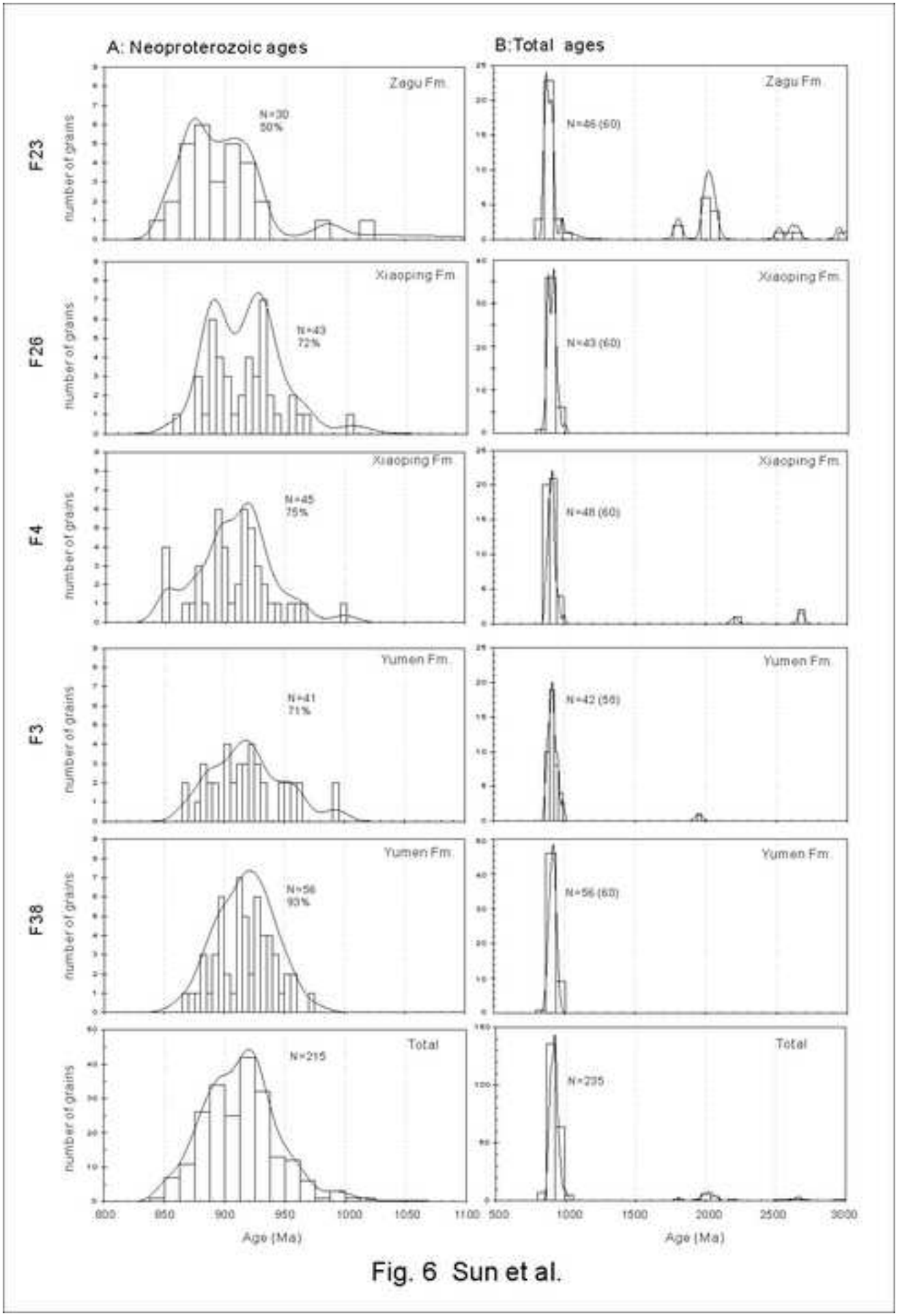

Fig. 6 Sun et al.

Click here to download high resolution image

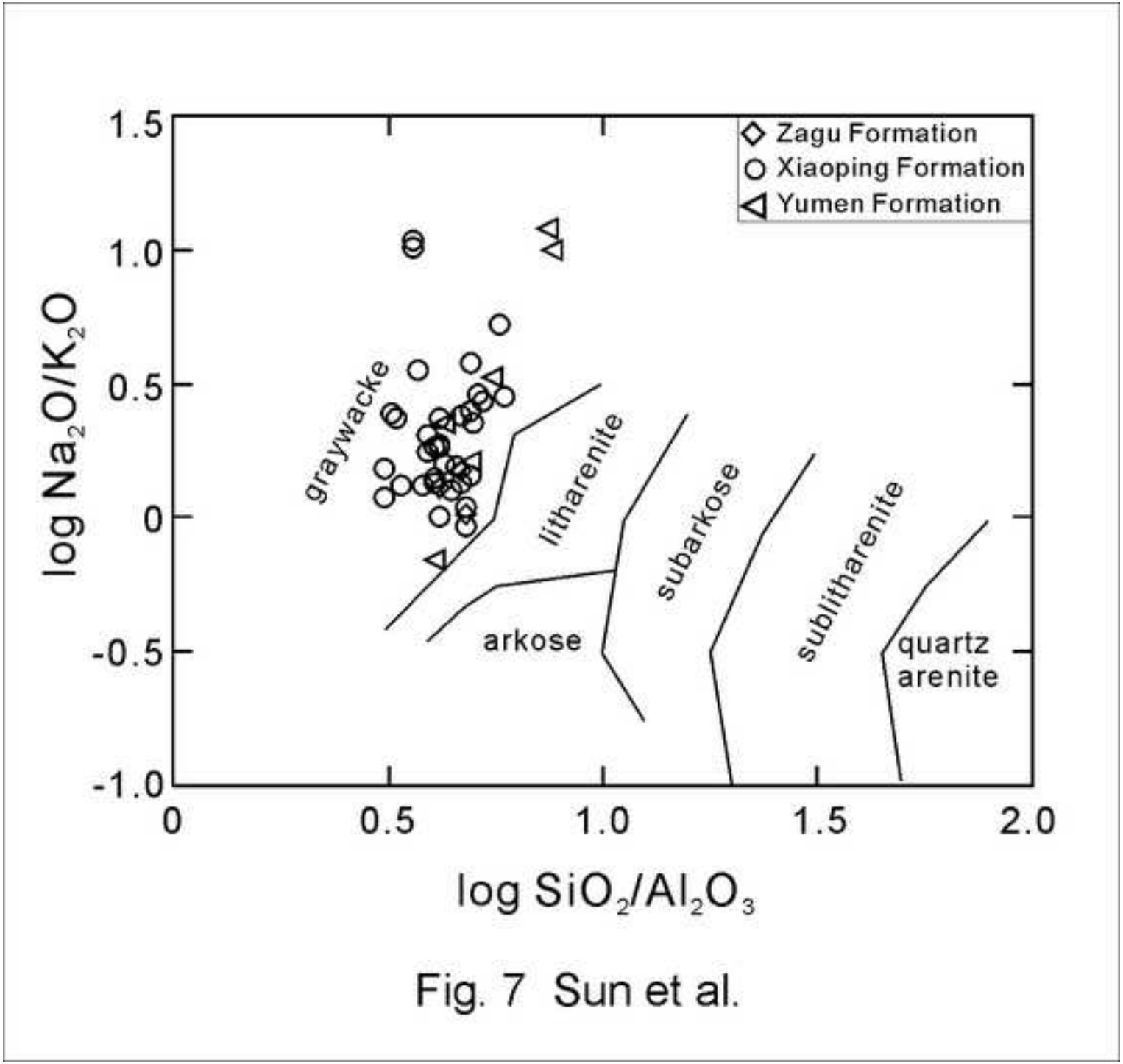

Fig. 7 Sun et al.

Click here to download high resolution image

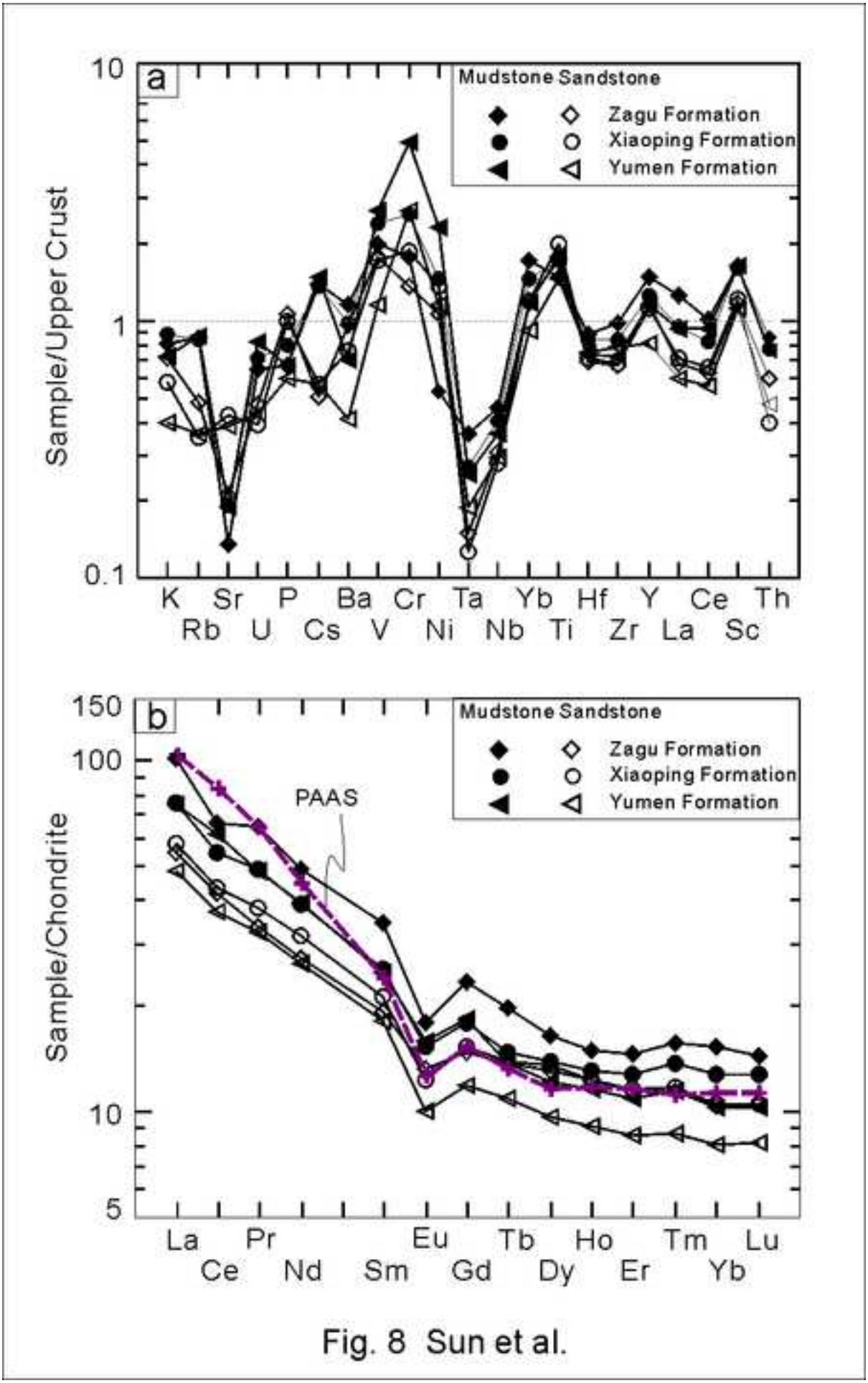

Fig. 8 Sun et al.

Click here to download high resolution image

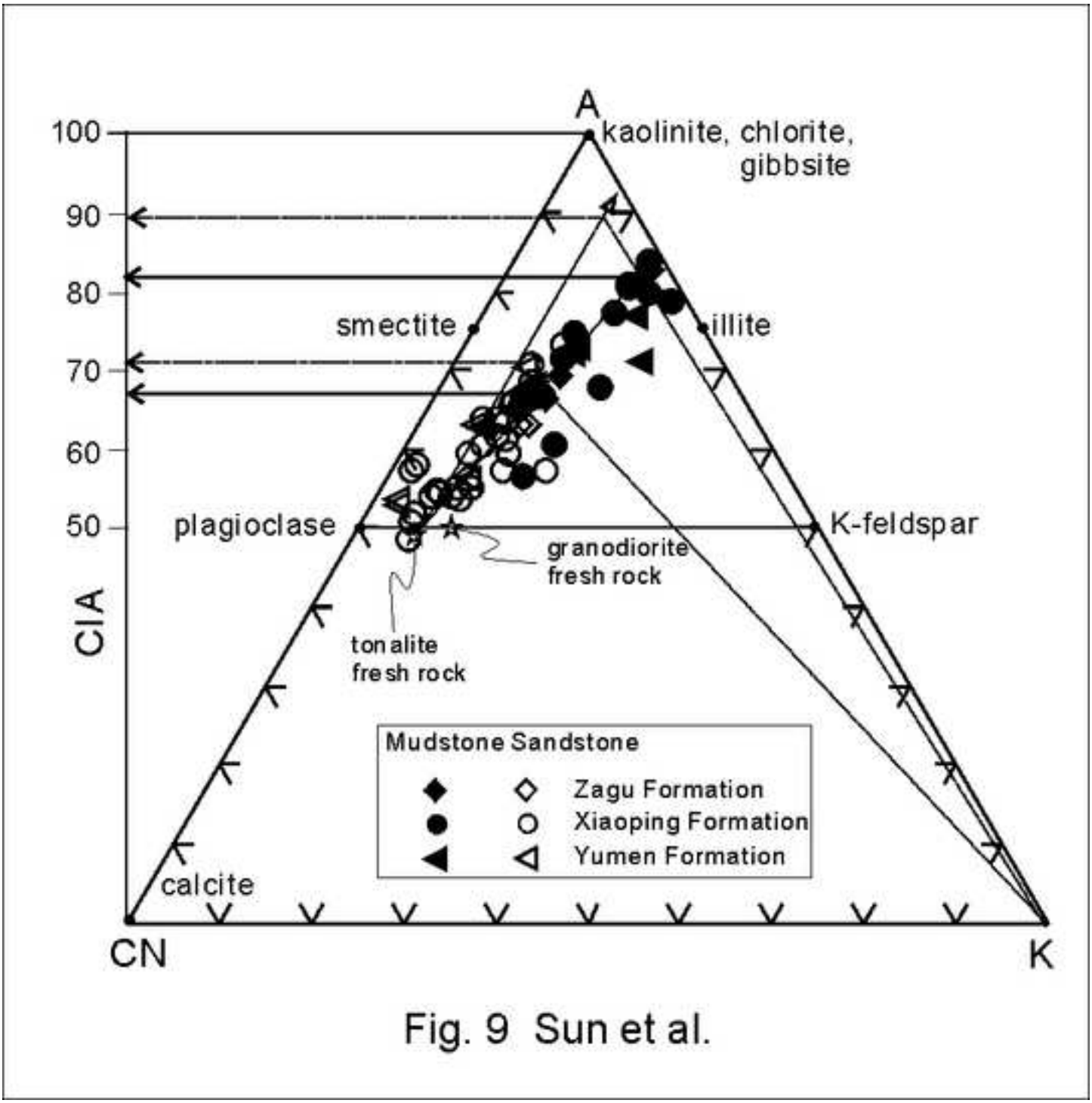

Fig. 9 Sun et al.

Click here to download high resolution image

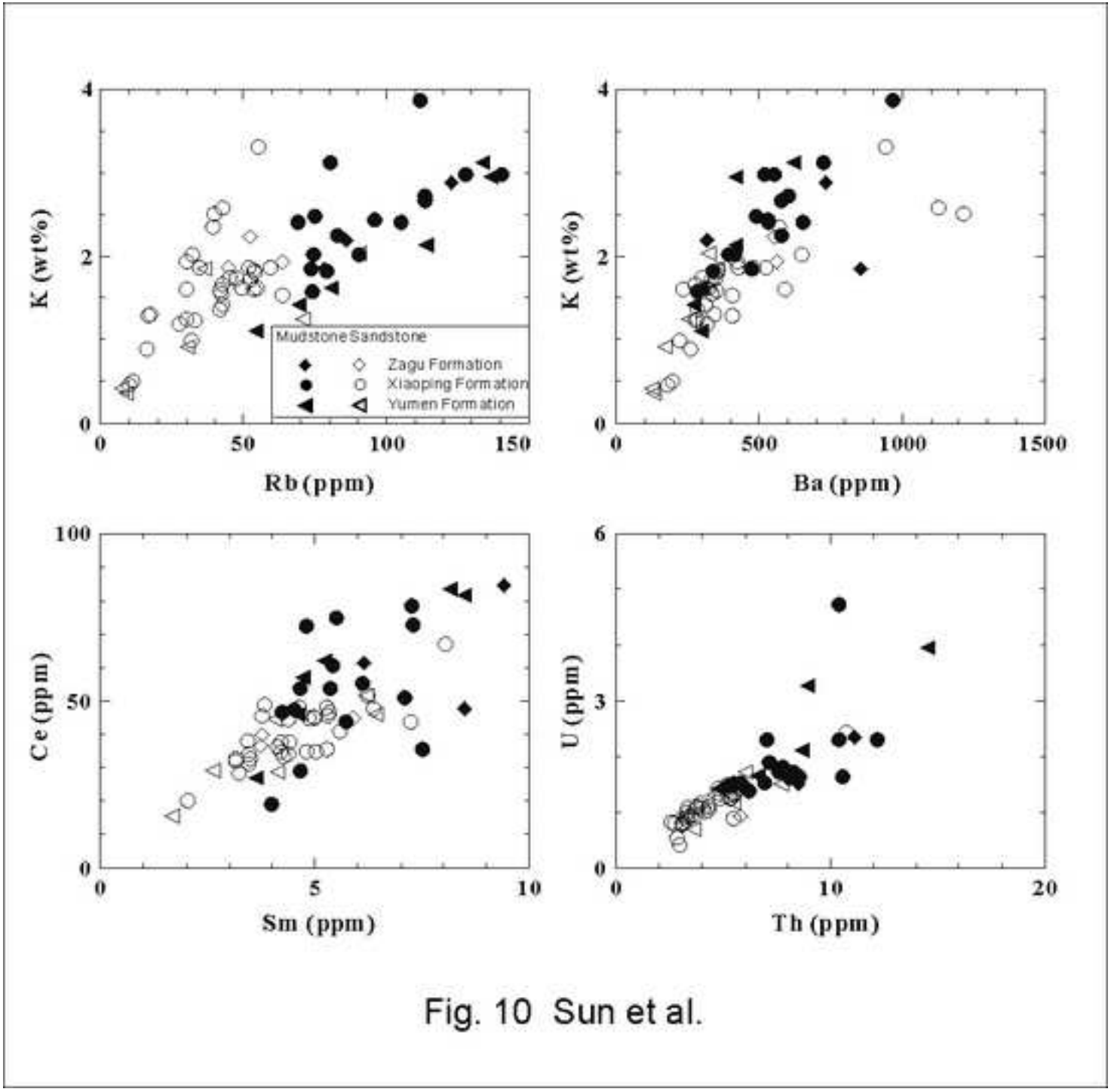

Fig. 10 Sun et al.

Click here to download high resolution image

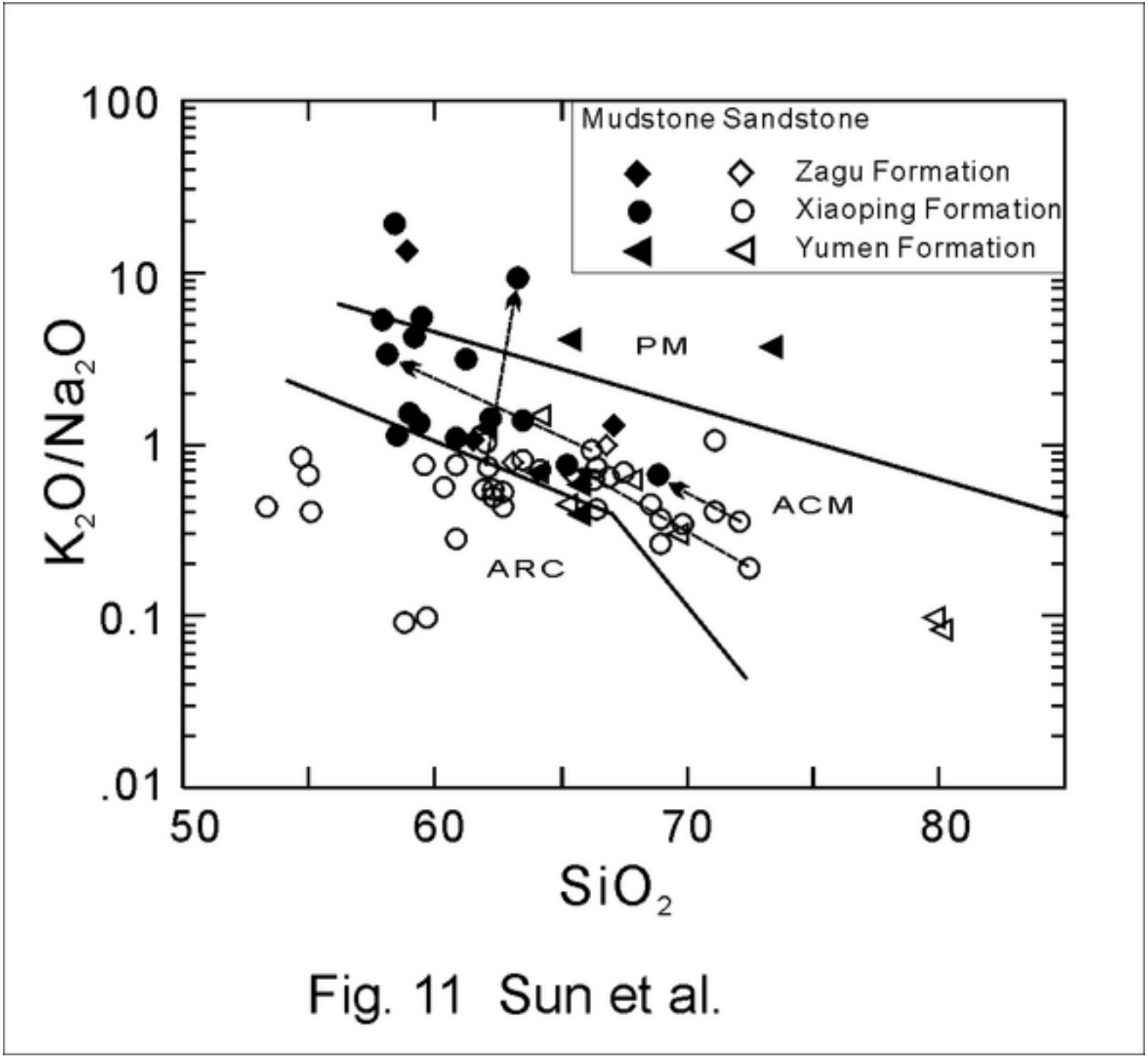

Fig. 11 Sun et al.

Click here to download high resolution image

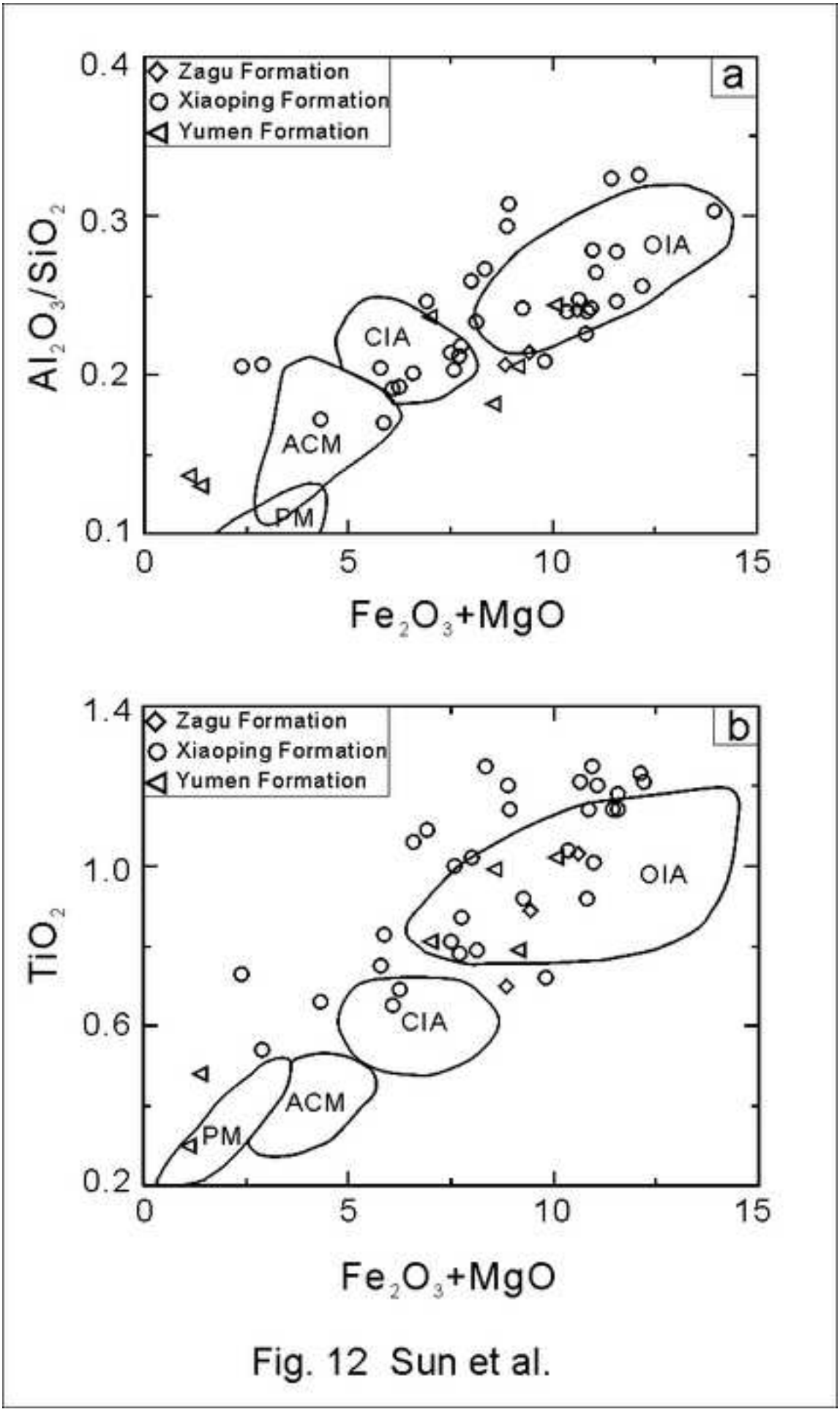

Fig. 12 Sun et al.

Click here to download high resolution image

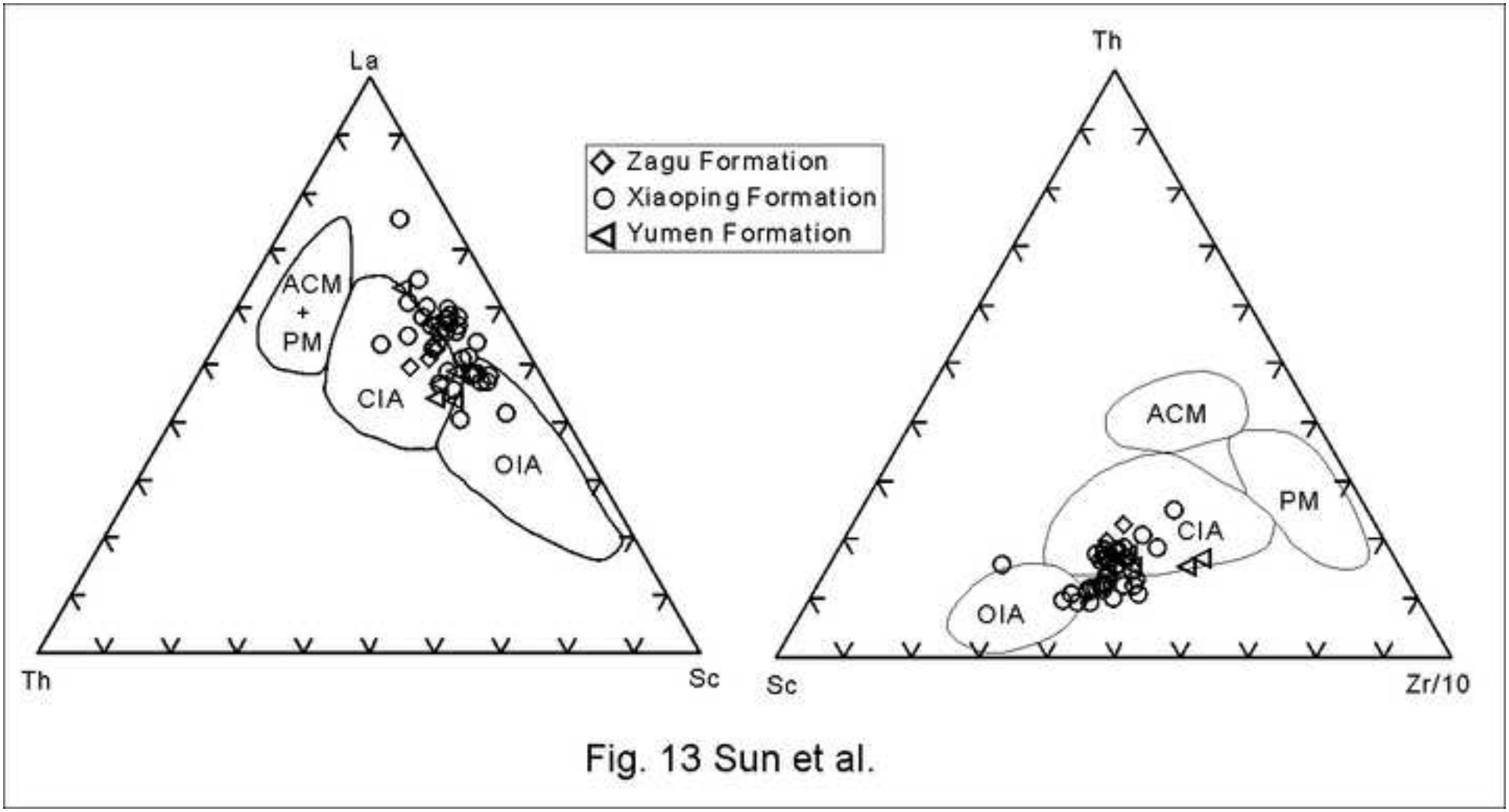

Fig. 13 Sun et al.

Click here to download high resolution image

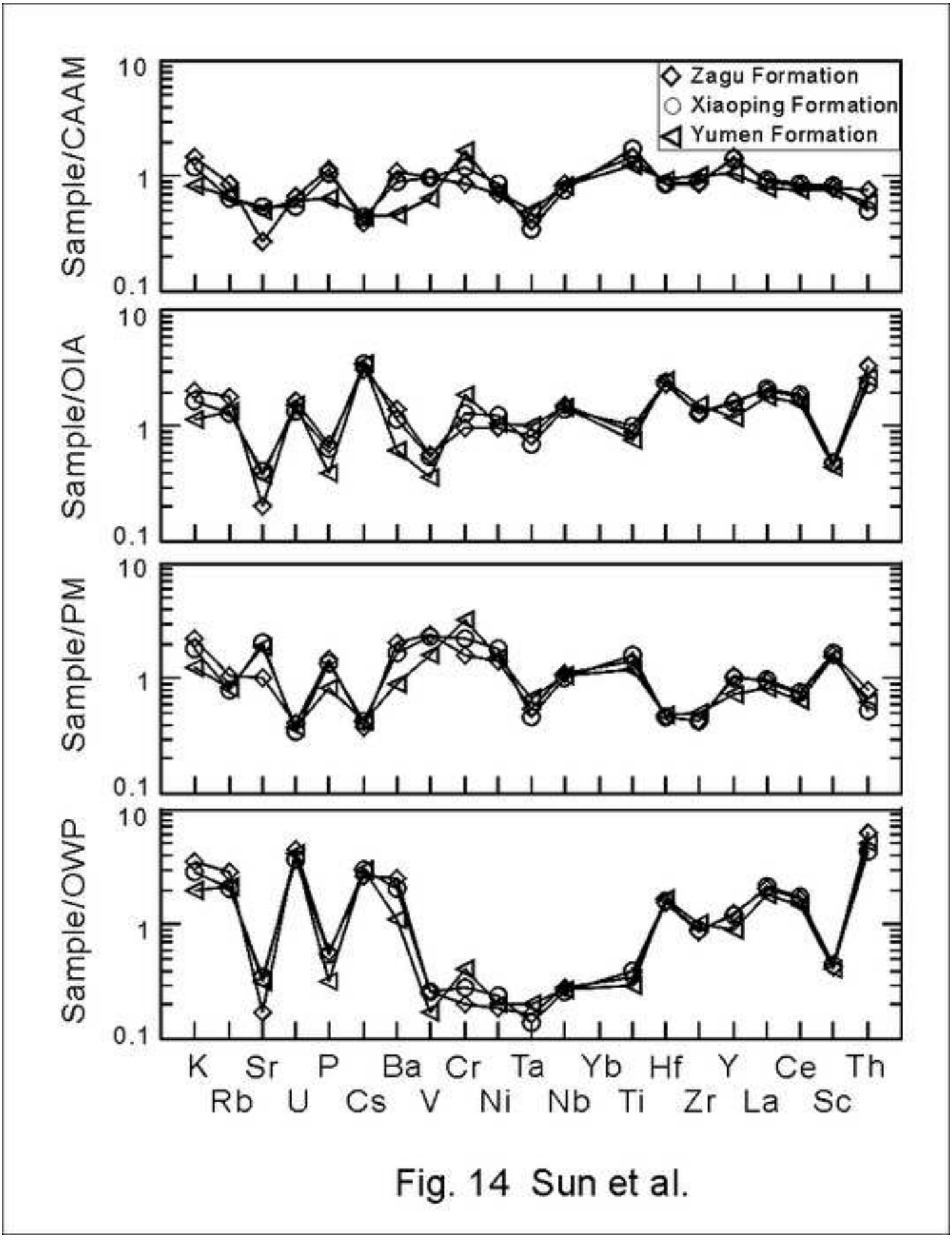

Fig. 14 Sun et al.

Click here to download high resolution image

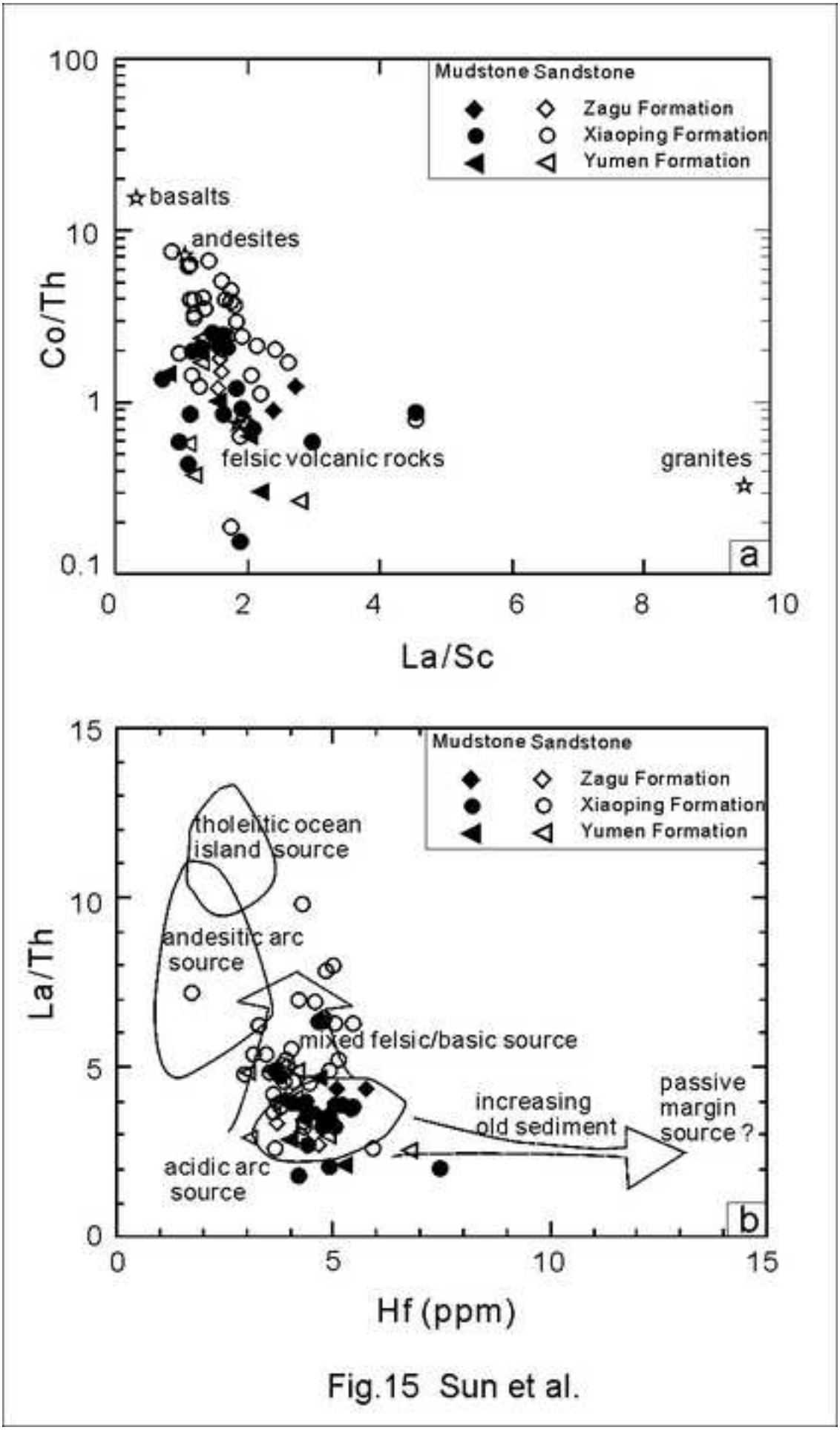

Fig.15 Sun et al.

Click here to download high resolution image

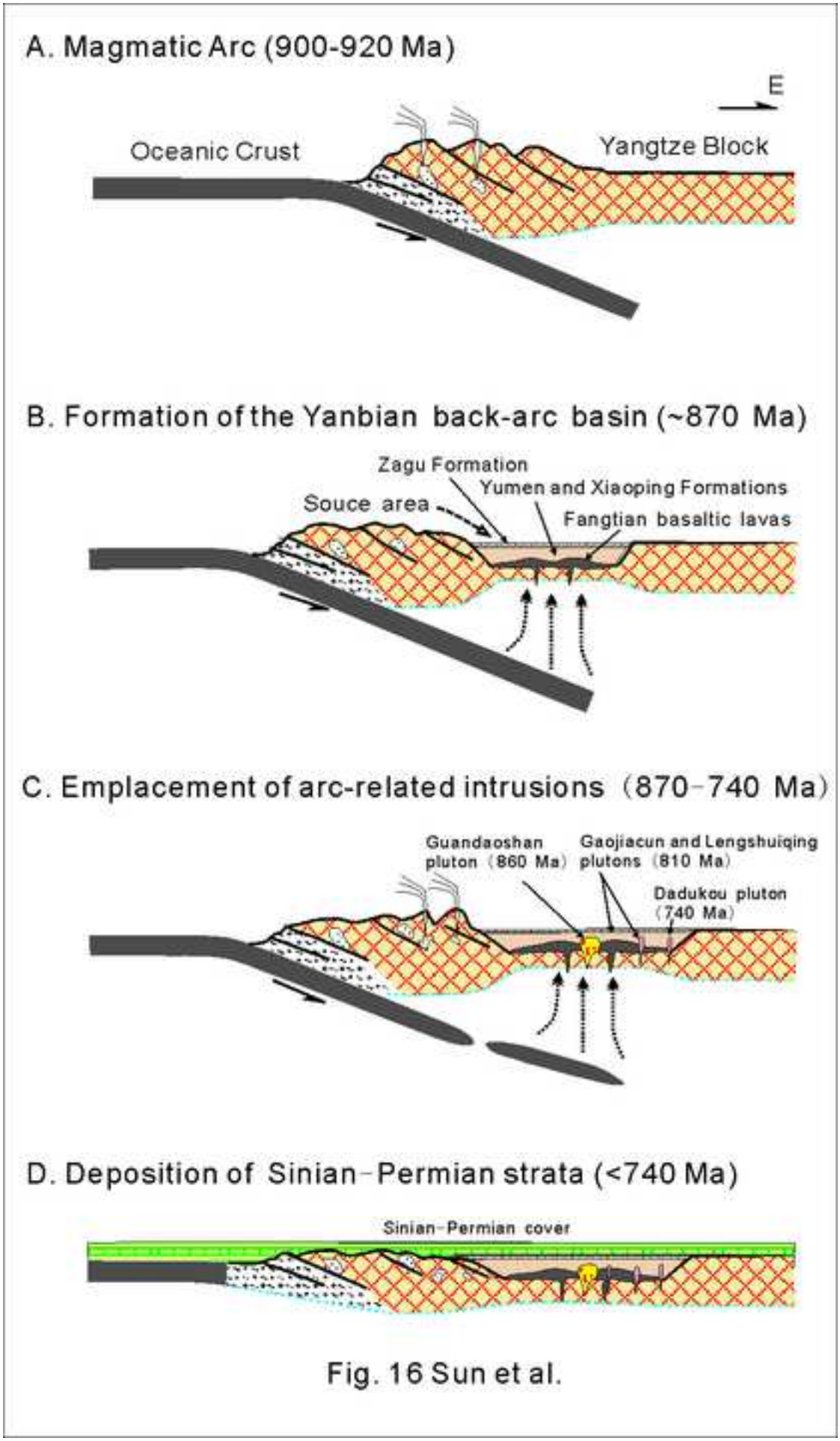

Fig. 16 Sun et al.